5-24-2012

Characterization of Normal Development and Injury in the Premature Baboon Brain

Jennifer Griffith
Washington University in St. Louis

Washington University in St. Louis

Division of Biology and Biomedical Sciences

Neurosciences

Dissertation Examination Committee:
Jeffrey Neil, Chair
Joseph Ackerman
Philip Bayly
Terrie Inder
John Olney
David Van Essen

Characterization of Normal Development and Injury in the Premature Baboon Brain

by

Jennifer Lynn Griffith

A dissertation presented to the
Graduate School of Arts and Sciences
of Washington University in
partial fulfillment of the
requirements for the degree
of Doctor of Philosophy

May 2012

Saint Louis, Missouri

ABSTRACT OF THE DISSERTATION

Characterization of Normal Development and Injury in the Premature Baboon Brain

by

Jennifer Lynn Griffith

Doctor of Philosophy in Biology and Biomedical Sciences

Neurosciences

Washington University in St. Louis, 2012

Professor Jeffrey Neil, Chairperson

Nearly 13% of infants born in the United States each year are preterm – that is, born before 37 weeks gestation. Although improvements in clinical care have contributed to survival rates that now exceed 85%, premature infants are at high risk for motor, sensory, cognitive and behavioral disabilities. In order to develop therapeutic interventions to prevent these adverse neurodevelopmental outcomes, we must first understand the nature of cerebral injury associated with premature birth and the mechanisms by which it leads to altered brain development. A baboon (*Papio papio*) model of preterm birth was used to evaluate cerebral development from 90 days of gestation (dg) to term (~ 185 dg). Conventional magnetic resonance imaging (MRI) and diffusion tensor imaging (DTI) was obtained on fixed brains. In addition, histopathology was obtained. Analysis of this model led to the following conclusions. (1) MRI/DTI findings during brain maturation closely paralleled those from live premature infants, indicating that the preterm baboon is a good model of human development. (2) Both qualitative MRI scoring and quantitative analysis of DTI parameters correlated with pathologic abnormalities in cerebral white

matter. In particular, reduced oligodendrocyte number was associated with increased radial diffusivity and decreased diffusion anisotropy, while astrocytosis corresponded to increased apparent diffusion coefficient. (3) The birth weight of control animals correlated strongly with cerebral development as measured with MRI/DTI, with lower weight corresponding to less mature brain. Since birth weight may be an indicator of the quality of the intrauterine environment, it may better predict cerebral growth and maturation than gestational age. (4) Clinical therapies differentially affect cerebral development and provide opportunities for neuroprotection. Positive pressure and high frequency ventilation were associated with more cerebral injury (as measured using both histology and MRI/DTI) than nasal continuous positive airway pressure. (5) High-dose erythropoietin, a novel neuroprotective agent, had no adverse effects on cerebral development and may increase the potential for cerebral repair by inducing proliferation of cells in the subventricular zone.

Acknowledgements

I am sincerely grateful to Drs. Jeffrey Neil and Terrie Inder for their exceptional mentorship and scientific guidance, and for their ceaseless encouragement. I am also indebted to Drs. Jacqueline Coalson, Ms. Vicki Winter and the staff at the Bronchopulmonary Dysplasia Resource Center, San Antonio, TX for provision of baboon tissue and clinical data; Dr. Donald McCurnin at the University of Texas Southwestern Medical Center, Dallas, TX, Dr. Carl White at the University of Colorado Health Sciences Center, Denver, CO, and Dr. Sandra Juul at the University of Washington, Seattle, WA for design of the ventilation and erythropoietin baboon trials; Drs. Sandra Rees and Michelle Loeliger, University of Melbourne, Australia and Drs. Nuri Farber and Shanna Zhang at Washington University, St Louis for histopathological analysis; Dr. Chris Kroenke at the Oregon Health and Science University, Portland, OR for development of diffusion tensor imaging acquisition and processing; Drs. Philip Bayly and Josh Shimony and Mr. Adrian Epstein for technical assistance with data collection and processing; Ms. Mischa van Prooijen and Ms. Stephanie Cousins for help with data processing and analysis; Dr. Michael Wallendorf for guidance on statistical analysis; and all the WUNDER team members, past and present, for years of enthusiasm and support. Finally, I would like to thank the National Heart, Lung and Blood Institute (RO1 HL074942) for financial support of the project, and the National Institute of Health (1T90 DA022871) and the Mallinckrodt Institute of Radiology for fellowship support.

Table of Contents

List of Figures and Tables

Chapter 1
Background

Introduction

Premature birth is a significant public health problem in the United States. In 2007, 12.7% of all births – nearly 550,000 infants – were preterm (less than 37 weeks gestation), and 2% of births were very preterm (less than 32 weeks gestation) (Heron et al., 2010). This represents a 20% increase since 1990 (Muglia and Katz, 2010). As the rate of preterm birth has risen, medical efforts have been focused toward decreasing perinatal morbidity and mortality. Advances in the care of premature infants, including antenatal steroid administration, improved ventilatory management and postnatal surfactant therapy have contributed to survival rates that now exceed 85% (Fanaroff et al., 2007).

Though the majority of premature infants survive, they do so at high risk of neonatal complications and long-term disabilities. The incidence of major neonatal morbidities, including bronchopulmonary dysplasia (22 - 40%), sepsis (22 – 50%), severe intraventricular hemorrhage (12%) and necrotizing enterocolitis (7%) remains high despite improved medical management (Wilson-Costello et al., 2005; Fanaroff et al., 2007). Children born preterm also have high rates of long-term neurodevelopmental disability. Major motor deficits, such as cerebral palsy, and neurosensory impairments, such as deafness or visual deficits, occur in 5 – 15% of preterm survivors (Marlow et al., 2005; Wilson-Costello et al., 2005; Moster et al., 2008). More recently, it has been recognized that up to 50% of children born preterm develop a clinically significant cognitive, behavioral, or attention deficit (Taylor et al., 2000; Anderson and Doyle, 2003; Aarnoudse-Moens et al., 2009). Not surprisingly, cognitive impairments such as poor

executive function, combined with problems in behavior and attention, negatively affect academic achievement. Some type of special education is required by 25 – 50% of school-aged children born preterm, and by middle school, up to 20% will have repeated a grade (Taylor et al., 2000). The short- and long-term sequelae of preterm birth are a burden on individual infants and their families, and on society in general. The economic impact of premature birth in the United States – including medical, educational and lost productivity costs – was recently estimated to total $26.2 billion annually (Committee on Understanding Premature Birth and Assuring Healthy Outcomes, 2006).

The social and economic consequences of premature birth provide powerful motivation to understand brain development in preterm survivors. Acute perinatal factors that are associated with preterm birth, such as ischemic events or intrauterine infection, predispose to subsequent abnormal cerebral development. In addition, the *ex utero* environment contributes many risk factors not found *in utero*, including variability in blood oxygenation during ventilation, administration of a variety of medications, and repeated exposure to invasive and potentially painful procedures; these factors may have added deleterious effects on the developing brain. To understand the impact of perinatal and environmental factors, however, we must first understand normal development of the fetal brain.

Normal Development of Premature Brain

Early development. Cerebral development begins when the neural tube closes, which in humans occurs on embryonic day 30. At this stage, the brain is organized into a

single layer of proliferative neuroepithelial cells called the ventricular zone (VZ) (Bystron et al., 2008) (Figure 1.1). The proliferative cells undergo many rounds of cell division, causing a substantial thickening of the VZ. Around embryonic day 31-32, the first neurons begin migrating tangentially along the pial surface from various origins, forming a transient layer known as the preplate (PP) (Bystron et al., 2008). Around this same time, proliferative cells in the VZ switch to asymmetrical cell division: one daughter cell remains proliferative, while the other is destined to become a neuron or glial cell (Noctor et al., 2004). Some of the proliferative cells in the VZ downregulate their epithelial characteristics and become radial glial cells, so called because these bipolar cells have processes that extend from the ventricular surface to the pial surface of the cerebrum. Radial glia are presumed to have an important role in neuronal migration, serving as a radial scaffold, but they are also capable of dividing to produce more progenitors or postmitotic cells like astrocytes, oligodendrocytes or even neurons (Fishell and Kriegstein, 2003).

Some of the progenitor cells produced by dividing radial glia are known as intermediate progenitors, which accumulate along the edge of the VZ furthest from the ventricle. This new layer is called the subventricular zone (SVZ) (Bystron et al., 2008) (Figure 1.1). In primates, early SVZ progenitors are primarily neurogenic, dividing to produce pairs of neurons that will migrate toward the pial surface (Noctor et al., 2004). Around embryonic day 40, some of the neurons at the pial surface of the PP begin to express the protein reelin, which terminates the migration of these neurons (Marin and Rubenstein, 2003; Bystron et al., 2006). As the first radially migrating neurons reach the reelin-expressing cells in the PP, they form a progressively thickening layer called the

cortical plate (CP) (Bystron et al., 2008) (Figure 1.1), which eventually becomes the cortex. The PP neurons on the other side of this CP eventually contribute to the subplate (SP) (Figure 1.1), another transient developmental zone of the neocortex. The role of the SP is not totally understood, but it is generally thought to serve as a waiting compartment for thalamocortical axons, acting as a scaffold to guide their navigation and providing transient connections with the CP (Kanold, 2004).

The mammalian neocortex is divided into six layers, numbered according to their distance from the pial surface. The reelin-expressing cells in the PP will eventually become layer I of the cortex, maturing into the largely cell-free marginal zone (MZ). Otherwise, migrating neurons arrive at the CP in an inside-out sequence. The neurons of layer VI are born and arrive earliest, while the last neurons to arrive will become layer II. The projection neurons of the deeper cortical layers are thought to originate from VZ progenitors, while SVZ progenitors generate neurons that will migrate to the more superficial layers (Noctor et al., 2004; Dehay and Kennedy, 2007). The majority of interneurons originate in the basal telencephalon and migrate tangentially, although in humans, SVZ progenitors also produce interneurons that migrate radially to the CP (Kriegstein and Noctor, 2004; Noctor et al., 2004). Peak migration of cortical neurons occurs between the third and fifth month of gestation and is completed around the seventh month (Gressens, 2000).

The area between the SVZ and the CP, through which cortical neurons are migrating throughout this period of gestation, is known as the intermediate zone (IZ) (Bystron et al., 2008) (Figure 1.1). In addition to containing axonal projections that will eventually become cerebral white matter (WM), the IZ provides a scaffold through which

neurons migrate. Cells originating in the basal telencephalon that will eventually become inhibitory interneurons in the cortex, migrate tangentially through the IZ, even as the first CP neurons are still migrating through it radially (Kriegstein and Noctor, 2004). Although there is no consensus on the boundaries of the IZ, it is generally agreed that the IZ includes the growing band of efferent axons from projection neurons in the cortex and afferent axonal projections from extracortical sites (Bystron et al., 2008). Later in gestation, these axons are joined by many corticocortical fibers. The onset of myelination and the arrival of interstitial cells (cells that terminate their migration in the IZ) characterize the maturation of the IZ to white matter (Bystron et al., 2008).

Development during late gestation. By the third trimester of gestation, migration of neurons and glia is largely complete, and the general organization of cortical and subcortical structures is set. Microstructural development from 26 – 40 weeks primarily involves maturation of large pyramidal neurons and extension of dendrites into layer I of the cortex along radial glial cells (Marin-Padilla, 1970). Subsequent cellular changes include formation and connection of additional cell processes. Migrating interneurons arrive in the cortex and create local circuit connections (Marin-Padilla, 1970). The arrival of thalamocortical afferent fibers and disappearance of radial glia are some of the final steps in cortical maturation during late gestation (Gilles et al., 1983).

Gyration and sulcation are the primary macrostructural changes notable during this same period. The pattern has been described by both histopathology and imaging studies (Chi et al., 1977; Gilles et al., 1983; van der Knaap et al., 1996). The lateral and central sulci are the first to appear, by 20 weeks gestation; sulci on the medial wall of the

occipital lobe develop next, followed by parietal, temporal and occipital sulci. The frontal and anterior temporal sulci develop last. Each sulcus is initially little more than a shallow depression in a smooth surface that deepens into a groove with time. As a sulcus deepens, its banks become steeper, so that the rounded gyri on either side of the sulcus become squared off. Primary sulci develop branches (secondary sulci), which in turn branch further (to form tertiary sulci). The microstructural forces responsible for the development of gyri and sulci are not fully understood, but there is at least some evidence that cortical gyration may depend on tension from underlying WM axons (Van Essen, 1997).

WM maturation is primarily characterized by the onset of myelination, which occurs at different times in various WM tracts, beginning midway through gestation and continuing throughout the first two years of life. The description of the sequence and timing of myelination that follows is derived from two large autopsy studies published in the mid-1980s that remain the most comprehensive evaluations of histopathological myelination in premature and newborn infants to date (Gilles et al., 1983; Brody et al., 1987; Kinney et al., 1988). Myelin first appears around 20 weeks gestation in the pons and cerebellum. In the cerebral WM, myelination proceeds from the region around the central sulcus to the poles. The first cerebral structures to be myelinated are the posterior limb of the internal capsule (PLIC) and the optic tract, around 32 weeks gestation, followed quickly by the corona radiata a few weeks later. Around term gestation, myelination begins in several more regions: the anterior limb of the internal capsule (ALIC), the cingulum, and the optic radiations. The corpus callosum (CC) is one of the latest cerebral tracts to show histopathological myelination, around 1 – 2 postnatal

months. WM regions vary not only in *onset* but in *duration* of myelination, and the two parameters are not necessarily related. For example, the PLIC and corona radiata begin myelination early and proceed quickly (i.e., have a short myelinative phase), while the optic tract has a long myelinative phase, though it also myelinates early. It is important to note that even though histopathology might be considered the gold standard of evaluation of brain maturation, different methods may provide different answers. In these two autopsy studies, which were undertaken by the same group of pathologists, the onset of myelination was consistently 5 – 20 gestational weeks earlier in one study (Gilles et al., 1983) than in the other (Brody et al., 1987; Kinney et al., 1988). This difference was attributed to differences in tissue processing and histological stain.

Impact of Premature Birth on Brain Development

Normal brain development is a highly orchestrated process throughout gestation, but the third trimester in particular is a time of rapid cerebral growth and maturation. When development during this period occurs *ex utero*, a variety of risk factors are introduced that may alter this complex series of events. An acute ischemic or infectious event by itself can induce premature labor and have devastating consequences for the developing brain. Even when preterm birth is not associated with an acute event – as in half of all preterm births where the cause *is not* known (Muglia and Katz, 2010) – neonatal intensive care required to keep infants alive involves medications, procedures and other stimuli that may be directly deleterious or cause significant stress associated with adverse neurodevelopment.

Neuropathological descriptions of cerebral injury. Although there is a great deal of variability in the severity of cerebral injury associated with preterm birth, the periventricular location and microstructural pattern of most types of injury are remarkably consistent among infants. Descriptions of lesions from 40 or 50 years ago are consistent with more recent pathological studies, although the most severe injury seems to be rarer now than it was then, probably as a result of improved neonatal care.

White matter injury. Fifty years ago, premature infants – particularly those born very preterm – had low survival rates, which meant large numbers of infants were available for neuropathological examination. On autopsy, over half of the infants were found to have lesions in the periventricular WM, a pattern of pathology termed "perinatal telencephalic leucoencephalopathy" or "periventricular leukomalacia of infancy" (Banker and Larroche, 1962; Gilles and Murphy, 1969). The latter, abbreviated PVL, is commonly used today, although its definition has expanded as new pathological insights have emerged. PVL has two components: foci of necrosis surrounded by diffuse gliosis (Gilles and Murphy, 1969; Marin-Padilla, 1997). The focal necrotic component has long been used to diagnose PVL in the live premature infant, primarily because its echogenicity makes it easily recognizable on CUS, particularly days to weeks after the injury occurs (Maalouf et al., 2001; Inder et al., 2003a; Miller et al., 2003). In the acute phase of injury (< 24 hours), these foci exhibit coagulative necrosis and axonal spheroids (Marin-Padilla, 1997; Folkerth, 2007). These spheroids dissolve during the subacute period (3-5 days), and the foci are marked by macrophage infiltration and the emergence of reactive astrocytes (Marin-Padilla, 1997). The pathology continues to develop during

the chronic stage of injury, which may last weeks to months. Eventually necrotic foci evolve to focal glial scars or, if the lesion is large enough, will cavitate to form periventricular cysts as macrophages clear necrotic tissue (Marin-Padilla, 1997; Folkerth, 2007). If the area of necrosis is very large, WM volume loss can be pronounced and lead to thinning of the corpus callosum and other surrounding tracts.

The diffuse component of PVL has long been recognized, but its presence in the majority of preterm infants and contributions to adverse neurodevelopmental outcomes has been understood only recently (Volpe, 2003). Necrotic foci are nearly always accompanied by diffuse gliosis in the surrounding WM (Gilles and Murphy, 1969; Marin-Padilla, 1997). In the acute phase, WM surrounding necrotic foci is marked by injury of oligodendrocytes and activated microglia (Kinney and Back, 1998). The microglia continue to proliferate in the subacute phase, which is marked by increased cytokines and free radical injury to oligodendrocytes (Haynes et al., 2003). The diffuse component of PVL in its chronic stage is characterized by the marked presence of reactive astrocytes, and eventually with myelin delay or deficiency, presumably caused by oligodendrocyte death (Leviton and Gilles, 1984; Haynes et al., 2003; Billiards et al., 2008). There is some evidence that oligodendrocytes may migrate toward the focal necrotic areas of PVL, perhaps to replenish oligodendrocyte populations, although even in the face of this potential for recovery and repair, myelination deficiencies are noted (Billiards et al., 2008). Even if the density of oligodendrocytes is restored, their maturation or production of myelin may still be impaired, accounting for the myelin deficiencies noted in pathological studies.

Because the majority of infants survive, it is impossible to know the incidence of PVL as defined histopathologically. Instead, *in vivo* imaging studies must be used. Large periventricular cysts that devastated the WM used to be very common, but today are found in fewer than 5% of infants (Maalouf et al., 2001). The diffuse component of PVL, in contrast, is found in up to 70% of all premature infants (Inder et al., 2003a). A complete discussion of imaging findings is found in part IV of this chapter.

The fact that the vast majority of premature infants have the same periventricular pattern of lesions, though to varying degrees, probably reflects the maturationally-dependent nature of WM injury. Even some of the first pathological reports of PVL suggested that the predominant vulnerability of periventricular WM was related to its early myelination (Gilles and Murphy, 1969). More recent studies have shown that the period of highest risk for PVL, from 23 to 32 weeks post-conception, coincides with a particular stage of oligodendroglia maturation, known as late oligodendrocyte progenitors, or pre-oligodendrocytes (pre-OLs)(Back et al., 2001). When these progenitor cells mature to immature (pre-myelinating) oligodendrocytes, around 32 weeks post-conception, the incidence of PVL decreases dramatically. Activated microglia, which are a prominent feature of periventricular WM injury, are known to release reactive oxygen and nitrogen species (Haynes et al., 2003), and the pre-OL is more vulnerable to oxidative and nitrosative injury and subsequent apoptosis than immature oligodendrocytes (Back et al., 2002). It is not surprising, therefore, that the anatomic pattern of oligodendrocyte maturation – and not cerebral blood flow – predicted the pattern of WM injury in a fetal sheep model of ischemia-reperfusion (Riddle et al., 2006).

Hemorrhage. Perinatal ischemic events, with or without reperfusion, commonly result in hemorrhage. Circulatory autoregulation is immature in the preterm infant, and decreased cerebral perfusion pressure due to transient drops in systemic hypotension – a common event in premature infants – is poorly compensated (Volpe, 2009). As with WM injury, the primary location of hemorrhage is periventricular, though unlike WM injury, the vulnerability depends on the existence of vascular "watershed" zones in this region (Folkerth, 2007). The vessels of the germinal matrix are particularly vulnerable, and drops in cerebral perfusion lead to ruptured capillaries in this area (Marin-Padilla, 1996). Acute germinal matrix hemorrhage (GMH) is characterized by infiltrates of macrophages and leukocytes, and chronically, appear as regions of hemosiderosis and gliosis (Folkerth, 2007). Large hemorrhages can disrupt the ependymal surface to cause intraventricular hemorrhage (IVH), which is sometimes associated with ventricular dilatation (Folkerth, 2007). In its most severe form, the pressure from intraventricular blood compresses deep venous structures in surrounding parenchyma, causing a so-called periventricular hemorrhagic infarct (PHI) in this WM (Volpe, 2009). GMH-IVH with associated PHI occurs in about 5% of all premature infants and in about 20 – 30% of those that are born 24 – 26 weeks gestation or less than 750 g (Larroque et al., 2003). The consequences of this most severe type of hemorrhage are similar to those of cystic PVL.

Gray matter injury. For decades, the common assumption has been that cerebral injury in premature infants is primarily limited to WM. But recent evidence from autopsy studies suggests that certain types of gray matter injury may accompany periventricular WM damage. Of infants with PVL, neuronal loss was found in the

thalamus (38 - 55% of cases), globus pallidus (33%) and hippocampus (33%) while significant gliosis was found in the caudate (60% of cases), thalamus (56%), putamen (50%), globus pallidus (60%), hippocampus (47%), and cortical GM (20 – 31%) (Pierson et al., 2007; Ligam et al., 2009). Cerebellar abnormalities have been similarly appreciated in recent years. As in cerebral GM, cerebellums in infants with PVL show a high incidence of neuronal loss and gliosis in the dentate nucleus (29% and 43% of infants, respectively), cerebellar cortex (24% and 29%) and basis pontis (21% and 100%) (Pierson et al., 2007). Cerebellar hemorrhage, which is often associated with supratentorial injury, is found in 2% of premature infants weighing 750 – 1500 g at birth, and in 17% of those weighing less than 750 g (Limperopoulos et al., 2005). These under recognized GM pathologies in premature infants may turn out to have important consequences for developmental outcome.

Pathogenetic mechanisms. Some of the pathogenetic mechanisms underlying cerebral injury in the premature infant have been described above, but it is worth bringing them into context here. The majority of evidence points to the pre-oligodendrocyte (pre-OL) as the key target of injury in developing WM (Back et al., 2001; Back et al., 2002; Haynes et al., 2003; Riddle et al., 2006) (Figure 1.2). The two major mechanisms leading to death of pre-OLs are inflammation, usually the result of maternal intrauterine infection or postnatal sepsis, and ischemia (Volpe, 2009). Both inflammation and ischemia lead to the activation of microglia, which release cytokines and reactive oxygen and nitrogen species (Back, 2006). Pre-OLs are more vulnerable to death from free radicals than other cell types like reactive astrocytes and oligodendroglia at other stages of maturation,

which are resistant to nitrosative and oxidative damage (Haynes et al., 2003). Both ischemia and inflammation also lead to excessive levels of extracellular glutamate, in part by inducing its release from axons and activated microglia (Back, 2006). A downstream effect of receptor-mediated glutamate excitotoxicity in pre-OLs is the generation of oxygen and nitrogen free radicals, which lead to cell death. The particular vulnerability of pre-OLs is probably related to their high levels of expression of cytokine and glutamate receptors and low production of antioxidants (Khwaja and Volpe, 2008).

Mediating environmental factors. Some neonatal care practices or other aspects of the NICU environment may also influence brain development. Infants are exposed to oxidizing agents such as supplemental iron and oxygen, which can generate free radicals that destroy vulnerable pre-OLs (Dommergues et al., 1998; Haynes et al., 2003). Certain modes of ventilation, particularly high frequency oscillatory ventilation, may increase the risk of intraventricular hemorrhage in the preterm brain, although variations in clinical management may modify this risk (Gressens et al., 2002). There is increasing recognition that a variety of drugs given to treat or prevent respiratory dysfunction may have unintended consequences for brain. Postnatal steroids, once thought to improve respiratory function, are known to be associated with an increased risk for poor neurodevelopmental outcome (Murphy et al., 2001). Inhaled nitric oxide has similarly been shown to be potentially deleterious (Gressens et al., 2002). Infants in the neonatal intensive care unit (NICU) are exposed to a variety of visual, auditory and tactile experiences wildly different from those *in utero*, which have the potential to alter cortical development. Invasive procedures and handling may also alter development, as they are

frequent during a premature infant's stay in the NICU and may cause pain. In addition, the use of sedatives and analgesics in these infants, as well as anesthetic agents – including nitrous oxide, isoflurane and fentanyl – may promote apoptosis of cortical neurons (Olney et al., 2000; Jevtovic-Todorovic et al., 2003; Johnson et al., 2008). As the effects of these therapies and stimuli become increasingly recognized, efforts are being made to limit their use, yet some procedures and other aspects of care are necessary for an infants survival. Therefore, a neuroprotective agent would be particularly helpful for premature infants. Such neuroprotective strategies will be discussed in more detail in Chapter 6.

Characterization of Premature Brain using MRI

The classic method used to study brain maturation was neuropathological analysis of autopsy specimens. The sheer amount of work involved in obtaining specimens, preparing slices, achieving reliable staining with a variety of agents, and quantifying the results means that very few such analyses have been published. Those that have been, however, are invaluable for their level of detail and systematic analysis (Gilles et al., 1983; Brody et al., 1987; Kinney et al., 1988; Marin-Padilla, 1997). There are limitations to neuropathological studies, however. Autopsy specimens used to characterize normal development are carefully selected to include only cases with a non-neurological cause of death and with no history of major neurological impairment or disease. Still, the cause of death in most of the autopsy specimens used in these studies is spontaneous abortion or accident; these brains might not represent true normal development. It is also

increasingly difficult to obtain large numbers of autopsy cases needed for such descriptive studies, not least because survival rates of preterm infants have been increasing in recent years.

Comparison of MRI to other imaging modalities. Imaging techniques are clinically relevant because they can be applied to the live human infant. Cranial ultrasound (CUS) is a common bedside technique for assessing cerebral injury because of its portability and ease of use. Hemorrhages (germinal matrix, intraventricular or parenchymal), ventricular dilatation and cystic white matter lesions are readily seen on CUS, but it is less reliable than MRI at detecting small punctate hemorrhagic WM lesions or diffuse WM abnormalities that are common in premature infants (Maalouf et al., 2001; Inder et al., 2003a; Miller et al., 2003). The US transducer is limited to positions on the skull where there is little or no bone, so that certain areas of the brain – notably, the cerebral convexities – are not visible on US images. Computed tomography (CT) studies provide a better field of view than CUS and are shorter than typical MRI scans. Concerns about exposing the developing brain to ionizing radiation have prevented the use of CT in human preterm neonates (Neil and Inder, 2004).

Magnetic resonance imaging (MRI) is a safe method to obtain high-resolution images of the premature brain *in vivo*. The MR signal in most clinical images arises from the hydrogen nuclei in water. The abundance of these nuclei allows for high spatial resolution imaging of biological tissue. Conventional MR imaging relies on the fact that hydrogen nuclei in water have different magnetic resonance properties in different types of tissues. These properties include proton density, and the relaxation time constants T1,

which represents recovery of longitudinal magnetization with time, and T2, which represents the decay of the magnetization in the transverse plane due to interactions of nuclei with their environment. The T1 and T2 relaxation time constants differ among tissue types. These differences are exploited using different MR pulse sequences: by varying image acquisition parameters, images can be "weighted" for T1- or T2-dependent contrast. For instance, the T2 relaxation time of water in cerebrospinal fluid (CSF) is longer than that in brain tissue; on a T2-weighted image, CSF will appear bright relative to the brain. In current clinical practice, T1- and T2-weighted images are obtained in premature infants to assess qualitative cerebral development (cerebral volume, gyration, myelination) and injury (hemorrhage, ventricular dilatation, cystic or diffuse WM abnormalities).

In diffusion-weighted MRI, image contrast depends on small displacements (~10 μm) of water. The motion of water in different tissues can be described by quantitative physical properties. Water molecules, which would otherwise be characterized only by Brownian motion, may be influenced by other factors in biological tissue. The overall magnitude of water diffusion is therefore called the apparent diffusion coefficient (ADC). In biological tissue *in vivo*, ADC depends on structural characteristics, such as cellular density and organization. But changes in ADC can also be seen on a physiologic time scale: for example, ADC decreases within minutes after stroke (Moseley et al., 1990). ADC is therefore valuable in the clinic to evaluate both acute injury (within minutes to hours) and structural changes that occur as a result of normal development or chronic injury (within days to months).

To obtain information about the spatial heterogeneity of water diffusion, diffusion is measured in several (> 6) directions, known as diffusion tensor imaging (DTI). In CSF, the motion of water is the same in all directions, that is, isotropic. In brain tissue, water motion is restricted by microstructure, and these restrictions are often not isotropic. In this case, tissue ADC values differ depending on the direction in which the measurement is made: indeed, in DTI, the acronym "ADC" refers to the average apparent diffusion coefficient. The extent to which water diffusion differs depending on direction can be quantified using a calculation of diffusion anisotropy, such as relative anisotropy (RA) or fractional anisotropy (FA). The classic example is mature WM: water diffusion is smaller perpendicular to axons, due to restricted motion through layers of myelin, than parallel to them. RA values in myelinated WM are therefore high, while in CSF they are close to zero. The value of water ADC in the direction along which diffusion is greatest is called the axial diffusivity, and the value of diffusion perpendicular to this direction is called the radial diffusivity. RA, axial and radial diffusivity are highly useful for evaluating the organization and maturation of cerebral tissue in the developing brain.

Imaging normal brain development. *Fetal imaging.* Ideally, normal brain development during gestation could be described by fetal MR imaging. The majority of fetal MR scans are conventional imaging studies, but a few diffusion-weighted imaging studies have been performed (Righini et al., 2003; Bui et al., 2006; Prayer et al., 2006). Fetal MR studies provide valuable insight into normal development, but are limited by image quality. Because of the tendency for fetal movement, imaging protocols use fast sequences, which can be more susceptible to artifacts (Prayer et al., 2006; Liu et al.,

2008). Image resolution is also often lower in these scans because the radiofrequency coil used to receive MR signals must fit around the mother's abdomen rather than around the infant's head, as in studies of premature infants. Improved resolution offers better characterization of anatomical and microstructural changes in the developing brain.

Conventional imaging. As the biological and structural properties of brain tissue that determine T1 and T2 relaxation times vary as a function of age, brain maturation can be evaluated qualitatively on conventional T1- and T2-weighted imaging. One of the primary determinants of tissue relaxation time constants is the content of water, which has long T1 and T2. Relative to the adult brain, fetal brain tissue has a high water content, which decreases during gestation and throughout the first year of life (Neil and Inder, 2004). A corresponding decrease in T1 and T2 relaxation times of both gray and white matter occurs during this period (Barkovich et al., 1988; Paus et al., 2001). Although T1 and T2 could be measured quantitatively to evaluate brain maturation, qualitative assessment of GM/WM contrast on T1- and T2-weighted images is far more common, in both clinical and research imaging. Tissue contrast depends on water content, as well as anatomical and microstructural organization: more structured or tightly organized tissue has shorter T1 and T2 (Neil and Inder, 2004). By late gestation, GM is highly organized with a radial orientation, while WM is still loosely organized, as described in the previous section. GM has shorter T1 and T2 times than WM, and therefore appears darker than WM on T2-weighted images and brighter than WM on T1-weighted images (McArdle et al., 1987b; Barkovich et al., 1988). By term gestation, the organization of GM has increased in complexity, although it is no longer radially orientated; WM is highly organized into bundles of axons, which become even more

tightly arranged as myelination proceeds during the first 12 months of life. WM relaxation times therefore decrease much more rapidly during the first year than do GM relaxation times, and around 6 months, WM T1 and T2 become shorter than those of GM, causing a "flip" in GM/WM intensities (McArdle et al., 1987b; Barkovich et al., 1988; Dietrich et al., 1988; Neil and Inder, 2004). After an isointense period around 6 – 12 months of life, during which GM and WM are poorly differentiated, GM becomes brighter than WM on T2-weighted images and darker than WM on T1-weighted images (Barkovich et al., 1988; Dietrich et al., 1988). This pattern is the same as the normal adult pattern of tissue intensities.

Myelination can also be evaluated on T1- and T2-weighted imaging. Compared to immature WM, myelinated tracts are tightly bundled and have an increased lipid content, which contributes to decreased T1 and T2 relaxation times (Paus et al., 2001). Myelinated WM will therefore appear darker than unmyelinated WM on T2-weighted images and brighter on T1-weighted images. In the autopsy studies described in part II, the temporal sequence of myelination was generally the same across studies, while the exact timing of the appearance of myelin in different regions depended on the method of staining. In a similar way, the chronology of myelination is consistent across MRI studies, although the actual timing for individual WM tracts varies depending on the MR acquisition parameters and grading scheme used. Myelination in the brain stem (pons) and cerebellum is visible on MR images at birth and precedes myelination in the cerebral hemispheres (McArdle et al., 1987b; Barkovich et al., 1988; Dietrich et al., 1988). The posterior limb of the internal capsule, optic radiations and corpus callosum are the first cerebral tracts to show MR evidence of myelination (birth – 3 months), followed by the

anterior limb of the internal capsule (3 – 6 months), and finally the hemispheric WM in the frontal, parietal and occipital lobes (8 – 12 months).

Other features of cerebral development can also be appreciated on conventional MRI. Very preterm infants have bands of hypointensity on T2-weighted images in frontal periventricular WM; the bands disappear by term-equivalent age, suggesting that the areas of hypointensity correspond to transient populations of migrating glia (Childs et al., 1998). Cortical gyration and sulcation can also be assessed on T2- or T1-weighted imaging, although grading schemes for gyral development are generally limited to qualitative evaluation (van der Knaap et al., 1996).

Diffusion imaging. Compared to conventional MRI, DTI has the advantage of being quantitative, and therefore provides a relatively objective method for evaluating brain development. As with T1- and T2-weighted MRI, the major factors influencing changes in diffusion parameters during development relate to decreasing brain water content and increasing microstructural tissue complexity (Beaulieu, 2002). Fetal brain tissue is much more "watery" and loosely organized than tissue in the adult brain. The overall magnitude of water diffusion is much greater in the preterm brain, and ADC in premature infants is about three times higher than that in the adult brain (Neil et al., 1998). Although water content is similar in GM and WM in fetal brains, ADC is lower in GM than WM during late gestation (Neil et al., 2002). By late gestation, the cortex is densely packed with the membranes of cells and their processes, which hinder water diffusion, whereas axons in the immature white matter are only loosely organized. As gestation continues, ADC decreases in both tissues, but more rapidly in the WM as bundles of axons organize, membranes proliferate and myelination begins. By term,

GM/WM contrast on ADC maps is reduced and by childhood has disappeared completely (Neil et al., 1998; Mukherjee et al., 2002).

Developmental changes in brain anisotropy are also related to tissue microstructure. In the adult brain, water diffusion in the cerebral cortex is isotropic, and RA values are near zero. In contrast, between 15 and 32 weeks, RA in the fetal brain is transiently anisotropic (McKinstry et al., 2002; Huang et al., 2009). Midway through gestation, the overall architecture of the cortex is radially orientated, due to the predominance of the apical dendrites of pyramidal neurons and the radial glia stretching from the ventricular surface to the marginal zone (Bystron et al., 2008). As additional neuronal connections are made, the radial orientation of the cortex is lost and anisotropy drops to zero (McKinstry et al., 2002).

Anisotropy in fetal WM is low and increases during development in two stages. WM development includes a "premyelination" stage, which is characterized by axonal changes – organization of axons into tight bundles, increasing axon caliber, proliferation of microtubule-associated proteins, increasing conduction velocity and Na^+/K^+-ATPase activity in axonal membranes – and an increase in the number of immature oligodendrocytes. This premyelination stage of WM development is associated with the first increase in RA (Wimberger et al., 1995; Drobyshevsky et al., 2005). Indeed, changes in anisotropy indicate the maturation of WM tracts weeks before conventional MRI (Neil et al., 1998) or histopathological (Gilles et al., 1983) evidence of myelination. A second increase in anisotropy occurs as a result of axon myelination. As with histopathological evidence of myelination and changes on conventional T1- and T2-weighted imaging, increases in anisotropy in the PLIC, CC and optic radiations precede

the ALIC and hemispheric WM (Neil et al., 1998; Partridge et al., 2004; Dubois et al., 2008a). Finally, it is important to note that although WM anisotropy is increasing around the same time as ADC is decreasing, the changes in the two are not correlated (Provenzale et al., 2007), and thus changes in these two parameters with development probably reflect different aspects of WM maturation.

Comparison of MRI with histological description of development. As described above, interpreting MRI features of cerebral development in live premature infants relies on comparing these features to histopathological characteristics of autopsy specimens. It is interesting that the first MRI studies to establish features of normal brain maturation were published at nearly the same time as the first autopsy studies to extensively define myelination histopathologically. These methods have long complemented one another, yet there is an important difference. To characterize normal preterm development, *in vivo* MRI studies include prematurely-born infants at minimal clinical risk, while autopsy studies include spontaneously-aborted fetuses or prematurely-born infants with non-neurologic causes of death. A few authors have attempted to better characterize histopathological correlates of imaging by using *ex vivo* MRI. In one study, T1-weighted MR imaging was performed prior to histological analysis in 17 *ex vivo* human brains, ranging from 15–36 weeks gestational age (Kostovic et al., 2002). The advantage of this study was that the same brains were used for both methods, and the laminar organization of the fetal cerebrum was shown in detail in both histological and MR slices. However, the slices of MR images and histological stains presented side-by-side in this and two later papers by the same group outlining the development of cerebral

connections and transient lamina (Kostovic and Jovanov-Milosevic, 2006; Rados et al., 2006) often came from brains that differed in gestational age by as much as two or three weeks. Also, though the MR imaging in this study had higher resolution than that in many *in vivo* studies, a significant opportunity was missed by not including any diffusion imaging. A second group performed DTI on 50 aborted fetuses, ranging from 12 – 42 weeks gestational age (Trivedi et al., 2009). Increased anisotropy in the intermediate zone/WM was correlated with increasing area of neurofilament expression. Anisotropy in the germinal matrix and subplate was correlated with the number of neuron-specific enolase-positive cells. The close qualitative correspondence between anisotropy and histopathology in fetal brains suggests that if there are alterations in cerebral development or other neuropathological abnormalities in infants born prematurely, they are likely to be detected using DTI.

MRI abnormalities in preterm populations. *Conventional imaging.* Two main features of abnormal cerebral development on MRI have been noted in preterm populations: WM neuropathologies and delayed brain maturation. Although it is likely that delays in gyration or myelination occur as a consequence of WM injury, in general, these two features have been assessed independently on conventional MRI.

Since the feasibility and utility of MRI in premature infants was realized in the late 1980s, attempts have been made to grade or quantify brain maturation using MRI. One approach is to standardize qualitative assessments using grading systems derived from large study populations. Rubrics to evaluate GM/WM differentiation and myelination (McArdle et al., 1987b; Dietrich et al., 1988) cortical gyration (van der

Knaap et al., 1996), or total brain development, including evidence of neurogenesis and glial cell migration (Childs et al., 2001) have been proposed, but none has been widely adopted. An alternative approach is to measure the diameter, area, or even volume of brain structures to evaluate brain growth (Huppi et al., 1998b; Nguyen The Tich et al., 2009). Even these quantitative values must be interpreted carefully, however, since brain metrics can vary depending on image resolution and GM/WM contrast.

Conventional MRI is also useful for identifying hemorrhagic and parenchymal lesions days to weeks after premature birth (McArdle et al., 1987a; McArdle et al., 1987c) (Figure 1.3). When preterm infants are imaged within the first few days of life, abnormalities including intraventricular or germinal layer hemorrhage, ventricular dilatation, focal T1-weighted hyperintensities and diffuse high signal intensity on T2-weighted images are common findings (Maalouf et al., 1999; Miller et al., 2003). The cystic lesions traditionally used to diagnose PVL by cranial US can be detected on T1- or T2-weighted MRI (McArdle et al., 1987a). However, in study populations consisting of consecutively enrolled preterm infants, cystic lesions are found on less than 5% of infants, while diffuse noncystic abnormalities are found in 30 – 75% (Maalouf et al., 2001; Inder et al., 2003a). When conventional imaging is performed at term-equivalent age, which can be weeks or months after preterm birth, prematurely-born infants have evidence of chronic injury compared to term-born control infants. Diffuse WM atrophy, ventriculomegaly, immature gyration and enlarged subarachnoid space are present at term-equivalent age(Maalouf et al., 1999; Maalouf et al., 2001; Inder et al., 2003b). These structural changes are often seen alongside diffuse T2 hyperintensity, which increases with postnatal age: in one study, the incidence increased from 21% in the first

postnatal week, to 53% a few weeks later, to 79% at term-equivalent (Maalouf et al., 2001). Diffuse noncystic WM abnormality marked by persistent T2-weighted signal changes therefore probably represents chronic evolution of WM injury in preterm infants (Volpe, 2003).

Though less widely recognized, gray matter abnormalities are another feature of abnormal cerebral development in preterm infants. As mentioned above, cortical gyration can be evaluated by conventional MRI (van der Knaap et al., 1996). Delayed gyral development occurs in ~30% of premature infants at term-equivalent age, while signal change in the cortex occurs in less than 5% (Inder et al., 2003b). As both of these findings were highly related to the presence of WM abnormalities, it is likely that alterations in GM represent disturbance in neuronal development subsequent to WM injury. Volumetric segmentation of high-resolution T2- and T1-weighted images at term-equivalent age showed that preterm infants had reduced cortical and deep nuclear GM volumes compared to term-born controls (Inder et al., 1999b; Inder et al., 2005b). On neurodevelopmental follow-up at one year of age, infants with moderate to severe disability had significantly reduced cortical and deep nuclear GM volumes (Inder et al., 2005b).

Many of the common MRI findings in preterm infants are assumed to be the imaging correlates of neuropathological findings from autopsy studies. Only two studies have direct comparisons of *in vivo* MRI and subsequent postmortem examination, in part because the vast majority of infants survive. T1-signal hypointensities in WM indicated areas of cellular necrosis, while increased T1 signal represented hemorrhage (extreme hyperintensity) or hypercellularity (moderate hyperintensity)(Schouman-Claeys et al.,

1993). On T2-weighted imaging, recent hemorrhage was associated with low signal intensity, while older hemorrhage was shown by high signal intensity; regions of low T2 signal in the basal ganglia and thalami were consistent with neuronal abnormalities (Felderhoff-Mueser et al., 1999). Both of these studies indicated that areas of diffuse cellular changes such as gliosis or apoptosis might be missed or underestimated on conventional MRI. It is possible that these more subtle neuropathological WM abnormalities may be represented by the diffuse high T2 signal intensity that has been so commonly reported in recent MRI studies.

Nearly as soon as MRI was first used to image cerebral maturation *in vivo*, it was shown to be useful at predicting neurodevelopmental outcome. In an early paper describing normal stages of GM/WM differentiation in children less than three years old, developmentally delayed children reached each of these stages at a later age than children with normal neurodevelopment (Dietrich et al., 1988). This study was only the first of many to show that delayed myelination is associated with neurodevelopmental disability. Intraventricular hemorrhage associated with parenchymal involvement, punctate signal abnormality in periventricular WM, and abnormal signal in the PLIC on preterm or term-equivalent MRI were all predictive of cerebral palsy or other motor deficits (Aida et al., 1998; Valkama et al., 2000; Roelants-van Rijn et al., 2001). Moderate to severe MRI abnormalities at term-equivalent age, including T1 hyperintensities, ventriculomegaly, or severe IVH, have also been associated with abnormal cognitive development by 12 – 24 months. (Murphy et al., 2002; Miller et al., 2005; Bassan et al., 2006; Woodward et al., 2006). MRI findings in preterm infants, particularly at term-equivalent age, may be

useful to identify infants at high risk for poor neurodevelopmental outcomes and to guide them toward appropriate interventional therapies.

Diffusion imaging. DTI has many advantages over conventional MRI for assessing cerebral injury in the premature brain. Because it is quantitative, images can be evaluated not just for presence or absence, but *degree* of injury. Furthermore, DTI is more sensitive than conventional MRI for detecting subtle WM abnormalities (Inder et al., 1999a; Miller et al., 2002). As the improved sensitivity of DTI has been more widely recognized, and as technical barriers to acquire and process DTI data have been lowered, the use of diffusion imaging to evaluate cerebral injury in premature infants has increased dramatically within the past decade.

One of the first advantages of diffusion imaging to be recognized was that it could be used to detect acute WM injury earlier than conventional MRI or CUS. A case report of an infant born at 30 weeks gestation documented markedly restricted diffusion (i.e. decreased ADC) in the periventricular region at 5 days of age; T2-weighted MRI and CUS did not detect significant abnormality in this acute period (Inder et al., 1999a). When the scan was repeated at 10 weeks of age, the injury had evolved to cystic lesions, surrounded by WM with increased ADC. By 18 months of age, the infant had developed spastic quadriparesis and global developmental delay. The evolution of diffusion abnormalities in this premature infant was similar to those seen in term born infants with perinatal ischemic events, who showed decreased ADC in cerebral WM one day after injury, psuedonormalization by seven days and increased ADC after that (McKinstry et al., 2002). This case report showed that diffusion-weighted imaging could be used to evaluate injury in the premature brain on an acute physiological time scale.

Serial imaging of premature infants has shown that those with evidence of WM injury on an early conventional MRI scan (T1-weighted focal hyperintensities or areas of hypointensity representing cavitations in periventricular WM) had higher ADC and lower RA in WM at term-equivalent age compared to preterm infants with no evidence of WM injury on early MRI (Huppi et al., 2001; Miller et al., 2002). Infants with overt periventricular cystic or hemorrhagic lesions on MRI at term-equivalent age have higher WM ADC compared to preterm infants with normal WM; notably, diffuse high T2-signal intensity is also associated with higher ADC, even in the absence of overt focal lesions (Counsell et al., 2003). Extensive WM signal abnormalities, but not isolated focal lesions, are associated with higher ADC and lower anisotropy (Cheong et al., 2009). Finally, WM anisotropy at term-equivalent age appears to be related to gestational age at birth: preterm infants (born at 29 weeks or later) had lower anisotropy particularly in WM tracts at term-equivalent age compared to term-born control infants, with very preterm infants (born at less than 29 weeks gestation) having further significant reductions (Anjari et al., 2007; Rose et al., 2008). Higher ADC and lower RA in the WM of premature infants may represent delay in normal maturation, as suggested by comparison to term-born controls, or evolution of injury, as suggested by the association with conventional MRI signal abnormalities.

To understand whether one or both of these processes is involved, some studies have investigated whether decreased anisotropy is related to changes in radial or axial diffusivity. In theory, increased RA could be the result of increased radial diffusivity, decreased axial diffusivity, or disproportionate changes in both. Animal models have shown that dysmyelination is associated with increased radial diffusivity and no change

in axial diffusivity (Song et al., 2002; Song et al., 2005; Budde et al., 2007), while primary axonal disease or injury was associated with isolated decreases in axial diffusivity (Budde et al., 2007; Budde et al., 2009). Prematurely-born human infants have significantly higher radial diffusivity WM compared to term-born infants (Counsell et al., 2006). Preterm infants who have extensive WM signal abnormality on conventional MRI have yet higher radial diffusivity than preterm infants without signal abnormality (Cheong et al., 2009). The effects on axial diffusivity are less consistent. The alteration in radial diffusivity supports the hypothesis that dysmyelination is the primary WM injury in premature infants, consistent with many studies showing oligodendroglia to be the most vulnerable cell population in premature WM (Back et al., 2001; Back et al., 2002; Riddle et al., 2006) and a primary mediator of WM injury (Haynes et al., 2003; Billiards et al., 2008). Diffusion changes at term-equivalent age are therefore probably markers of WM injury, although diffusivity and anisotropy parameters are probably also influenced by delayed maturation.

Regional diffusion abnormalities have been identified in many studies, but the regions and type of diffusion abnormality (ADC, RA, axial and radial diffusivity) have not been entirely consistent (Huppi et al., 2001; Miller et al., 2002; Counsell et al., 2006; Anjari et al., 2007; Rose et al., 2008; Cheong et al., 2009). However, there are some general trends. Regions with higher ADC generally include unmyelinated hemispheric WM (frontal, occipital, centrum semiovale). Lower anisotropy, and the associated increase in radial diffusivity, has been found most consistently in WM tracts, including the PLIC, CC and to a lesser extent, the optic radiations. Notably, these are the regions identified as showing DTI evidence of myelination during the last few weeks of gestation

(Neil et al., 1998; Mukherjee et al., 2002; Partridge et al., 2004; Dubois et al., 2008a), supporting the theory that vulnerability of WM is maturationally-dependent.

Certainly diffusion abnormalities in any one WM region or tract do seem to be related to long-term neurodevelopmental outcomes. The PLIC in particular is an oft-studied region, perhaps because its early myelination makes it easy to delineate on diffusion parameter maps, and because abnormalities in its neurodevelopmental correlate – motor function – are detectable within months of birth. Decreased anisotropy in the PLIC at term-equivalent age or earlier is strongly associated with the development of cerebral palsy or other gait and motor disabilities by 18 months – 4 years of age(Arzoumanian et al., 2003; Drobyshevsky et al., 2007; Rose et al., 2007). Abnormalities in ADC may also be predictive of outcome. One study of preterm infants without overt WM pathology imaged at term-equivalent age found that increased ADC in the centrum semiovale was significantly correlated with lower developmental quotient (Krishnan et al., 2007). Diffusion imaging may therefore prove to have greater utility for predicting neurodevelopmental outcomes than conventional imaging because even subtle changes in ADC or RA may prove to have prognostic value.

Although diffusion abnormalities in WM suggest underlying microstructural and cellular alterations, the ideal comparison would be between diffusion imaging and histopathological analysis. Two studies have been able to do this analysis, despite the limited availability of premature brains for autopsy. In the first, conventional MRI and diffusion-weighted imaging was performed in an infant born prematurely (at 28 weeks gestation) and scanned at 39 days of life, shortly after cystic PVL was diagnosed by CUS (Roelants-van Rijn et al., 2001). Conventional MRI showed periventricular cysts and

extensive T2-weighted hyperintensity in surrounding WM, while DWI showed a large area of decreased ADC in the periventricular region, suggestive of a recent or evolving injury. A few days following imaging, postmortem examination revealed histopathological findings of extensive apoptosis, gliosis and cytotoxic edema in the periventricular WM, which corresponded well with the area of MRI abnormality (Roelants-van Rijn et al., 2001). The second study compared fetal diffusion weighted imaging with fetopathologic examination performed after medical termination of the pregnancies (Guimiot et al., 2008). Based on previously published normative values for ADC in fetuses, twelve fetuses had normal ADC, while nine had increased ADC. This delineation was supported by conventional MRI findings: all of the infants with increased ADC had T1 hypointensities and T2 hyperintensities, while only one of the twelve infants with normal ADC did. The ADC abnormality was highly associated with histopathological findings of vasogenic edema and astrogliosis, but not with microgliosis, or neuronal or oligodendroglial abnormalities. Both of these studies are extremely valuable because they clarify the histopathological correlates of ADC abnormalities. Unfortunately, neither study used DTI, and the assumption that anisotropy decreases in preterm infants reflect dysmyelination related to oligodendroglial injury remains unproven.

Significance of Premature Baboon Model

Advantages of the preterm baboon model. Animal models remain invaluable to understand the pathologic consequences of preterm birth and to evaluate putative

mechanisms of injury or develop neuroprotective therapies. Most animal models involve the deliberate introduction of an ischemic or, less commonly, an inflammatory insult, in recognition that these are the two upstream factors though to lead to preterm human injury. For example, the Rice- Vannucci model requires unilateral ligation of the carotid artery and exposure to hypoxia for several hours in seven-day-old rat pups (Rice et al., 1981). This model has been well characterized because it is inexpensive and reproducible, yet because the rat has a lissencephalic cortex and very little white matter, its brain development is less relevant to the human infant than that of a higher-order species. The ferret, which has a gyrencephalic cortex that folds postnatally, is a useful model to understand normal development (Barnette et al., 2009); but an injury model has yet to be fully developed. Recognizing that intrauterine ischemia due to placental insufficiency may play a large role in postnatal brain injury in the premature infant, other groups have developed fetal injury models in sheep (Rees et al., 1997) and guinea pigs (Nitsos and Rees, 1990). Compared to rodents, these animals have brains more anatomically similar to humans, and gestations on a time scale that allow for better translation to the timing of human gestation. By varying the timing of ischemic insults, cerebral injury has been shown to depend on the timing, duration and frequency of ischemia (Rees et al., 2008). Despite the value of each of these animal models, none is particularly relevant to the preterm human infant in a typical NICU.

The premature baboon model (Figure 1.4) provides a unique opportunity to understand cerebral injury in the premature human infant. The Southwest Foundation in San Antonio developed this model of premature delivery and neonatal care of baboon infants in the early 1990s to study bronchopulmonary dysplasia (BPD), a pulmonary

complication of premature birth. For the same reasons that this model was highly relevant to the investigation of BPD, it is unique among animal models used to understand the encephalopathy of prematurity. The baboon brain is anatomically and developmentally much more similar to the human than rodent, ovine or other non-primate models (Figure 1.5). In addition, unlike the animal models described above, the premature baboon model receives no direct insult to induce injury in the developing brain. Rather, baboon infants receive standard care in a neonatal intensive care unit (NICU). This relevance to the human premature infant provides motivation to evaluate cerebral development and injury in the premature baboon using both *in vivo* methods, such as electroencephalography (EEG), and *ex vivo* studies, including MRI and histopathology.

Normal development in preterm baboon model. An advantage of any preterm animal model is that it allows comparison of experimental animals to control animals with true normal cerebral development. As a primate, the baboon is a particularly valuable model for this purpose. High-resolution maps of T1 and T2 relaxation times were recently obtained in fetal baboons at 56 – 185 days gestation (term ~ 185 days) (Liu et al., 2008). A study of postnatal brain maturation obtained maps of T2 relaxation times in nine baboon infants from 1 – 30 months of age (Miot-Noirault et al., 1997). The maturation of GM and WM by changes in relaxation times was carefully evaluated in both cases, but these studies have little clinical relevance, as T1 and T2 maps are rarely obtained in human infants.

To characterize normal development in the premature baboon model, animals are delivered at a specific gestational age and euthanized immediately. Gestations are timed by characteristic maternal sex skin changes at conception. Establishing the gestational ages of equivalent brain development in baboon and human infants was accomplished by comparing the extent of cerebral gyration, cortical growth, astrocyte development and myelination (Dieni et al., 2004). At 125 days of gestation (dg) in the baboon, all six layers and major gyri of the cortex were present, and myelination had begun in the PLIC and deep nuclear GM; this was comparable to 26 – 28 weeks of human gestation. The baboon brain grew rapidly between 125 and 140 dg, and by the end of this period, mature myelin could be found in the PLIC and frontal and parietal hemispheric WM. The baboon at 140 dg is therefore equivalent to 32 – 34 weeks gestation in the human. From 140 to 160 dg, the brain grew more slowly overall, although cortical thickness increased significantly; the 160 dg baboon infant is therefore equivalent to the term human infant.

Preliminary investigation of these gestational control brains using *ex vivo* T1- and T2-weighted MR imaging revealed increasingly complex cortical gyration between 125 and 160 dg and decreasing GM/WM contrast with increasing gestational age, as is the case in human infants (Inder et al., 2005a). Diffusion imaging showed increasing anisotropy in the WM from 90 dg to term (185 dg); the PLIC and CC had particularly high anisotropy values, even by 140 dg (Inder et al., 2005a; Kroenke et al., 2005). In the cortex, anisotropy was high at 90 dg and decreased by 160 dg (Kroenke et al., 2005). The decrease in anisotropy varied regionally, occurring first and fastest in areas of the cortex nearest the lateral sulcus and precentral gyrus, and corresponded to increasing cortical thickness during this period (Kroenke et al., 2007). Maps of ADC showed

decreasing diffusion throughout the brain; WM/GM contrast was high at 90 dg and disappeared by term (185 dg) (Kroenke et al., 2005). Though diffusion changes in the cortex with increasing gestational age have been well characterized, a similar analysis remains to be done for WM, particularly as there is a selective vulnerability of cerebral WM in the premature infant. *The first goal of this study, therefore, was to more fully characterize normal WM development – particularly its DTI characteristics and histopathological correlates – in the premature baboon.*

Pattern of injury in preterm model and relevance to humans. Preliminary investigation of the premature baboon model revealed that the frequency and distribution of cerebral injury was very similar to that seen in human infants. The two most common cerebral injuries in the prematurely delivered baboon, as in humans, are WM damage and hemorrhage (Dieni et al., 2004). The variability in type and extent of histopathological WM injury closely mimicked descriptions of human PVL: diffuse astrocytosis (50% of baboon infants) and ventriculomegaly (25%) are common, while cystic damage is rare (6%). Isolated subarachnoid hemorrhage (38%) is more common than intraventricular hemorrhage (IVH) (6%). Some prematurely delivered baboons also show evidence of neuronal loss in the cortex and basal ganglia, though GM damage is much less common than WM injury (Dieni et al., 2004).

In studies of human infants, it is difficult to separate injury associated with *ex utero* development or therapeutic interventions from injury that either preceded or was the direct effect of premature labor and delivery. Because all animals in this baboon model are the result of uncomplicated pregnancies and elective deliveries, differences

between the brains of gestational controls and premature animals are likely due to the impact of the *ex utero* environment and/or therapeutic interventions. For this reason, studies with relatively small numbers of baboon infants have been able to show significant differences in cerebral histopathology attributable to different modes of ventilation (Loeliger et al., 2006; Loeliger et al., 2009a), inhaled nitric oxide administered to improve respiratory outcomes(Rees et al., 2007) or hemodynamic stabilization by closure of patent ductus arteriosus (Loeliger et al., 2009b; Loeliger et al., 2010). Differences in cerebral outcomes have not been comprehensively evaluated by MRI, despite the importance of imaging, particularly diffusion imaging, in evaluating cerebral integrity and predicting outcomes in human preterm infants. *The second goal of this study was to 1) identify the DTI characteristics of cerebral injury in the premature baboon and determine the histopathological correlates of DTI abnormality, and 2) evaluate the effect of a novel therapeutic agent, erythropoietin, on cerebral injury and development.*

Figures

Figure 1.1. (*A*) T2-weighted axial magnetic resonance image and (*B*) color-coded map of relative anisotropy in baboon brain at 90 days of gestation, equivalent to 18 – 20 weeks gestation in the human infant. The transient layers of the developing neocortex are visible in both images. From ventricular margin to pial surface, VZ: ventricular zone; SVZ: subventricular zone; IZ: intermediate zone; SP: subplate; and CP: cortical plate. Other landmarks include GE: ganglionic eminence; V: lateral ventricle; P: putamen; Th: thalamus. Colors in (*B*) indicate the principal orientation of water diffusion; red: medial-lateral diffusion; green: anterior-posterior diffusion; blue: superior-inferior diffusion.

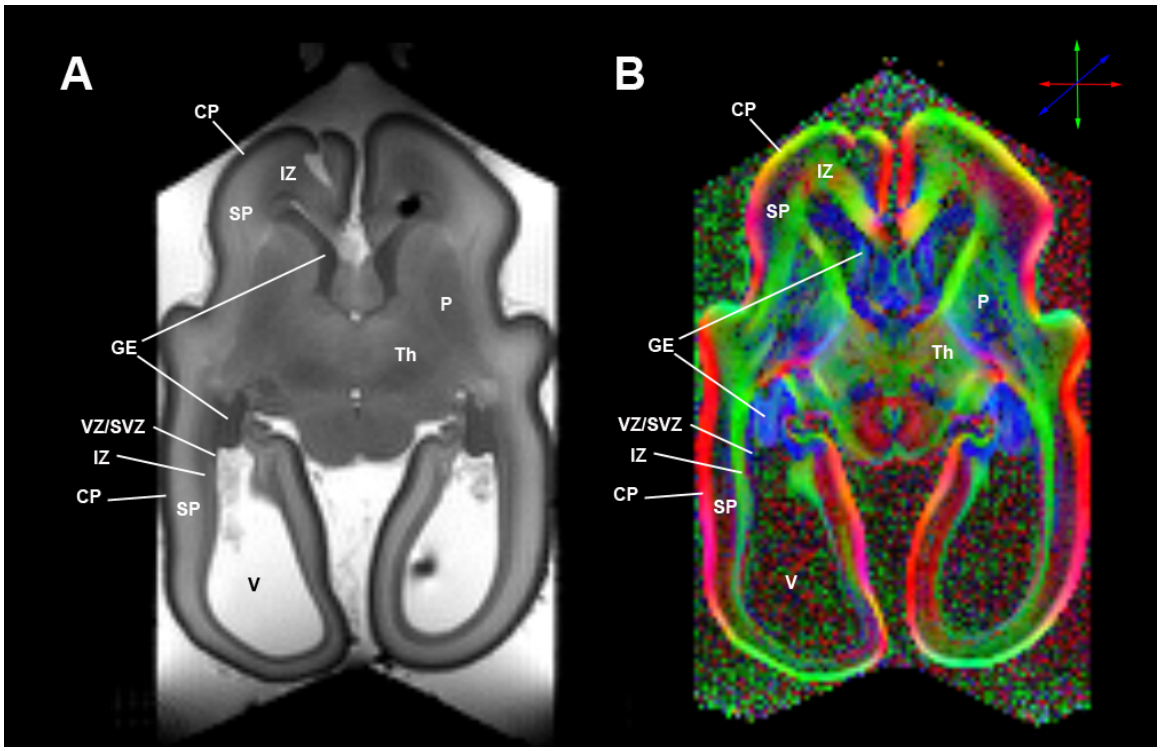

Figure 1.2. Schematic of the pathogenetic mechanisms of cerebral WM injury in preterm infants. Upstream mechanisms, namely inflammation and ischemia, induce the activation of microglia. Microglia in turn release cytokines and free oxygen and nitrogen radicals that damage pre-oligodendrocytes (pre-OLs), the primary cellular target of WM injury. Inflammation and ischemia also cause an increase in extracellular glutamate, by inducing its release from axons and activated microglia, which causes receptor-mediated excitotoxicity in pre-OLs. Both excitotoxicity and oxidative/nitrosative damage induce necrosis of pre-OLs.

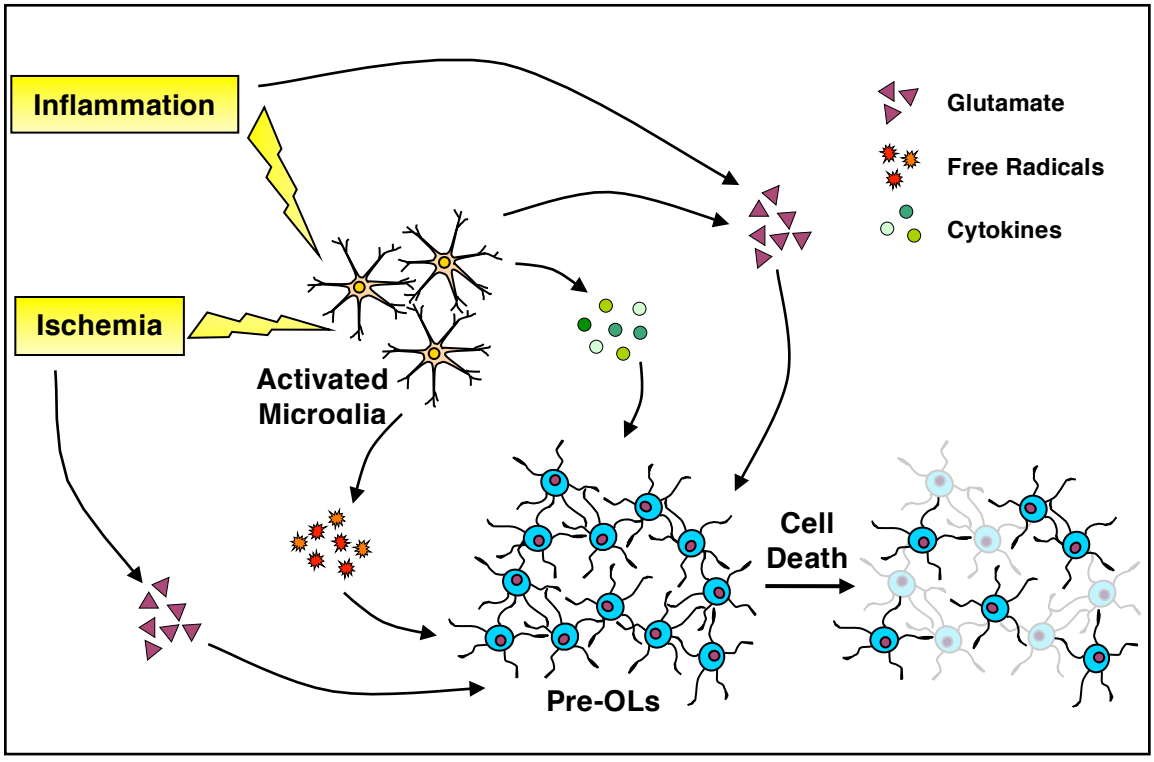

Figure 1.3. Common MRI abnormalities in preterm human infants at term-equivalent postmenstrual age. (*A*) T2-weighted axial MRI of infant with no WM abnormality. (*B*) Infant with many moderate to severe abnormalities, including germinal matrix hemorrhage extending into the deep nuclear gray matter (*white arrowhead*), ventricular dilatation (*black arrow*) and WM volume loss (*long white arrow*). (*C*) Infant with diffuse WM signal changes in the periventricular region (*black arrowheads*).

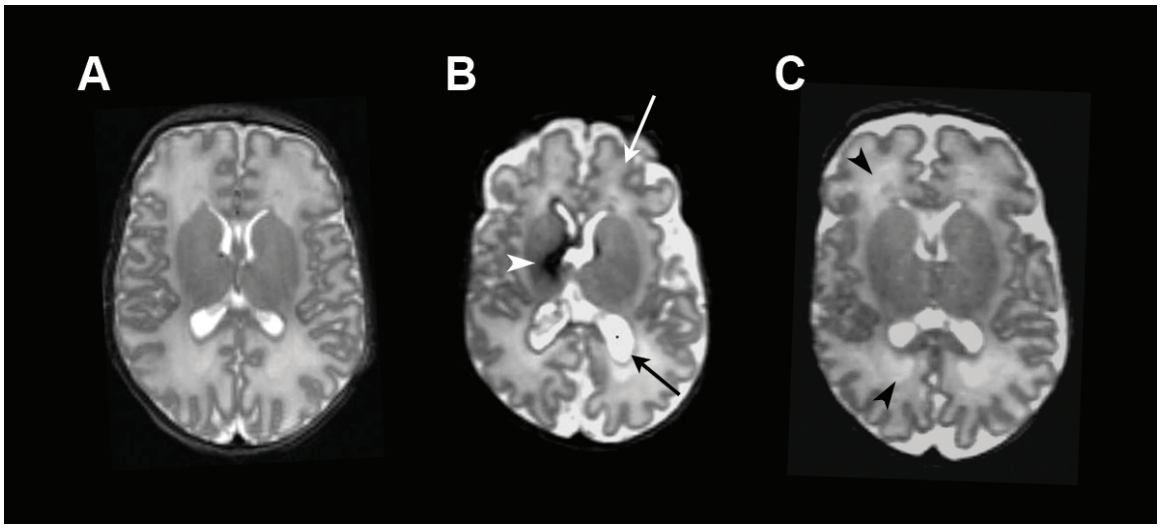

Figure 1.4. Schematic depicting the timing of events in the premature baboon model. Baboons are delivered at 125 days of gestation, equivalent to 26 – 28 weeks human gestation, and treated in an animal intensive care unit for 14 or 28 days prior to sacrifice.

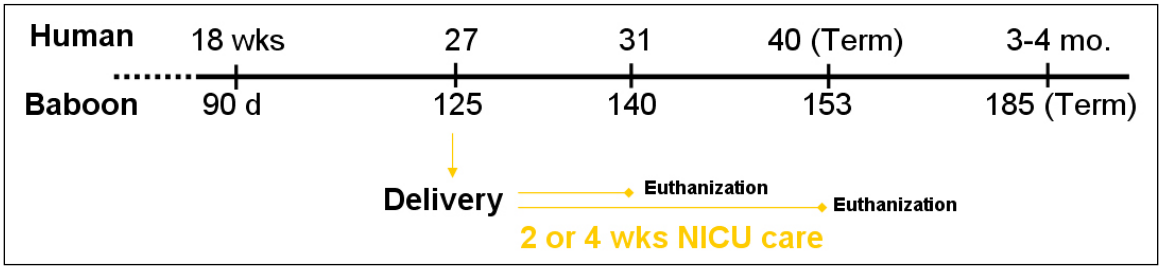

Figure 1.5. Representative axial slices of *ex vivo* T2-weighted MRI of baboon brains from three points in gestation (*top row*) and T2-weighted MRI in live premature human infants at equivalent development (*bottom row*). Baboons were delivered and euthanized at 125 (*A*), 140 (*B*) or 153 (*C*) days of gestation. Live human premature infants were imaged at 28 (*D*), 32 (*E*) and 37 (*F*) weeks postmenstrual age (images not to scale). Note the similarities in cortical gyration, WM volume and signal characteristics of cortex, WM and deep nuclear gray matter in each pair (*A* – *D*; *B* – *E*; *C* – *F*).

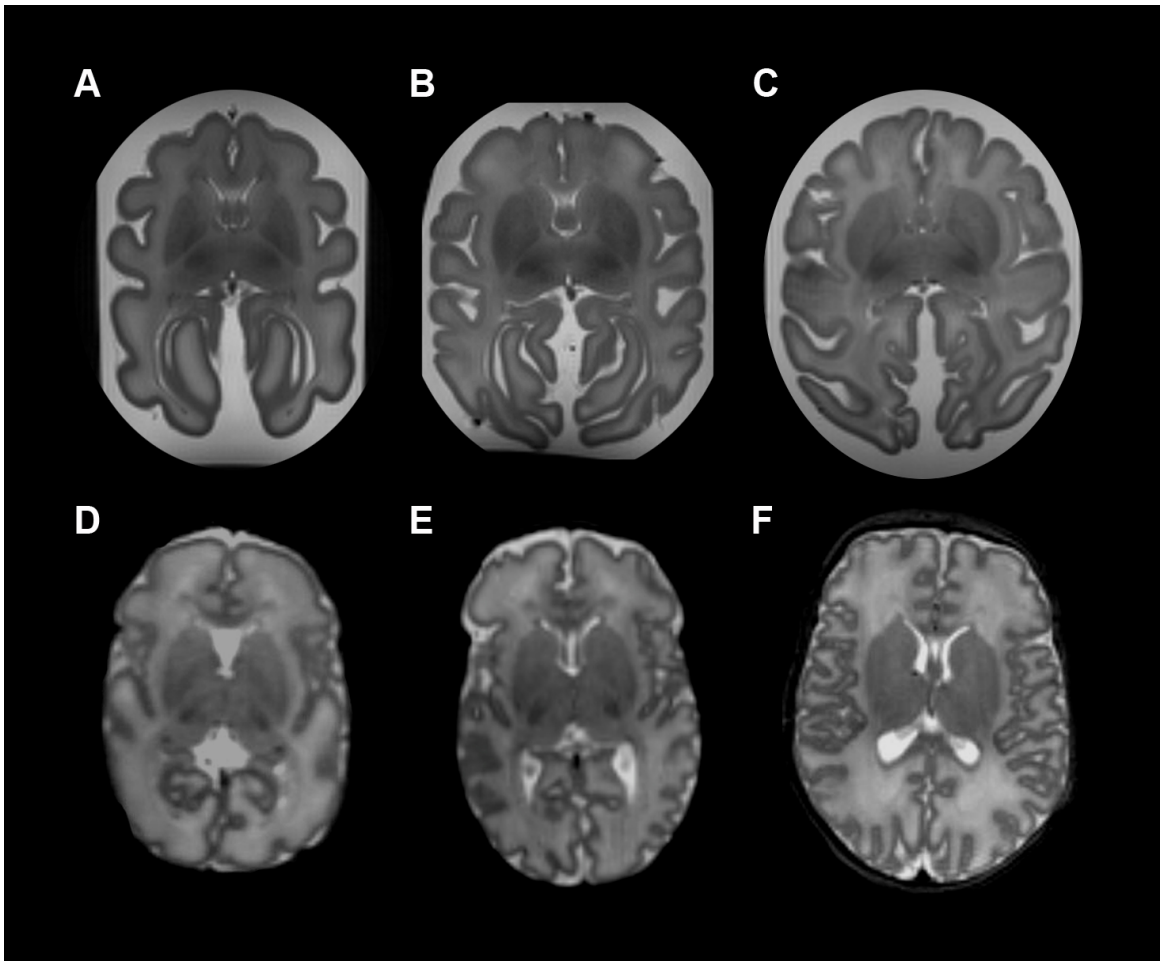

Chapter 2

Normal Growth and White Matter Development in the Preterm Baboon Brain

Abstract

Normal cerebral development during gestation has typically been characterized using neuropathology spontaneously aborted fetuses or magnetic resonance imaging (MRI) in premature infants. Despite efforts to exclude infants with cerebral abnormalities from these analyses, it is not clear that the study populations represent true normal development. We aimed to characterize normal cerebral development, paying particular attention to white matter (WM) maturation, in the preterm baboon brain. Baboons were delivered by elective hysterotomy at five time points during gestation or delivered naturally at term (~185 days gestation, dg). Cerebral WM maturation was evaluated using MRI, diffusion tensor imaging (DTI) and histopathology. Between 90 and 185 dg, WM maturation was associated with decreasing T1 and T2 MR relaxation times; increasing diffusion anisotropy and decreasing apparent diffusion coefficient (ADC); and increasing density of oligodendrocytes and myelinated fibers. Diffusion changes in WM generally were seen earlier in gestation than MRI or histopathology. WM maturation occurred first in the internal capsule, followed by the optic radiations, corpus callosum, centrum semiovale and parietal WM, while frontal and occipital WM appeared to mature latest. Overall, the pattern of WM maturation on MRI, DTI and histology paralleled that in humans, indicating that the preterm baboon is a reasonable model of human cerebral development during gestation.

Introduction

Characterizing normal cerebral development during gestation in humans has long been a challenge. Some of the most complete descriptions have come from autopsy studies of dozens of specimens, usually fetuses delivered after spontaneous abortions or premature infants with accidental or non-neurological causes of death. Due to the difficulty of obtaining large numbers of specimens, comprehensive descriptions of normal development are limited to a handful of studies, which are valuable for their detailed and systematic analyses (Gilles et al., 1983; Brody et al., 1987; Kinney et al., 1988). To evaluate only normal development, specimens were generally excluded from these autopsy studies if there was evidence of major neurological impairment or disease. Still, spontaneously aborted fetuses or premature infants may have subtle cerebral injury or delay from compromised intrauterine environment and/or acute perinatal events associated with premature delivery. Therefore, there is no way to be certain that these brains represent "normal" development.

Magnetic resonance imaging (MRI) can be used on live human infants and is therefore more clinically relevant than neuropathological analyses. Changes in MRI characteristics from 24 weeks postmenstrual age through the first postnatal year relate to changes in brain tissue water content and tissue microstructure (McArdle et al., 1987b; Barkovich et al., 1988; Dietrich et al., 1988; Childs et al., 2001; Paus et al., 2001). Diffusion tensor imaging (DTI), in which contrast depends on small (~10 μm) displacements of water, has been used to quantify these microstructural changes in cerebral development (Neil et al., 1998; McKinstry et al., 2002; Mukherjee et al., 2002;

Partridge et al., 2004; Provenzale et al., 2007; Dubois et al., 2008a). To characterize normal development during gestation, MRI and DTI studies have studied populations of "healthy" preterm infants, which generally include infants born before 37 weeks gestation who are the products of otherwise unremarkable pregnancies and who have normal neurologic examinations at the time of imaging. Despite this effort to screen for relatively healthy premature infants, the effects of preterm birth and the intensive care environment on the brain cannot be separated from those of normal development.

Ideally, normal brain development during gestation could be described by fetal imaging. Fetal MRI studies have described normal brain development from the eighteenth gestational week to term (Righini et al., 2003; Bui et al., 2006; Prayer et al., 2006). Although these studies provide valuable insights about brain development during the second half of gestation, they are often limited by image quality. Because of the tendency for fetal movement, imaging protocols use fast acquisition sequences, which can be more susceptible to image artifacts (Prayer et al., 2006; Liu et al., 2008). In addition, image resolution is often lower in these scans because the radiofrequency coil used to send and receive the MR signal must fit around the mother's abdomen rather than around the infant's head, as in studies of premature infants. Improved image quality offers better characterization of anatomical and microstructural changes in the developing brain.

The premature baboon (*Papio papio)* model provides a unique opportunity to characterize normal cerebral development. This model is highly relevant because the premature baboon has cerebral anatomy and development that are very similar to that of the human preterm infant (Dieni et al., 2004). Baboon infants delivered prematurely at

five time points during gestation (90, 125, 140, 160 and 175 days of gestation, dg) or delivered naturally at term (~ 185 dg) were available for *ex vivo* MRI and histology. The ontogeny of the forebrain was previously described (Dieni et al., 2004) and used to define equivalent stages of brain development in the baboon and human (Table 2.1). Cortical development in the baboon was also previously described in detail (Kroenke et al., 2007). In the present study, we characterize normal development of cerebral white matter in the preterm baboon using MRI and DTI and compare imaging findings with histological markers of maturation.

Methods

Tissue Collection. Animal studies were performed at the Southwest Foundation for Biomedical Research, San Antonio, TX. All handling and procedures conformed to American Association for Accreditation of Laboratory Animal Care guidelines. Baboons (*Papio* sp.) were delivered by cesarean section and elective hysterotomy under general anesthesia at 90 (n = 5), 125 (n = 10), 140 (n = 11), 160 (n = 3) and 175 (n = 3) days of gestation (dg). Nine animals were delivered at term (185 ± 2 dg) by natural delivery. Timed gestations were determined by observing characteristic sex skin changes and confirmed by serial fetal ultrasound examinations. Except for those delivered at 90 dg, baboons received prenatal steroids (6 mg betamethasone or dexamethasone injected intramuscularly into pregnant baboon dams) at 123 and 124 dg. Baboon infants were euthanized immediately after delivery with sodium pentobarbitone (130 mg/kg, intravenously). Brains were extracted and immediately immersed in buffered fixative:

10% formalin (necropsies performed before 2004; in this study, the three 90d controls) or 4% buffered paraformaldehyde (necropsies 2005 and later).

Magnetic resonance imaging. Imaging studies were performed at Washington University in St Louis. Twenty-four brains were available for MRI: 90 dg, *n* = 3; 125 dg, *n* = 6; 140 dg, *n* = 6; 175 dg, *n* = 3; and term, *n* = 6. Imaging was performed using a 15-cm inner bore diameter, 4.7-tesla Oxford Instruments (Oxford, UK) magnet controlled by a Varian NMR Systems (Palo Alto, CA) console. All brains were placed in sealed cylindrical containers containing fixative; each gestational age required a container of different diameter. Medium-sized brains (125 and 140 dg) were imaged using a 6.3-cm inner diameter RF birdcage volume coil (Varian, Palo Alto, CA). Smaller (90 dg) and larger (175 and 185 dg) brains were imaged using custom-built inductively-coupled volume coils appropriate for the container size.

T1- and T2-weighted imaging. T2-weighted images were acquired using a spin-echo pulse sequence. T1-weighted images were acquired using a modified driven equilibrium Fourier transform (MDEFT) sequence. Because imperfections in slice-selection excitation profiles can cause signal loss, slices were acquired in an interleaved pattern. For all T1- and T2-weighted scans, the number of signal averages was 12. Depending on the number of slices, scan time was 75 – 120 min for T1-weighted images and 3 h – 5 h 30 min for T2-weighted images.

In order to optimize image contrast, it is useful to know the T1 and T2 relaxation time constants of the sample. In the baboon, as in humans, these time constants decrease

during gestation, and they decrease at different rates in gray matter (GM) and white matter (WM) (Liu et al., 2008). Therefore T1 and T2 maps were calculated for each gestational age. For the T2 map, a spin-echo image was acquired at TE = 20, 40, 60, 80, 100, 120, 140, 160, 180, 200, 500, and 1000 ms; TR = 5000 ms for all. For the T1 map, a spin-echo inversion recovery sequence was used with TI = 50, 100, 200, 600, 1000, 1400, 1800, 2200, 2600, 3000, 4000, and 5000 ms; actual recovery time (TR – TI) was 5000 ms and TE was 16.98 ms for all scans. Maps were calculated in Matlab (MathWorks, Natick, MA) by curve fitting on a voxel-by-voxel basis the T1- or T2-weighted images obtained at different values of TI or TE:

$$\text{T1 map:} \quad S = M_0(1 - 2e^{-TI/T1})$$

$$\text{T2 map:} \quad S = M_0(e^{-TE/T2})$$

T1 and T2 values of WM are presented in Table 2.2; GM values are also shown for comparison.

For T2-weighted images, TE was set to ½ ($T2_{GM}$ + $T2_{WM}$) to optimize the contrast-to-noise ratio, and TR > 3 x T1 so that T1 contrast was minimized. For T1-weighted images, TE and TR were short to maximize T1 contrast. TI was set to approximately ½ x T1. At 175 and 185 dg, T1 and T2 relaxation time constants in WM and GM were very similar (Table 2.2); this is comparable to the isointense period of brain development in humans during the first postnatal year (Dietrich et al., 1988). For the brains from these later periods of gestation, therefore, optimal image acquisition parameters were determined empirically. Scan parameters used to image brains at each gestational age are shown in Table 2.3.

The size of the brain increases dramatically over the course of gestation – at term, brain weight is nearly ten times that of the 90d brain – necessitating the use of different coils, as mentioned above. The voxel size chosen for each gestational age required trade-offs among desired image resolution, signal-to-noise ratio of the coil used, and overall scan time. To ensure the best comparison between diffusion and conventional images, the FOV, voxel dimensions, and slice positions were identical for T1-weighted, T2-weighted, and diffusion images. These parameters are listed in Table 2.3.

Brain Metrics. Simple quantitative brain metrics measured on MRI can be used to describe the range of variability in normal brain development (Garel, 2004). These metrics include fronto-occipital distance (FOD), length of the corpus callosum (LCC), bifrontal (BFD) and biparietal (BPD) distance, width of the basal ganglia (WBG), lateral ventricular width (LVD) and transverse cerebellar distance (TCD) (Figure 2.1). Brain weight was also measured at the time of imaging.

Diffusion Tensor Imaging. Because diffusion measurements are sensitive to temperature, T1- and T2-weighted imaging were always performed prior to diffusion imaging to allow samples stored in the fridge (4°C) to equilibrate to magnet bore temperature (~18°C). Diffusion data were acquired using a spin-echo pulse sequence modified by the addition of a diffusion-sensitization gradient pulse pair of duration δ of 11.5 ms, interpulse interval Δ of 50 ms, and magnitude G ranging from 3 – 25 Gauss/cm. Diffusion anisotropy was measured using a 25-direction, icosahedral sampling scheme that has been described previously (Kroenke et al., 2007). Each b value was unique in

both direction and amplitude, with amplitudes ranging from 187 – 11,300 sec/mm^2. All diffusion scans used TE of 70 ms; TR varied from 4700 – 6650 ms, depending on the number of slices in the image. As with T1- and T2-weighted imaging, slices were acquired in an interleaved pattern. Because inhomogeneities in the static magnetic field at high field strength can lead to signal loss in diffusion images, diffusion data were acquired in two blocks, each with two signal averages: a "positive" set of gradient pulse pairs, with vectors and magnitudes as described above, and a "negative" set, in which gradient vectors had the opposite direction but equal magnitudes to the positive set. These two sets were averaged during data processing, so that the effective number of signal averages was four. Total scan time for diffusion-weighted image acquisition varied from 18 – 24 h.

Raw diffusion data were phase-corrected using linear and non-linear methods of Bayesian probability analysis (Bretthorst, 2008a, b) so that background experimental noise was Gaussian with a mean value of zero. Diffusion tensor parameters were then estimated from the 25 signal amplitudes for each voxel using the modified DTI model selection algorithm and Bayesian probability analysis previously described (Kroenke et al., 2006). These parameters include the apparent diffusion coefficient (ADC), relative anisotropy (RA), axial diffusivity and radial diffusivity (Figure 2.2). Using Analyze v7.0 software (Rochester, MN), regions of interest were drawn manually on horizontal slices in frontal, parietal and occipital white matter, in the centrum semiovale, and in white matter tracts, including the corpus callosum (CC), the optic radiations (OR) and the anterior and posterior limbs of the internal capsule (ALIC, PLIC).

Histology. Histology was performed at the University of Melbourne, Australia. Seventeen brains were available for histological analysis: 90 dg, $n = 2$; 125 dg, $n = 4$; 140 dg, $n = 5$; 160 dg, $n = 3$; and term, $n = 3$. Five-millimeter coronal blocks from the right forebrain were processed to paraffin, and ten 8-μm sections were cut from the rostral surface of each block. Slices from three sections – (1) frontal, through the frontal horn of the lateral ventricle; (2) mid-parietal, at the level of the dentate gyrus and lateral geniculate nucleus; and (3) occipital, through the occipital horn of the lateral ventricle – were compared across gestational ages. To assess overall cerebral maturation, sections were stained with hematoxylin and eosin. To assess WM myelination, sections were stained with rat anti-bovine myelin basic protein (MBP, 1:100; Chemicon, USA).

Results

Conventional MRI. T1 and T2 relaxation times of GM and WM generally decreased during gestation, with the exception of T1 in GM, in which no clear trend was observed (Table 2.2). At each gestational age, T1 and T2 relaxation times in GM were shorter than those in WM. T2 maps are shown in Figure 2.3.

Brain weight increased linearly from 90 – 185 dg (Figure 2.4). The WBG and TCD also increased linearly with gestation (Figure 2.4). In contrast, measures of cerebral growth (FOD, BFD, BPD and LCC) increased non-linearly with gestation, with more rapid growth from 90 – 140 dg. The lateral ventricle was largest at 90 dg and decreased by half by 125 dg. Examples of T1- and T2-weighted images from which these metrics were derived are shown in Figure 2.5.

Evidence of myelination (WM with hypointense T2-signal) was first seen in the PLIC, appearing in some, but not all, of the 140 dg brains. By 175 dg, myelination in both limbs of the internal capsule, the OR and the centrum semiovale was visible. Myelinated WM also appears in parietal WM by 185 dg. There was no evidence of myelination in the frontal WM, occipital WM or CC.

DTI. Changes in WM diffusion with cerebral maturation can be appreciated qualitatively on ADC and RA maps (Figure 2.6), and on color-coded maps representing the principal orientation of water diffusion (Figure 2.7). Values of RA (Figure 2.8), ADC (Figure 2.9), axial diffusivity (Figure 2.10) and radial diffusivity (Figure 2.11) at each gestational age are represented graphically.

At 90 dg, WM anisotropy is generally low; however, even at this early time-point, the internal capsule and the corpus callosum are visible on RA maps. By 125 dg, anisotropy appears to have decreased in the ALIC and CC, and increased in the OR; no change was seen in the PLIC. Anisotropy in these four regions increases from 125 to 185 dg. Anisotropy in the centrum semiovale, frontal, parietal and occipital WM does not substantially increase until after 140 dg. ADC values decrease steeply in all WM regions from 90 – 140 dg; in most regions, WM ADC decreases little if at all after 140 dg. Notable exceptions are the ALIC and CC, in which ADC increases from 140 – 185 dg. Axial and radial diffusivity are generally highest at 90 dg in all WM regions. From 140 – 185 dg, axial diffusivity increases in the CC, ALIC, and to a lesser extent, in the OR and PLIC. During this same time period, axial diffusivity decreases in parietal and occipital WM and stays more or less the same in frontal WM and centrum semiovale. Radial

diffusivity decreases from 125 – 185 dg in all brains, but more steeply in OR, parietal WM, occipital WM and centrum semiovale than in other WM regions.

Histology. H&E staining revealed a substantial increase in gyration and sulcation during gestation (Figure 2.12). An increase in WM volume is also notable. The density of oligodendrocytes and myelinated fibers also increased with gestational age (Figure 2.13). At 90 dg, only a few sparsely distributed MBP-positive oligodendrocytes were present. By 125 dg, MBP-positive oligodendrocytes, along with a few sparse myelinated fibers, were present in the IC and OR. By 140 dg, the density of oligodendrocytes and myelinated fibers was substantially increased in the PLIC and OR, and a few fibers were visible in parietal WM and centrum semiovale. The first myelinated fibers appeared in the CC by 160 dg. In frontal, parietal and occipital regions, oligodendrocyte and myelinated fiber density increased in deep WM before subcortical WM. By 185 dg, the IC, OR and centrum semiovale had the greatest fiber density, and at least some myelinated fibers were present in all WM regions.

Discussion

In this study, we have described normal cerebral growth and WM development in the baboon during gestation. Although this data represents discrete gestational time points, rather than a continuous sampling across gestation, we have characterized cerebral development in several animals at each gestational time-point, which provides a unique description of the variation in cerebral development during normal gestation. There

appeared to be more variation in diffusion values than in cerebral growth metrics; the most variation was seen at 90 dg (Figures 2.4, 2.8 – 2.11). This suggests that early maturation is associated with more variation in tissue microstructure.

T1 and T2 relaxation times. T1 and T2 relaxation times in fixed baboon brains were ~ 50% shorter in both WM and GM than in a fetal baboon imaging study at equivalent gestational ages (Liu et al., 2008). This difference can be attributed to the effects of fixing the brain in 4% paraformaldehyde (Shepherd et al., 2009). Although the absolute relaxation times were shorter in fixed brains, the relative pattern was the same as in live infants: T2 times were generally shorter than T1 times, and GM relaxation times were shorter than those in WM. In addition, the T2 relaxation time in GM and WM and the T1 relaxation time in WM generally decreased with increasing gestational age. T1 and T2 times in WM and GM decrease with increasing postmenstrual age in human premature infants (Paus et al., 2001). Similarly, relaxation times decrease in fetal baboons from 56 dg to term (185 dg) (Liu et al., 2008). Decreasing water content of the immature brain, increasing lipid content of myelinated fibers and increasing organization of axons all contribute to shorter relaxation times (Neil and Inder, 2004). T1 times in GM did not show a clear trend across gestational ages. T1-weighted images also failed to show any evidence of myelination (T1 signal hyperintensity) at 175 and 185 dg, even though myelination was present on T2-weighted imaging. In human infants, evidence of myelination appears on T1-weighted images before T2-weighted images (Barkovich et al., 1988). This suggests that our T1 maps and T1-weighted images probably reflect tissue properties other than T1-weighting alone.

Maturation of WM regions. Overall, the sequence of myelination in the preterm baboon demonstrated by our MRI and DTI data paralleled descriptions in human infants. The first tract to show myelination on conventional T2- or T1-weighted images is the PLIC at term gestation (equivalent to the 153 dg baboon), soon followed by the OR (McArdle et al., 1987b; Barkovich et al., 1988; Dietrich et al., 1988; Childs et al., 2001). The ALIC and centrum semiovale show myelination on T1- or T2-weighted MRI during the first few months of life, with other regions – frontal WM, occipital WM and CC – becoming myelinated within the first year (Barkovich et al., 1988; Dietrich et al., 1988; Paus et al., 2001). Accordingly, the PLIC was the first cerebral region to appear myelinated, around 140 dg in the baboons, while term or near-term baboons, equivalent to human infants in the first few post-natal months, showed T2-weighted evidence of myelination in many WM regions. The regional sequence of diffusion changes also parallels that described in many diffusion imaging studies in human infants (Neil et al., 1998; McKinstry et al., 2002; Mukherjee et al., 2002; Partridge et al., 2004; Provenzale et al., 2007; Dubois et al., 2008a). In our baboons, as in these human studies, WM anisotropy increased in all WM regions during gestation, but RA in IC, CC and OR was much higher, indicating advanced progression of maturation, than in the frontal, parietal and occipital WM.

Relative timing of WM maturation and brain development. We were surprised to see an early decrease in RA in some WM regions. From 90 – 125 dg, RA decreased in the ALIC, CC and parietal WM, but stayed approximately the same in other regions. At the same time, there was generally a steep decrease in ADC, axial and radial

diffusivity. Other studies of WM diffusion in humans have not previously reported similar early diffusion changes, probably because the human developmental equivalent of the 90 dg baboon is ~ 18 – 20 weeks gestation, which is much earlier than the limit of viability of prematurely-born infants.

The early decrease in RA may reflect the early tangential migration of neurons and glia through immature WM during mid-gestation. Axial diffusivity is high at 90 dg, perhaps reflecting water diffusion along axons that guide migrating neurons; as migration is completed and WM fibers proliferate, axial diffusivity, and thus RA, would decrease. The migration of neurons peaks during the third to fifth month of gestation and is complete during the third trimester in humans (Gressens, 2000; Bystron et al., 2008). Translated to baboons, this would be equivalent to peak migration around 90 dg, and completion of migration between 125 and 140 dg. The increase in cellular density that results from migration probably corresponds to the decrease in ADC in the baboons before 125 dg. The peak migration and proliferation of cells would also correspond with a substantial increase in cerebral size. Indeed, more cerebral growth occurred before 140 dg in the preterm baboon than from 140 – 185 dg as shown by changes in BFD, BPD, FOD and LCC (Figure 2.4).

After 125 dg, our baboon findings paralleled DTI studies in human preterm infants. WM RA increased, with greater changes from 140 – 185 dg in most regions than before 140 dg. Axial diffusivity increased greatly after 140 dg, particularly in the ALIC, PLIC, CC, OR and centrum semiovale. In contrast, radial diffusivity decreased in these regions. The changes in axial and radial diffusivity generally offset each other, so that ADC decreased little if at all after 125 dg in most regions. The increased ADC in the

ALIC and CC seems to reflect the exceptionally large increase in axial diffusivity after 140 dg.

In some WM regions, increases in RA preceded MRI or histological evidence of myelination. For example, between 125 and 140 dg, RA increased in ALIC, PLIC, OR, frontal WM, parietal WM and centrum semiovale. Yet by 140 dg, the PLIC showed T2 evidence of myelination in only a few of the brains, and MBP-positive fibers were seen only in the PLIC and OR. Notably, the CC had among the highest values of RA throughout gestation, yet histological evidence of myelination did not appear until 160 dg, and even by 185 dg, there was no T2-weighted evidence of myelination. Part of the reason for this is that diffusion imaging is sensitive to the premyelinating phase of WM maturation, characterized by axonal changes – organization of axons into tight bundles, increasing axon caliber, proliferation of microtubule-associated proteins, increasing conduction velocity and Na^+/K^+-ATPase activity in axonal membranes – and an increase in the number of immature oligodendrocytes (Wimberger et al., 1995; Drobyshevsky et al., 2005). However, for a given WM tract, the steepest increase in anisotropy was associated with the greatest change in density of MBP-positive fibers. Comparison of RA maps and MBP immunostaining (Figure 2.14) shows the parallel in WM changes with maturation. As WM fibers are myelinated, the myelin membranes hinder water diffusion perpendicular to the axons, but diffusion parallel to axons changes little; the disproportionate change in radial and axial diffusivity are associated with an increase in RA (Beaulieu, 2002). Accordingly, in our baboon data, peak myelination in the PLIC occurred from 140 – 185 dg (Figure 2.13). During this time, there was little change in axial diffusivity (Figure 2.10) and a decrease in radial diffusivity (Figure 2.11). This

example represents a trend in our baboon data: the density of MBP-positive fibers parallels RA but not ADC values. Therefore, although both diffusion parameters are sensitive to WM maturation, they reflect different microstructural aspects of that process, as has been noted previously (Neil et al., 2002). In our baboon data, RA increases associated with WM maturation occurred later in gestation than decreases in ADC.

Evidence of myelination described by MBP-positive immunostaining is only one method to assess cerebral WM maturation. Other histological markers can and have been used to assess myelination – Black-Gold (Dieni et al., 2004), Luxol Fast Blue (Brody et al., 1987) or Loyez stain (Gilles et al., 1983). Though the sequence of WM maturation is generally the same across studies, the timing of myelination described varies by as much as 20 weeks of gestation (Brody et al., 1987). One advantage of immunohistochemical techniques (such as anti-MBP) or high-resolution Black-Gold staining is that individual fibers can be identified (Dieni et al., 2004), which may explain why studies employing these techniques consistently describe the appearance of mature myelin several weeks earlier in gestation than studies utilizing less sensitive stains such as Luxol Fast Blue.

Effects of fixation. Caution must be exercised when comparing diffusion values in the fixed baboon brain to those in live human infants. RA values are unchanged by fixation, whereas ADC, axial diffusivity and radial diffusivity are ~30% lower (Sun et al., 2003). Therefore, the values of RA in live and fixed tissue can be compared directly. In live tissue, changes in ADC can represent differences in tissue microstructure or acute physiological changes. In fixed tissue, alterations in ADC reflect only the changes in tissue microstructure (Sun et al., 2005). In the present study of normal development, we

are primarily interested in characterizing the decrease in ADC that results from increasing tissue density and organization. It is still worth noting that, however similar the premature baboon brain might be to the human brain, the ADC, axial and radial diffusivity values presented here cannot be applied to live premature human infants.

Another caveat is that the gestational control animals were delivered and sacrificed over a six-year period (2001 – 2007). Differences in fixation time or type of fixative (4% paraformaldehyde or 10% formalin) may lead to differences in MR signal characteristics and the reliability of immunohistochemistry. There appeared to be no relationship between duration of fixation and diffusion or histological characteristics in this or a previous study of the fixed preterm baboon brain (Kroenke et al., 2007).

Conclusion

This descriptive study provides a unique understanding of the maturation of cerebral WM in the primate brain. The window of development described here is much wider than that of most studies of live preterm infants, for whom the limit of viability is approximately 22 – 24 weeks gestation. Furthermore, the WM diffusion imaging and histological characteristics in these baboons with timed gestations are more representative of the normal variation in cerebral development than populations of live premature infants or autopsy specimens. The results of this descriptive study demonstrate that the preterm baboon model is highly relevant to the human infant. In addition, this description of normal development provides a baseline for comparison of preterm baboons treated for two or four weeks with standard neonatal care (Chapter 3 – 6).

Figures & Tables

Table 2.1. Baboon gestational ages and the corresponding human ages at which cerebral development is equivalent. Adapted in part from Dieni et al., 2004.

Baboon gestational age	Equivalent human development
90 dg	18 – 20 wks gestation
125 dg	26 – 28 wks gestation
140 dg	32 – 34 wks gestation
160 dg	Term (~40 wks)
175 dg	1 – 2 mo postnatal
Term (~ 185 dg)	3 – 4 mo postnatal

Table 2.2. T1 and T2 relaxation times of cerebral gray matter (GM) and white matter (WM) at each gestational age. Values listed are averages from two or more regions in each tissue type.

Baboon gestational age	T1 GM	T1 WM	T2 GM	T2 WM
90 dg	500 ms	1200 ms	120 ms	190 ms
125 dg	780 ms	1100 ms	110 ms	180 ms
140 dg	1100 ms	1400 ms	90 ms	140 ms
175 dg	600 ms	750 ms	60 ms	70 ms
185 dg	530 ms	650 ms	60 ms	70 ms

Table 2.3. Scan parameters used at each gestational age. For T2-weighted images, TR values ranged from 5 – 12 s, depending on the number of slices required. For T1-weighted images, TR was automatically set equal to 2 x TI, due to the timing requirements of our multi-slice MDEFT sequence.

Baboon gestational age	Voxel size (mm)	Field of View (mm) (matrix: 256 x 128)	TE (ms) in T2-w images	TI (ms) in T1-w images
90 dg	0.3 x 0.3 x 0.3	76.8 x 38.4	160	800
125 dg	0.5 x 0.5 x 0.5	128 x 64	160	700
140 dg	0.5 x 0.5 x 0.5	128 x 64	110	600
175 dg	0.7 x 0.7 x 0.7	179.2 x 89.6	100	550
185 dg	0.8 x 0.8 x 0.8	204.8 x 102.4	90	500

Figure 2.1. Brain metrics on coronal T2-weighted (*A – C*) or sagittal T1-weighted (*D & E*) MR images of the brain. Bifrontal distance (BFD) was measured on coronal slice just anterior to the lateral ventricles (A). Biparietal distance (BPD) and width of the basal ganglia (WBG) were measured at the level of the temporal horn of the lateral ventricles (*B*). The maximum transcerebellar distance (TCD) on any coronal slice (*C*) and maximum fronto-occipital distance on any sagittal slice (*D*) were also measured. The trace length of the corpus callosum (LCC) was measured on a mid-sagittal section (*E*). The widths of the left and right lateral ventricles were measured perpendicular to the ventricles on a coronal slice through the atria (*not shown*).

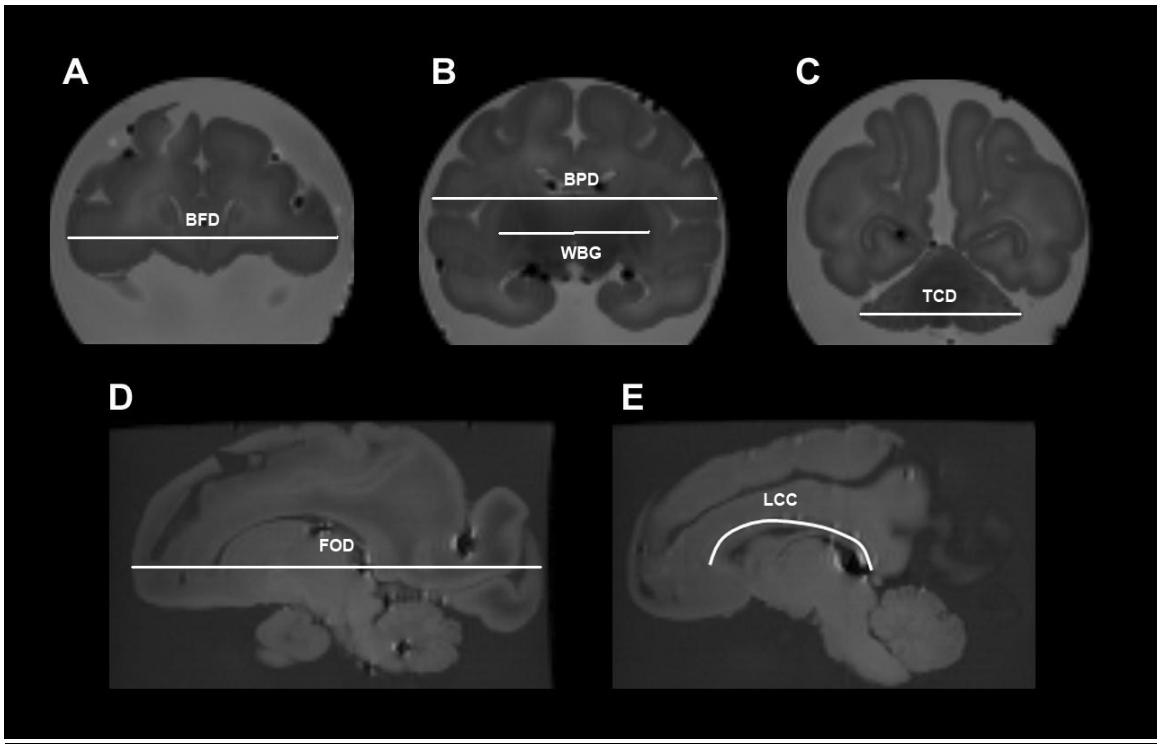

Figure 2.2. Calculation of the diffusion tensor and parameters. Panel *A* shows a voxel representing WM, outlined in red, on an axial image of a 140 dg brain. For each voxel in the image, the signal is described as a function of b-value (Panel *B*). The diffusion tensor **D** calculated for each voxel is a 3 x 3 matrix, which can be represented by the three eigenvalues λ_1, λ_2 and λ_3 (Panel *C*). In this example, the eigenvalue with the largest magnitude is defined as λ_1. The equations for calculating the diffusion parameters from the three eigenvalues are shown in Panel *D*. In this and subsequent chapters, the acronym ADC (apparent diffusion coefficient) refers to the mean diffusivity ( ).

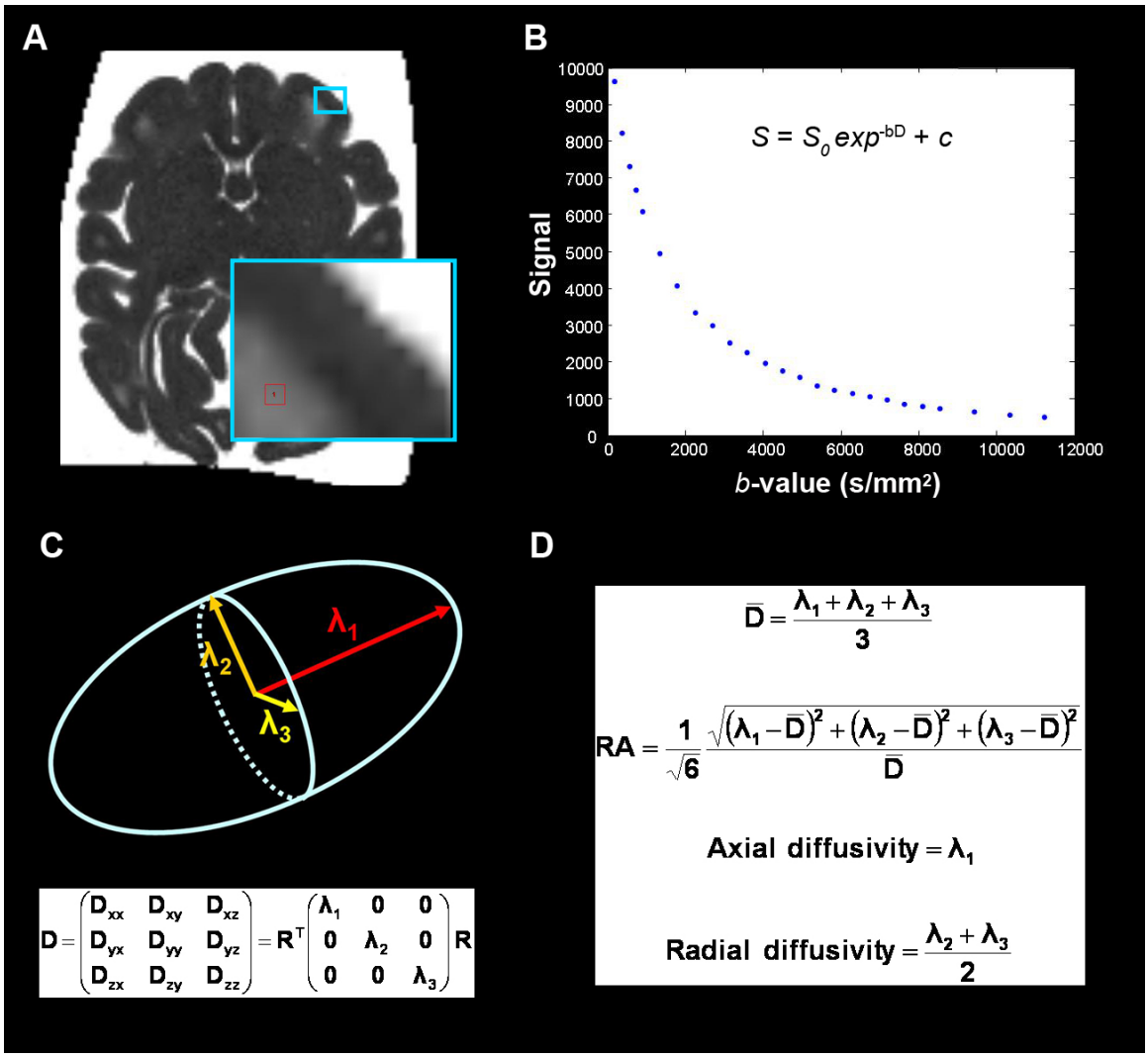

Figure 2.3. T2 maps across gestation. Scale bars indicate T2 relaxation time (s). Brains are not shown to scale. Note that T2 relaxation times of GM and WM decrease as gestational age increases.

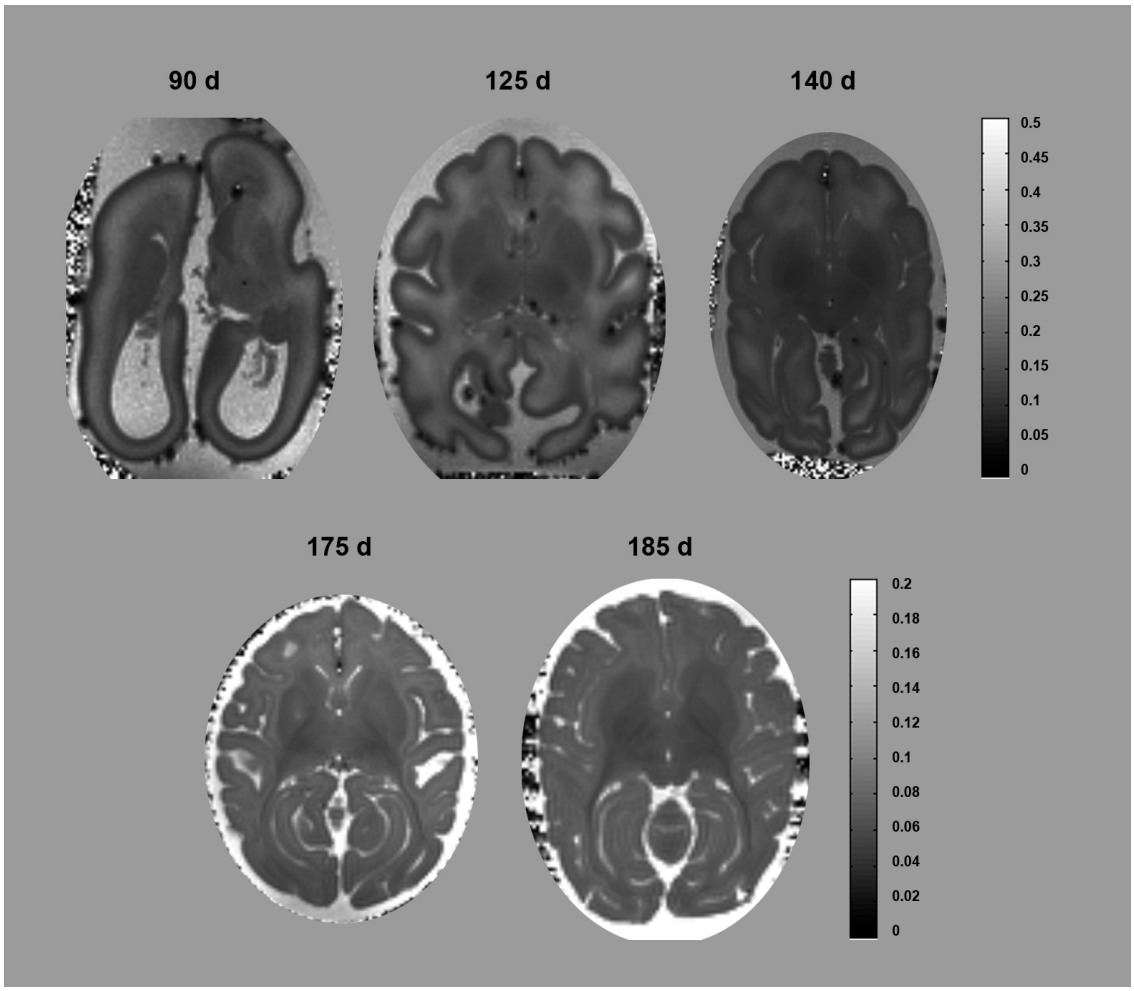

Figure 2.4. Scatter plots showing brain metrics across gestational ages.

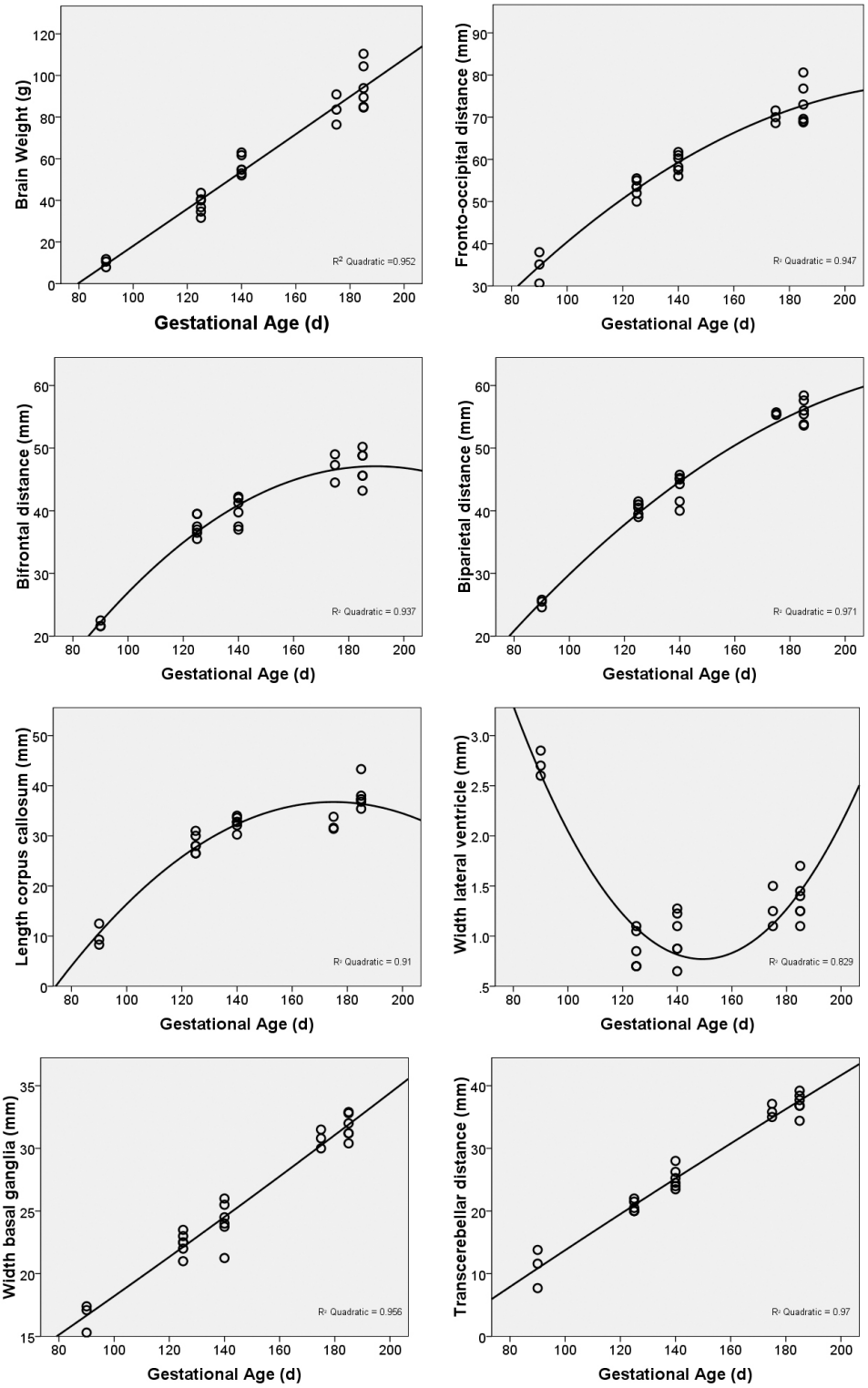

Figure 2.5. *(Top panel)* T2-weighted MR images of representative brains at each gestational age. *(Bottom panel)* T1-weighted images of the same brains. Mid-thalamic, axial slices are shown for comparison.

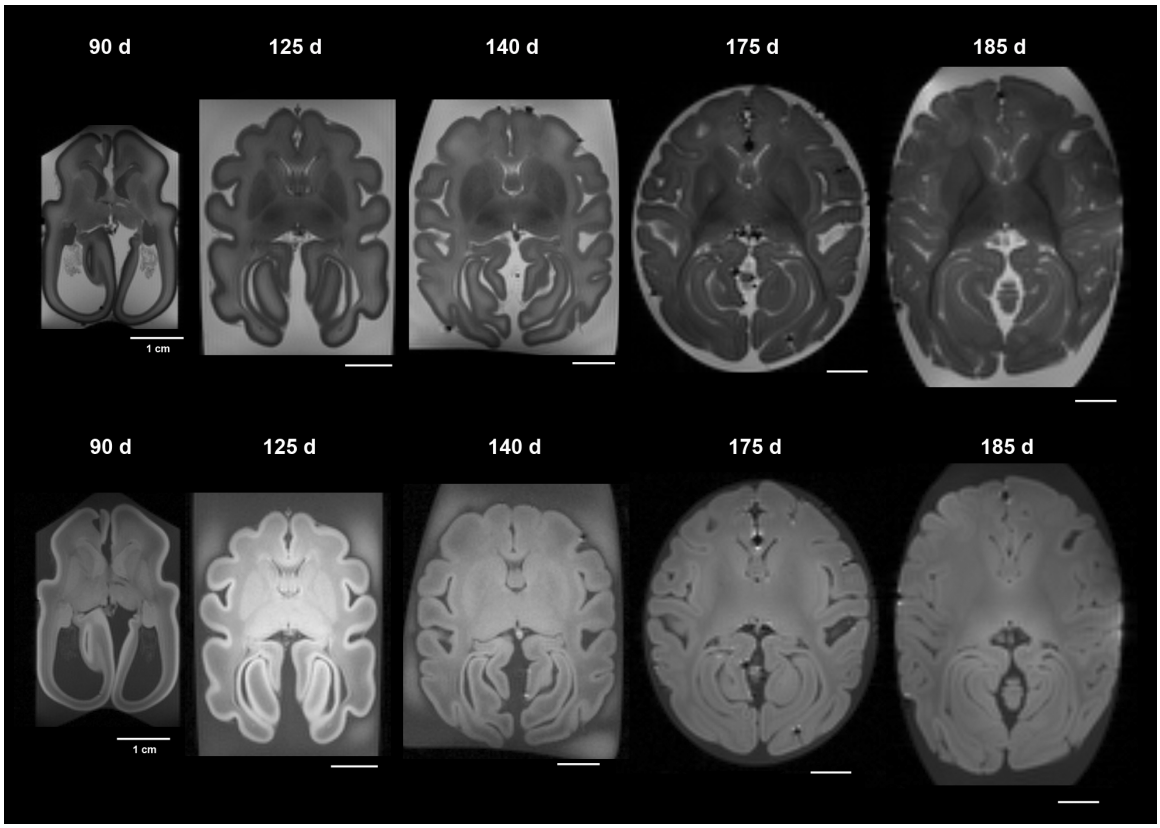

Figure 2.6. Axial slices of apparent diffusion coefficient (ADC, *top row*) and relative anisotropy (RA, *bottom row*) maps from representative brains at each gestational age.

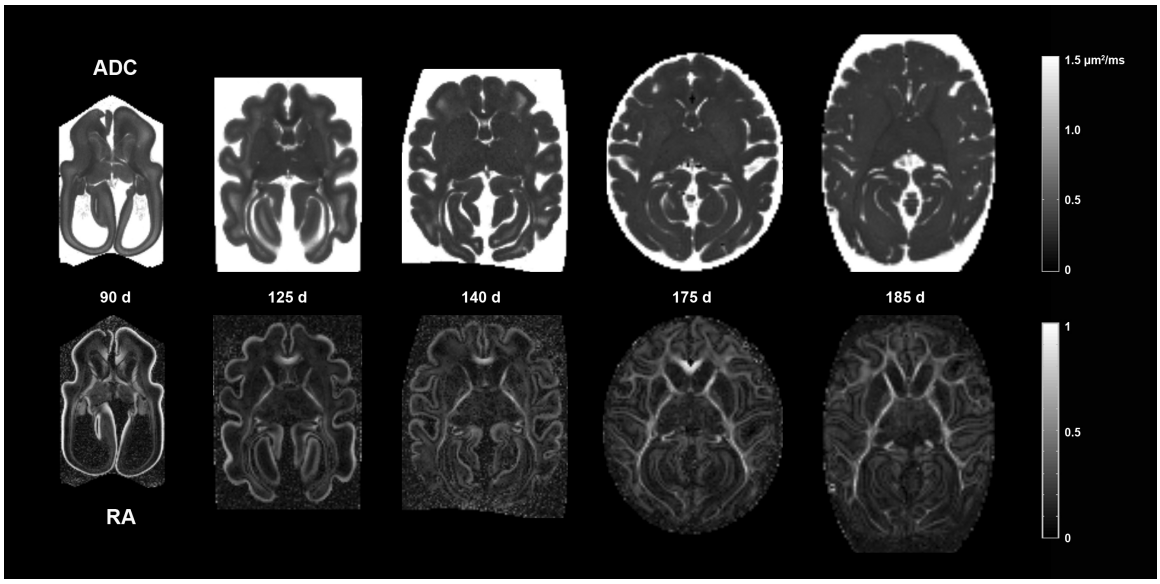

Figure 2.7. RGB color-coded maps representing the principal direction of water diffusion; mid-thalamic slices from representative brains at each gestational age are shown.

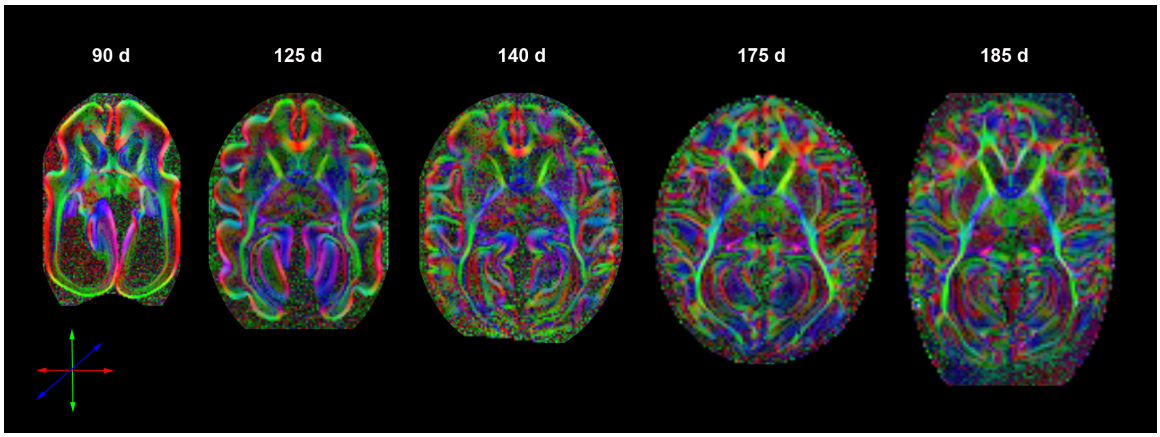

Figure 2.8. RA in WM regions across gestational ages.

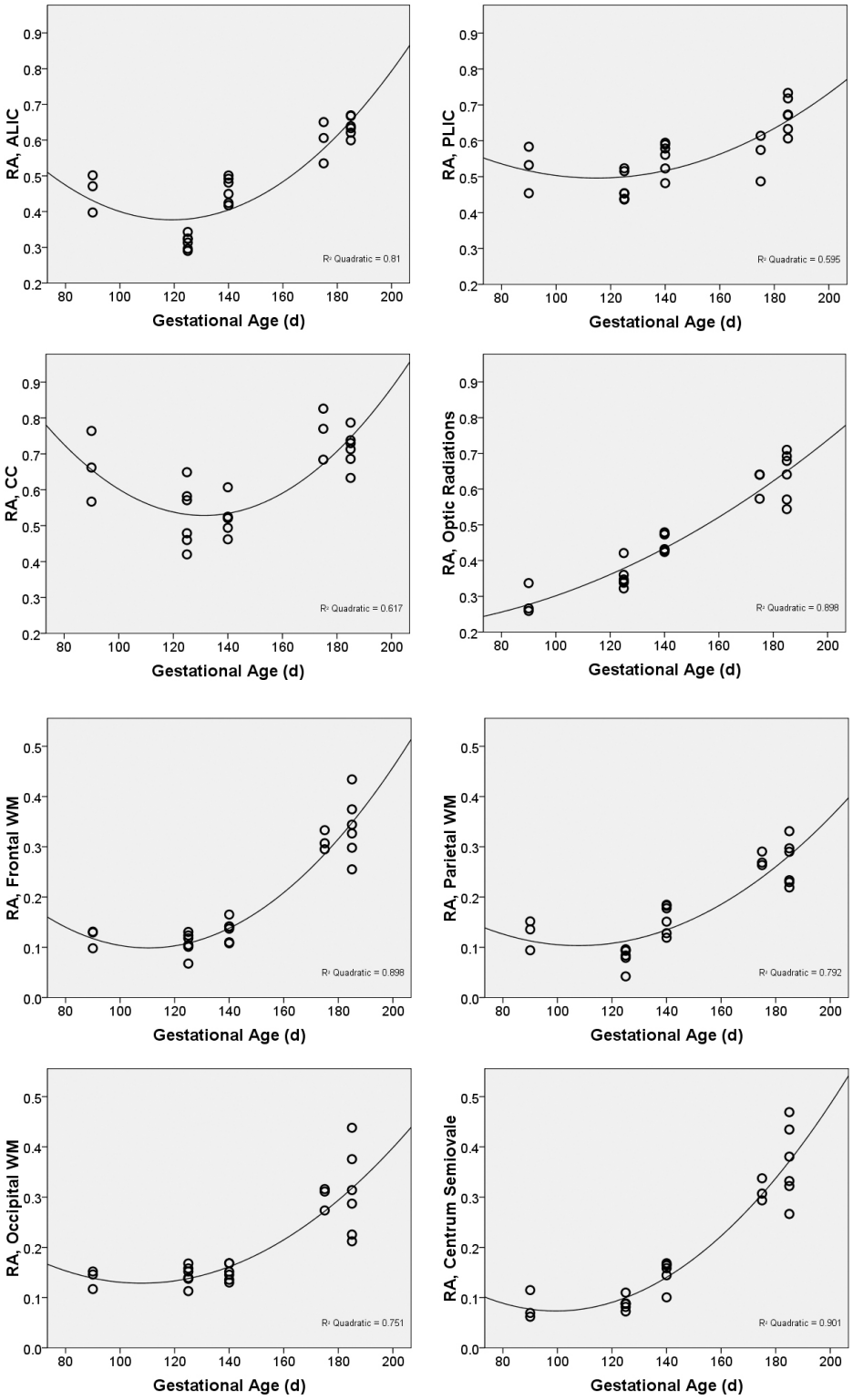

Figure 2.9. ADC ($\mu m^2/ms$) in WM regions across gestational ages.

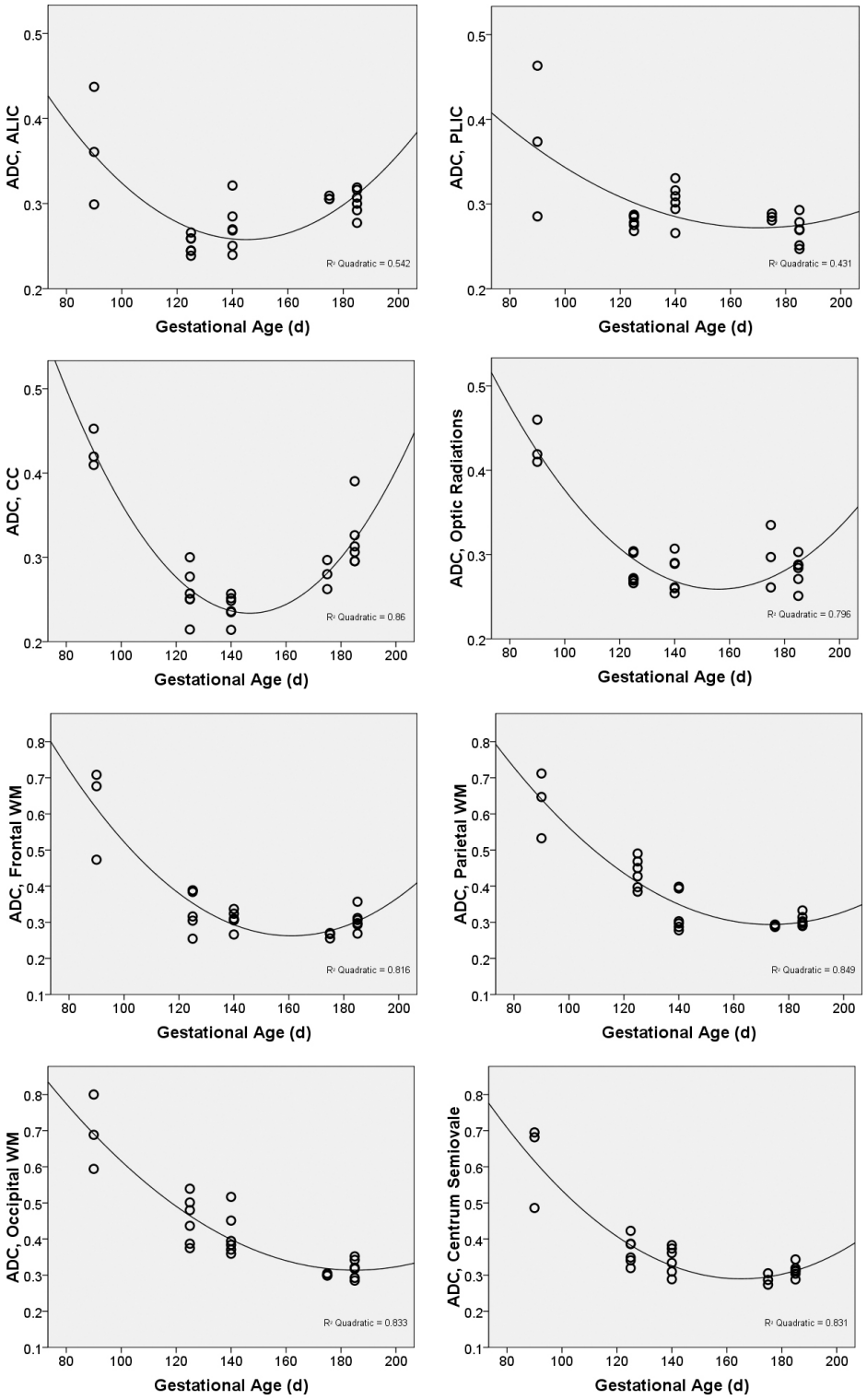

Figure 2.10. Axial diffusivity ($\mu m^2/ms$) in WM regions across gestational ages.

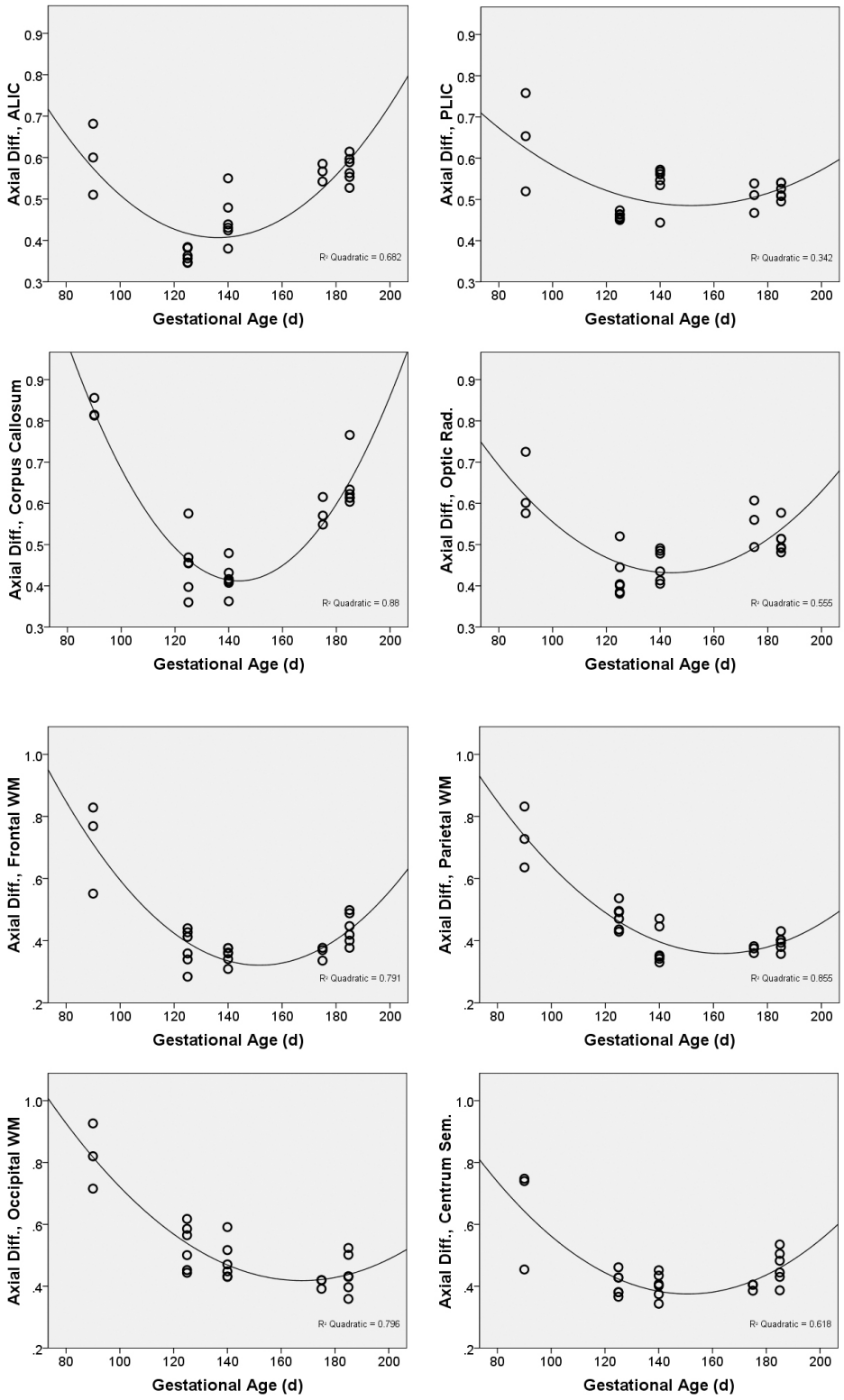

Figure 2.11. Radial diffusivity ($\mu m^2/ms$) in WM regions across gestational ages.

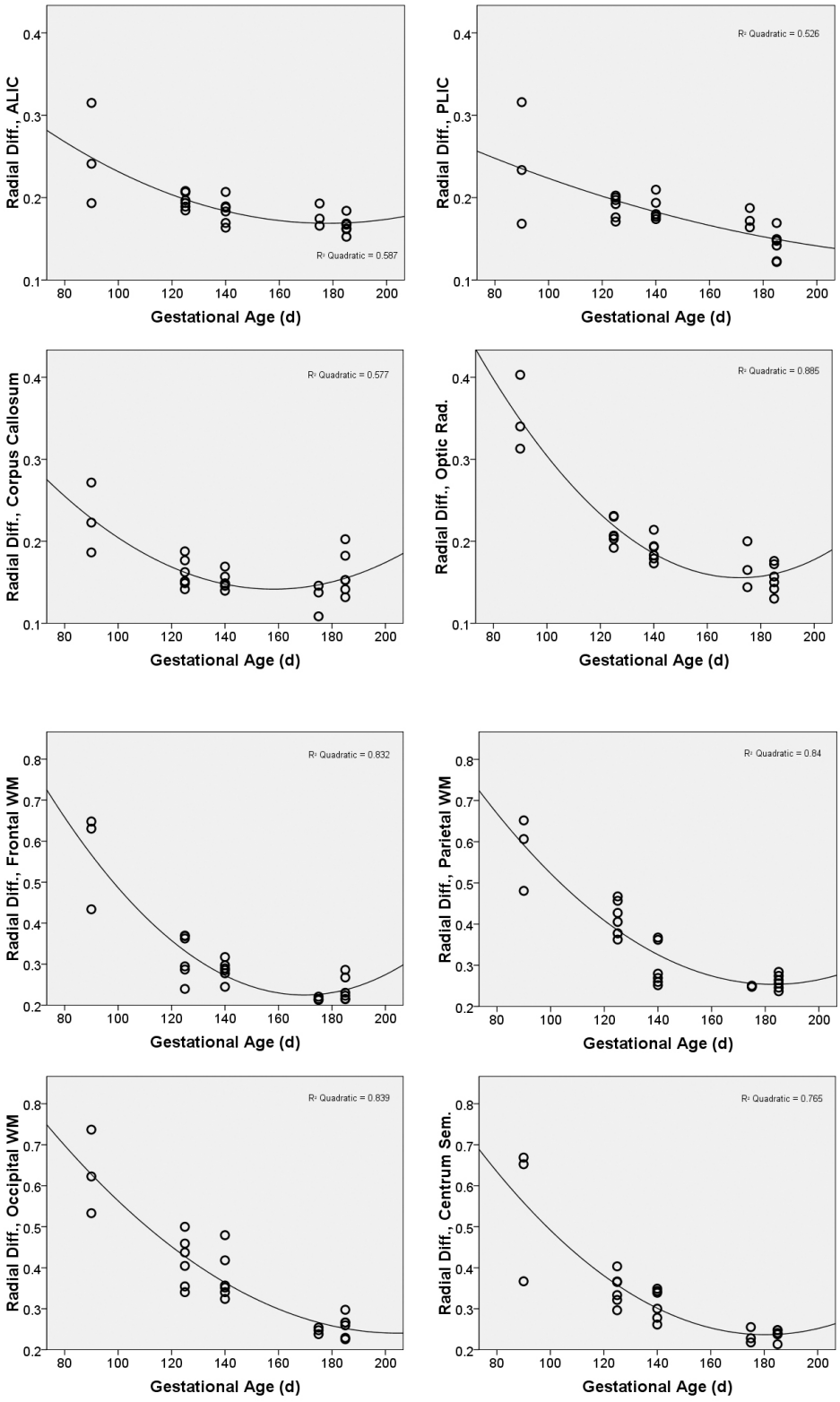

Figure 2.12. H&E staining of coronal slices at each gestational age *(top row)*. T2-weighted coronal MRI slices *(bottom row)* are shown for comparison; scale bar = 1 cm.

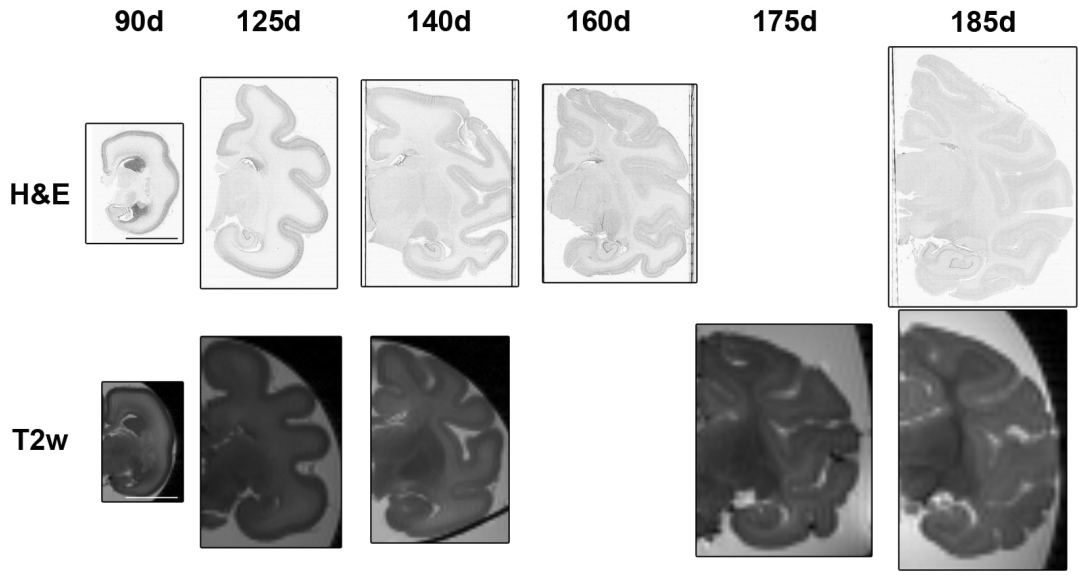

Figure 2.13. MBP immunostaining of coronal slices at each gestational age. *Top row*, right hemisphere; scale bar = 1 cm. Myelination and oligodendrocyte density in the internal capsule *(middle row)* and parietal WM superior to the lateral sulcus *(bottom row)* increase throughout gestation; scale bar = 200 μm.

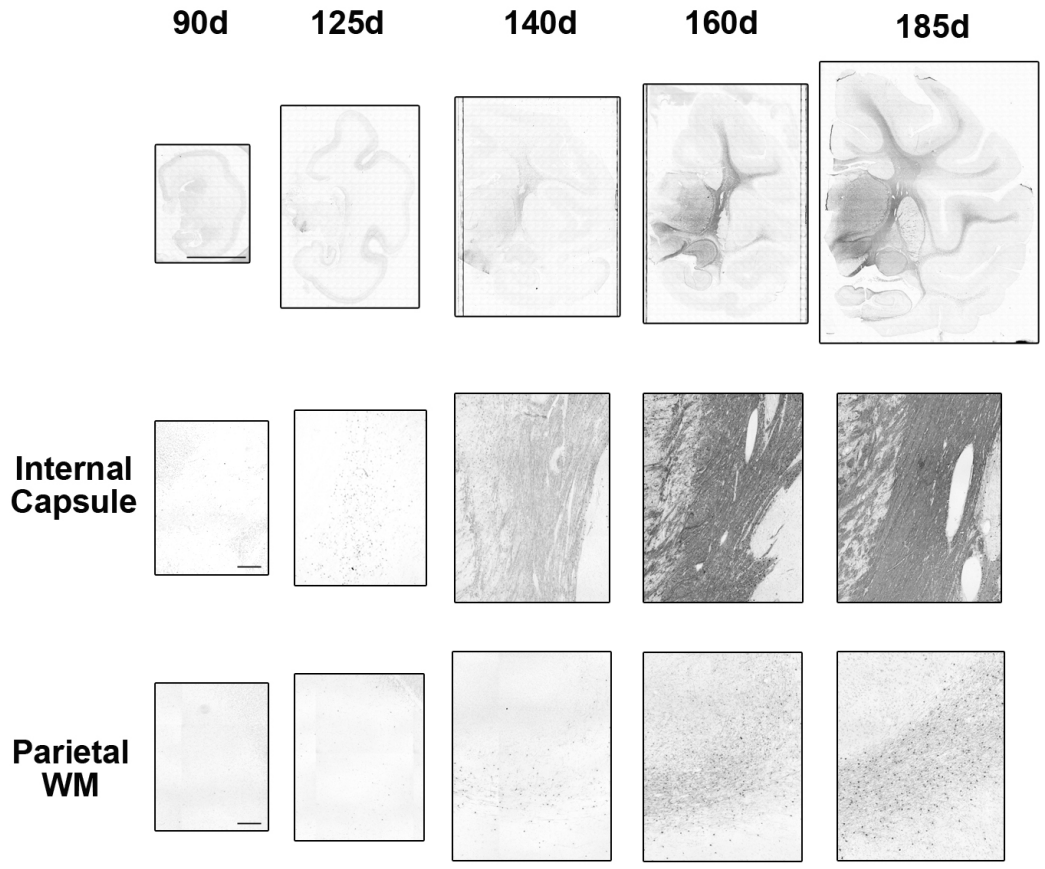

Figure 2.14. Coronal slices of brain immunostained for MBP *(top row)* and corresponding diffusion RA maps *(bottom row)*; scale bar = 1 cm.

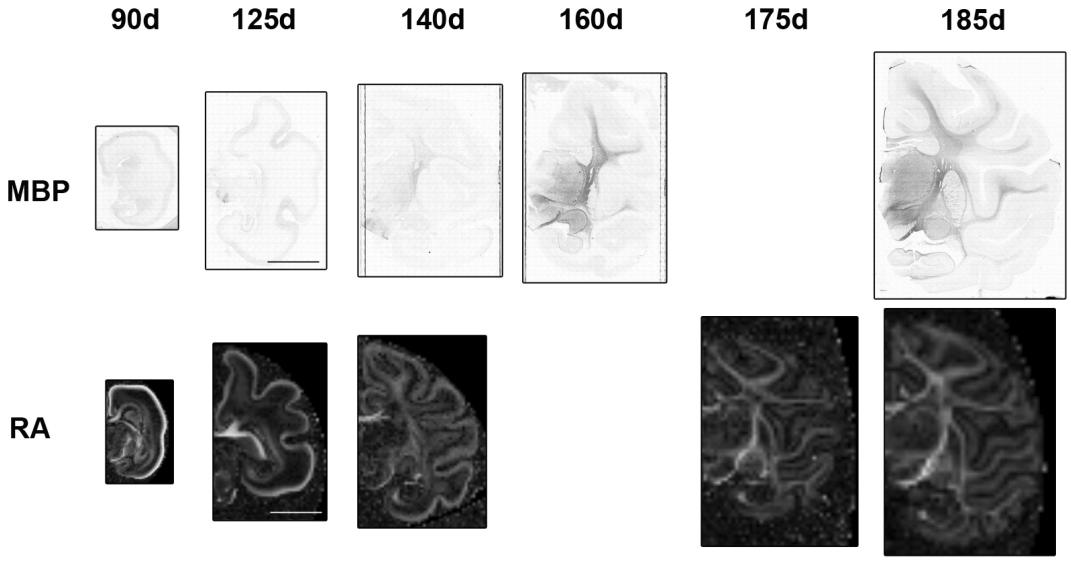

Chapter 3

Magnetic Resonance Imaging Correlates of Cerebral White Matter Pathology

Abstract

Cerebral white matter (WM) abnormalities on magnetic resonance imaging (MRI) and diffusion tensor imaging (DTI) correlate with neurodevelopmental disability in infants born prematurely. The microstructural nature of these MRI abnormalities is not clear. We investigated the histopathological correlates of MRI and DTI abnormalities in a preterm baboon model. Baboons were delivered at 125 d gestation (dg, term ~ 185 dg) and maintained in an animal intensive care unit for 14 d (*n = 24)* or 28 d (*n* = 19). Gestational control animals were delivered at 140 dg (*n* = 7) or 153 dg (*n* = 4). Cerebral WM in fixed brains was evaluated using magnetic resonance imaging (MRI), diffusion tensor imaging (DTI) and histopathology. Qualitative MRI scores of WM volume loss and ventriculomegaly non-specifically detected quantitative differences in WM and ventricular volumes. Diffuse astrocytosis was reflected by T2 signal hyperintensity and higher apparent diffusion coefficient (ADC) in WM. For the first time, we showed that the loss of oligodendrocytes in the premature primate brain is indicated by lower relative anisotropy characterized by higher radial diffusivity values and no change in axial diffusivity. The relationship between histopathology and MRI abnormalities was more pronounced in animals in the 28 d model, equivalent to the term human infant. These findings will allow investigators to better interpret the neuropathological nature of MRI and DTI abnormalities in premature infants with WM injury.

Introduction

Infants born prematurely now account for nearly 13% of all births (Heron et al., 2010). Though the vast majority of these infants survive, they are at high risk for a variety of long-term physical, behavioral, and cognitive impairments (Wilson-Costello et al., 2005; Moster et al., 2008). These adverse neurodevelopmental outcomes are often associated with cerebral white matter injury (WMI) present in the preterm infant at term-equivalent postmenstrual age (Miller et al., 2005; Woodward et al., 2006; Drobyshevsky et al., 2007). Based on human autopsy studies, this WMI is characterized by diffuse astrocytosis in central WM, prominence of activated microglia and preferential death of pre-oligodendrocytes (Gilles and Murphy, 1969; Marin-Padilla, 1997; Haynes et al., 2003). Focal necrosis, when present, is localized to deep periventricular WM. While histopathological evaluation of WMI remains the "gold standard," surrogate methods such as magnetic resonance imaging (MRI) are important because the majority of premature infants survive. To date, relatively few studies correlating MRI and neuropathology in the human preterm infant have been published. Two studies showed that conventional T1- and T2-weighted MRI accurately delineate cystic and hemorrhagic lesions, but do not detect subtle cellular abnormalities found at autopsy (Schouman-Claeys et al., 1993; Felderhoff-Mueser et al., 1999).

Diffusion tensor imaging (DTI) is more sensitive to subtle WM abnormalities than conventional MRI (Inder et al., 1999a; Miller et al., 2002). As DTI of premature infants has become increasingly common in the clinical setting, there is a growing awareness that many infants, even those thought to be at low clinical risk, have subtle

WMI (Volpe, 2003). Diffuse regions of WM have diffusion abnormalities characterized by increased apparent diffusion coefficient (ADC) and decreased anisotropy (Huppi et al., 2001; Miller et al., 2002; Counsell et al., 2003; Counsell et al., 2006; Anjari et al., 2007; Rose et al., 2008; Cheong et al., 2009). Despite an increasingly common assumption that DTI abnormalities in the preterm brain represent cellular changes like astrocytosis and loss of oligodendrocytes, only two studies have directly investigated how well diffusion imaging corresponds to histopathological findings. In the first, the only premature infant available for autopsy had severe, cystic WM lesions rather than the diffuse injury common in surviving infants (Roelants-van Rijn et al., 2001). A second study found that higher ADC in fetal brains reflected vasogenic edema and astrocytosis, but did not investigate diffusion anisotropy (Guimiot et al., 2008).

To correlate imaging findings with histopathology, a preterm animal model of WMI is required. The immature baboon (*Papio papio)* model was developed to study respiratory outcomes of ventilatory strategies, but also provides an opportunity to compare MRI findings with histopathology. This model is highly relevant to the preterm human infant with subtle WM injury because the baboon infants receive no "intentional" ischemic or inflammatory insult as in other animal models, but instead receive standard neonatal care (Dieni et al., 2004; Inder et al., 2005a). Baboons are delivered prematurely at 125 days of gestation (dg, term ~185 dg), equivalent to 26 weeks human gestation, and are treated in an animal intensive care unit for either 14 or 28 d prior to sacrifice. In the present study, we use conventional MRI and DTI of fixed brain to show the variability of cerebral WM characteristics in premature brains, and to explore the relationship between MR imaging parameters and histopathological markers of cerebral injury.

Methods

The animal portion of these studies was performed at the Southwest Foundation for Biomedical Research, San Antonio, TX. All animal husbandry, handling, and procedures were approved to conform to American Association for Accreditation of Laboratory Animal Care guidelines.

Delivery and Instrumentation. Pregnant baboon dams (*Papio papio*) were treated with 6 mg of intramuscular betamethasone 48 and 24 hours prior to elective hysterotomy under general anesthesia. Timed gestations were determined by characteristic sex skin changes and confirmed by serial fetal ultrasounds. Study animals were delivered at 126 ± 2 dg. At birth, animals were weighed, sedated, intubated and treated with 4 mL/kg bolus of exogenous surfactant (Survanta, courtesy Ross Laboratories, Columbus, OH) through the endotracheal tube.

Respiratory Management and Treatment. The management, monitoring and treatment strategies of all baboon infants in this analysis have been described in detail in previous publications (Yoder et al., 2000; Thomson et al., 2006; McCurnin et al., 2008; McCurnin et al., 2009).

The animals included in this analysis were administered a variety of ventilatory strategies. For 24 of the animals, initiation of positive pressure ventilation (PPV; InfantStar ventilator; Infrasonics, San Diego, CA) began immediately after delivery at 125 dg and continued for 14 days prior to euthanization with sodium pentabarbitone (130

mg/kg intravenously). In a second model, 19 animals were randomized to 28 days of positive pressure ventilation, high frequency oscillatory ventilation, or early (within 24 h of life) or delayed (within 5 d of life) extubation to nasal continuous positive airway pressure, according to antenatal assignment. Animals were euthanized after 28 d. Gestational control infants delivered by elective hysterotomy at 140 dg (n = 9) or 153 dg (n = 4) and euthanized immediately were included in the 14 d and 28 d groups, respectively. After sacrifice, brains were extracted, weighed and immersed in 4% paraformaldehyde in 0.1M phosphate buffer.

Cerebral outcomes of specific ventilatory strategies in this preterm baboon model have been previously evaluated by histopathology (Loeliger et al., 2006; Loeliger et al., 2009b; Loeliger et al., 2009a; Loeliger et al., 2010) and MRI (Chapter 5), and will not be discussed here.

Qualitative MRI. Imaging studies were performed at Washington University in St Louis, MO. Imaging was performed using a 33-cm clear bore, 4.7-tesla magnet controlled by a Varian INOVA console. The fixed brains were placed in sealed plastic containers filled with 4% paraformaldehyde, which fit inside a single-turn RF coil for imaging. T2-weighted images were acquired using a spin-echo pulse sequence, with TE = 100 ms (≈ T2) and TR set to 8–11 s, depending on the number of slices being acquired. Slice thickness was 500 μm; in-plane resolution was 500 μm x 500 μm.

MR images were scored qualitatively by two experienced readers blinded to treatment group. WM abnormality was graded using three 3-point scales previously described (Inder et al., 2003b) to assess the nature and extent of WM signal abnormality,

WM volume loss and ventriculomegaly. Representative MRI images of animals with normal and abnormal scores are shown in Figure 3.1.

Diffusion MRI. Diffusion data were acquired using a spin-echo pulse sequence modified by the addition of a diffusion-sensitization gradient pulse pair. The brains from all animals in the late sacrifice group and ten of those in the early sacrifice group were imaged using a 6-direction sampling scheme, with b = 2038 s/mm^2 (TE = 80 ms, TR = 3–7 s, 600-μm isotropic voxel size, diffusion gradient duration = 15 ms, delay between diffusion gradients = 50 ms, and diffusion gradient amplitude = 3.75 Gauss/cm). A reference image was obtained with b = 0 s/mm^2. The remainder of brains in the early sacrifice group were imaged using a 25-direction sampling scheme in which gradient strength was varied across each of the 25 gradient orientations to produce b-values ranging from 0 - 12,500 s/mm^2 (TE = 67 ms, TR = 3–7 s, 500-μm isotropic voxel size, diffusion gradient duration = 15 ms, delay between diffusion gradients = 50 ms, and diffusion gradient amplitude = 0-38 Gauss/cm).

Raw data from diffusion studies were phase-corrected using Bayesian probability analysis so that noise was Gaussian and centered about zero. A diffusion tensor was estimated for each voxel using a model selection algorithm. For the single b-value data, the signal was assumed to decay to zero; for the 25 b-value data, the data were modeled as a monoexponential function plus a constant (Kroenke et al., 2006). The mean and standard deviation of the eigenvalues of the diffusion tensor at each voxel were used to calculate the apparent diffusion coefficient (ADC) and relative anisotropy (RA), respectively. Axial diffusivity, equal to the principal eigenvalue, and radial diffusivity,

the mean of the two minor eigenvalues, were also determined. Using Analyze software, regions of interest were defined manually on horizontal slices in frontal, parietal and occipital white matter, in the centrum semiovale, and in white matter tracts, including the corpus callosum (CC) and the anterior and posterior limbs of the internal capsule (ALIC, PLIC).

Histology. Histopathological analysis was performed at the University of Melbourne, Australia. Details of the histopathological analysis have been previously published (Loeliger et al., 2006; Loeliger et al., 2009b; Loeliger et al., 2009a; Loeliger et al., 2010). Five-millimeter coronal blocks from the right forebrain were processed to paraffin, and 10 8-μm sections were cut from the rostral surface of each block. Analyses were performed on sections from each block for all brains. Areas were assessed using a digitizing program (Sigma Scan Pro v4, SPSS Science, Chicago, IL, USA) and counts performed using an image analysis system (Image Pro Plus v4.1, Media Cybernetics, Maryland, USA).

Volumetric analysis:, The cross-sectional area of the white matter and ventricle were measured In sections stained with hematoxylin and eosin, and the total volume estimated using the Cavalieri principle.

Areal density of astrocytes: Rabbit anti-cow glial fibrillary acidic protein (GFAP; 1:500, Sigma, St Louis, MO, USA) was used to identify astrocytes. GFAP-IR cells were counted (x660) in randomly selected areas (0.2 mm^2) in deep and subcortical white matter for each block.

Areal density of oligodendrocytes: Rat anti-bovine myelin basic protein (MBP, 1:100; Chemicon, USA) was used to identify oligodendrocytes. MBP-IR oligodendrocytes were counted (x660) in a randomly selected area (0.2 mm^2) in the deep and subcortical white matter in blocks from the frontal/temporal, parietal/temporal, and occipital lobes and the mean calculated.

Statistical analysis. Statistical analysis was performed using the Statistical Package for the Social Sciences, v17 (SPSS, Chicago, IL). Pearson's correlation coefficients were used to assess the relationship between histological parameters and qualitative MRI scores, and between histological parameters and diffusion values.

Results

Qualitative MRI scores. More than half of the animals received normal scores for WM signal, WM volume and ventriculomegaly in both the 14 d and 28 d models (Table 3.1). Approximately 12% had severe WM abnormalities (score = 3). The percentages with WM injury were similar for the two groups.

WM diffusion values. Figure 3.2 shows the variation in diffusion values in WM tracts. In the 14 d model, values in the ALIC, PLIC and CC tended to cluster around the median, with a few outliers, while there was somewhat more variability at 28 d, particularly in the CC. Diffusion values in hemispheric WM (frontal, parietal, occipital and centrum semiovale) can be seen in Figure 3.3. Overall, hemispheric WM had more

variability in diffusivity (ADC, axial and radial diffusivity) than WM tracts, but less variability in anisotropy (RA). Values in the 14 d and 28 d groups showed a similar amount of variation.

Relationship of qualitative MRI to histopathology. WM signal hyperintensity on T2-weighted MRI was correlated with lower WM volume, greater ventricular volume, and higher astrocyte density, particularly in subcortical WM (Table 3.2). Higher qualitative scores of WM volume loss, ventriculomegaly and total WM abnormality were correlated with lower WM volume, greater ventricular volume, and lower oligodendrocyte density in subcortical WM.

To determine how early imaging findings correlated with histological changes, separate correlation analyses were performed for the 14 d and 28 d models. At 14 d, higher qualitative injury scores were associated only with greater ventricular size. By 28 d, however, higher WM signal abnormality scores were associated with lower WM volume, greater ventricular volume, and higher astrocyte density in both deep and subcortical WM. Higher WM volume loss scores, ventriculomegaly scores and total WM injury scores reflected lower WM volume; greater ventricular volume; higher astrocyte density in both deep and subcortical WM; and lower oligodendrocyte density in subcortical WM.

Relationship of DTI to histopathology. Higher diffusivity (ADC, axial and radial diffusivity) was strongly correlated with lower WM volume, greater ventricular volume, and higher astrocyte density in deep WM (Table 3.3). These correlations tended

to be stronger in hemispheric (frontal, parietal and occipital) WM than in WM tracts (ALIC, PLIC, CC). Higher astrocyte density in subcortical WM correlated with higher axial diffusivity, but not with radial diffusivity. It was also correlated with higher RA in the occipital WM and centrum semiovale. In contrast, lower oligodendrocyte densities in deep and subcortical WM correlated with higher radial, but not axial, diffusivity. Lower RA was strongly correlated with greater ventricular volume and lower oligodendrocyte densities in both WM tracts and hemispheric WM.

When the 14 d model was analyzed separately, lower WM volume was significantly correlated with lower RA and higher diffusivity in the ALIC, CC, frontal and parietal WM and centrum semiovale. None of the other histopathology measures were significantly correlated with diffusion in this group. In the 28 d group, higher diffusivity was correlated with lower WM volume, higher ventricular volume, and higher astrocyte densities in both deep and subcortical WM. The oligodendrocyte densities were not correlated with any diffusion parameters when the 14 and 28 d models were analyzed separately.

Discussion

Technical considerations. Fixation affects diffusion parameters, so that one must exercise caution in interpreting data obtained from fixed tissue. RA values are unchanged by fixation, whereas ADC, axial diffusivity and radial diffusivity are reduced by ~30% (Sun et al., 2003). Thus, the relationship between RA values from live and fixed tissue is straightforward. The relationship between ADC values in live and fixed

tissue, on the other hand, is more complex. The acute reduction in ADC associated with injury likely reflects alterations in tissue physiology because ADC contrast between normal and acutely injured tissue is lost following fixation (Sun et al., 2005). In a sense, fixation "injures" all the tissue, reducing the ADC of previously healthy tissue to that of injured tissue. Alterations in ADC that survive fixation, such as those reported in this study, do not reflect acute physiologic change or injury. Rather they are a consequence of differences in tissue microstructure. Such differences might be an increase in tissue density related to brain maturation (leading to a lower ADC) or a decrease in tissue density related to injury or delayed maturation (leading to a higher ADC).

Another potential concern is that our analysis includes data obtained with two different sets of b values: a 6-direction, single amplitude acquisition, and a 25-direction, 25 amplitude acquisition. In particular, a 25 amplitude acquisition allowed modeling signal decay with a positive constant, whereas the single amplitude acquisition did not; the difference in model selection algorithms between the two data sets could introduce a potential source of bias in our analysis. Recalculating the correlations between DTI parameters and histopathology using only the 6-direction data, which included all of the late sacrifice animals and approximately half of the early sacrifice animals, gave the same pattern of correlations. Thus, we included all the data in the final analysis.

Imaging correlates of histopathology. Our results indicate that qualitative assessments of WM injury on T2-weighted MRI reflect histopathology. However, individual qualitative scores are non-specific. For instance, qualitative WM volume loss scores correlate not only with quantitative measurement of WM volume, but also with

ventricular volume and astrocyte density. Qualitative scoring of diffuse T2 signal hyperintensity reflects WM volume loss, ventriculomegaly and astrocyte density, but not oligodendrocyte density. This pattern of histopathological correlations is the same as that reflected by ADC. Indeed, we found that qualitative WM signal abnormality was correlated with ADC in hemispheric WM, and similar findings have been reported in the literature (Miller et al., 2002; Counsell et al., 2003; Cheong et al., 2009). These correlations may reflect the fact that a reduction in tissue density would be expected to both lengthen water T2 relaxation time constant (and cause signal hyperintensity on T2-weighted imaging) and increase water diffusivity.

Macrostructural changes in cerebral anatomy were reflected by diffusion values. Higher ADC, axial and radial diffusivity correlate with lower WM volume and greater ventricular volume. Ventricular dilatation and WM atrophy are known sequelae of preterm birth (Maalouf et al., 1999; Inder et al., 2003b; Nguyen The Tich et al., 2009), and WM, particularly in the periventricular region, may have disorganized or delayed maturation. Ventriculomegaly is also associated with lower RA in WM, which may be due to interrupted development of injured WM tracts.

Diffusion parameters are also sensitive to cellular neuropathological abnormalities in WM. Astrocytosis correlates with higher ADC and axial diffusivity, similar to the results of a fetal imaging study (Guimiot et al., 2008). An increased density of reactive astrocytes is typical of white matter lesions in later stages (Haynes et al., 2003), and is probably a response to death of other cell types. The loss of injured cells and subsequent tissue disorganization probably account for the higher diffusivity associated with astrocytosis. One of the cell types most vulnerable in the premature brain is the pre-

oligodendrocyte. Indeed, previous investigations in this baboon model have shown reduced oligodendrocyte densities in preterm brains compared to gestational controls (Rees et al., 2007; Loeliger et al., 2009b; Loeliger et al., 2009a). In the present analysis, lower oligodendrocyte densities correlate with higher radial diffusivity, but not axial. The reduction in myelination that would occur subsequent to the loss of oligodendrocytes can account for this pattern of diffusion changes, as loss of myelin is associated with higher radial diffusivity and no change in axial diffusivity, with a corresponding decrease in RA (Song et al., 2005; Budde et al., 2007; Wang et al., 2009).

In this analysis, DTI parameters in fixed brains correlated strongly with pathology by 28 d, which corresponds to term-equivalent postmenstrual age in human infants. In animals sacrificed after 14 d, however, pathological abnormalities did not correlate strongly with imaging findings. One explanation is that our pathological analysis was limited to investigation of chronic tissue changes (loss of mature oligodendrocytes, astrocytosis, WM volume loss) for technical reasons. Certain immunohistochemical methods, such as stains to identify activated microglia or necrotic cells, particularly pre-oligodendrocytes, are not feasible in paraformaldehyde-fixed tissue. It is possible that cerebral diffusion values in the 14 d model relate to subacute neuropathology, such as transient activation of microglia or necrosis of pre-OLs or other cell populations (Marin-Padilla, 1997; Back, 2006; Folkerth, 2007). In addition, microstructural changes are necessary before diffusion parameter differences are detectable in fixed tissue (Sun et al., 2005). Microstructural changes are likely more prevalent at 153 dg than 140 dg.

Conclusion

We have shown that MRI reflects microstructural and anatomical abnormalities that are characteristic of WMI in the preterm brain. Quantitative differences in WM and ventricular volumes are accurately – if not specifically – detected by qualitative MRI scores of WM volume loss and ventriculomegaly. Astrocytosis is reflected by T2 signal hyperintensity, and by increased ADC values associated with increases in both axial and radial diffusivity. Finally, we have shown for the first time that the loss of oligodendrocytes in cerebral WM in the premature primate brain is indicated on MRI by regions having decreased anisotropy characterized by higher radial diffusivity values and no change in axial diffusivity. These findings will allow investigators to better interpret the neuropathological nature of MRI and DTI abnormalities in premature infants with WMI.

Figures & Tables

Figure 3.1. Representative T2-weighted MRI (axial slices, top row, and coronal slices, bottom row) depicting WM abnormality in infants born at 125 dg and treated for 14 d. (*A*) Infant with normal WM scores. (*B*) Infant with grade 3 scores for WM signal abnormality (*white arrow*), ventriculomegaly (*black arrowhead*) and WM volume loss.

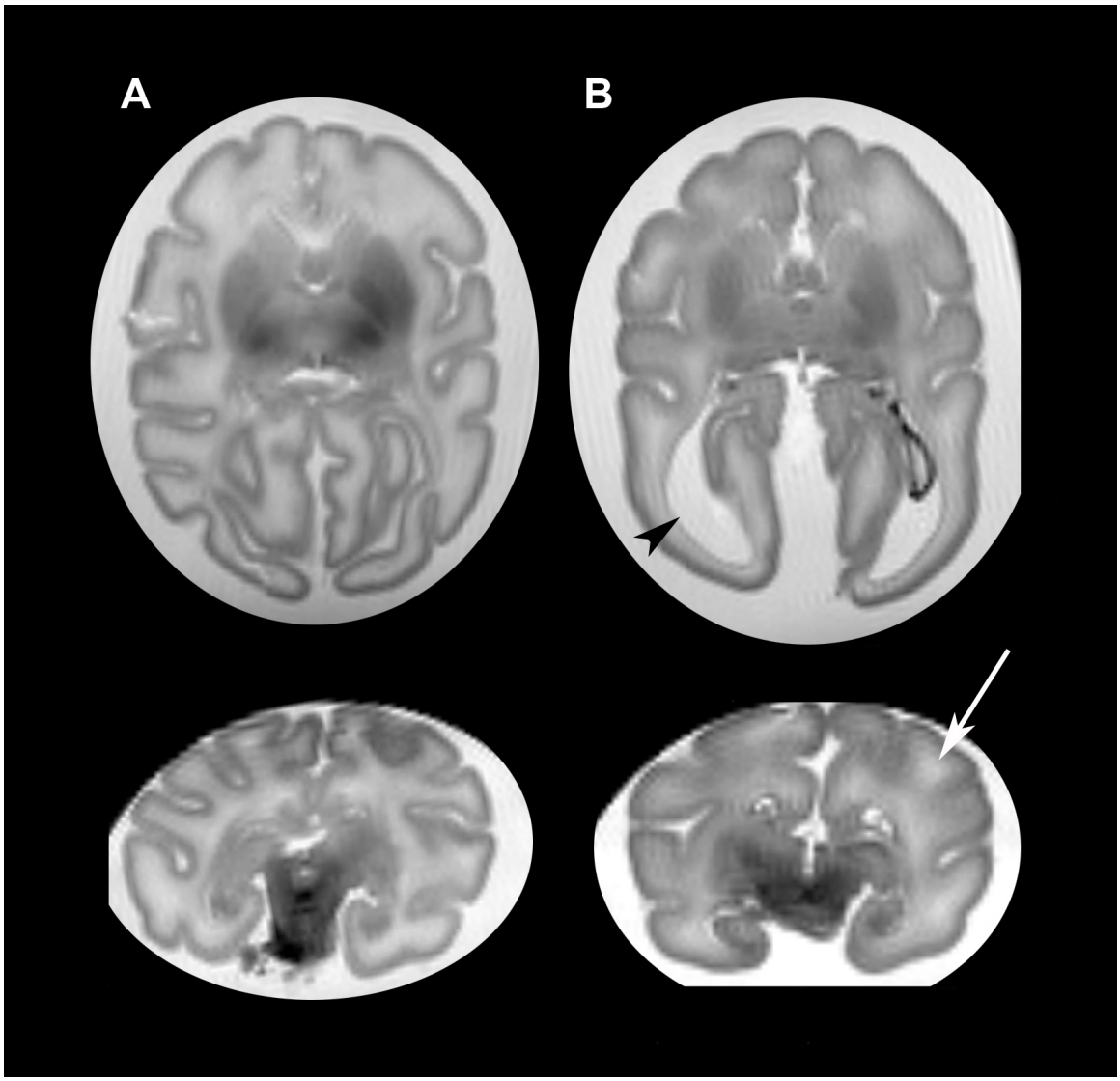

Table 3.1. Frequency of qualitative WM scores evaluated on conventional MRI in each model. Values are expressed as *N*/Total (%).

Qualitative Score	**Model**	**Frequency of Score**		
		1	**2**	**3**
WM Signal	*14 d*	13/26 (50)	10/26 (38)	3/26 (12)
	28 d	9/17 (53)	6/17 (35)	2/17 (12)
WM Volume Loss	*14 d*	19/26 (73)	4/26 (15)	3/26 (12)
	28 d	12/17 (71)	3/17 (18)	2/17 (12)
Ventriculomegaly	*14 d*	14/26 (54)	9/26 (35)	3/26 (12)
	28 d	9/17 (53)	6/17 (35)	2/17 (12)

Figure 3.2. Values of RA, ADC (μm^2/ms), axial (μm^2/ms) and radial diffusivity (μm^2/ms) in white matter tracts in the 14 and 28 d models. Box plots represent the median value (horizontal line), interquartile range (IQR; box) and range (error bars); shaded circles (●) or stars (*) indicate values greater than 1.5 or 3 IQRs from the end of a box. ALIC/PLIC: anterior/posterior limb of the internal capsule; CC: corpus callosum.

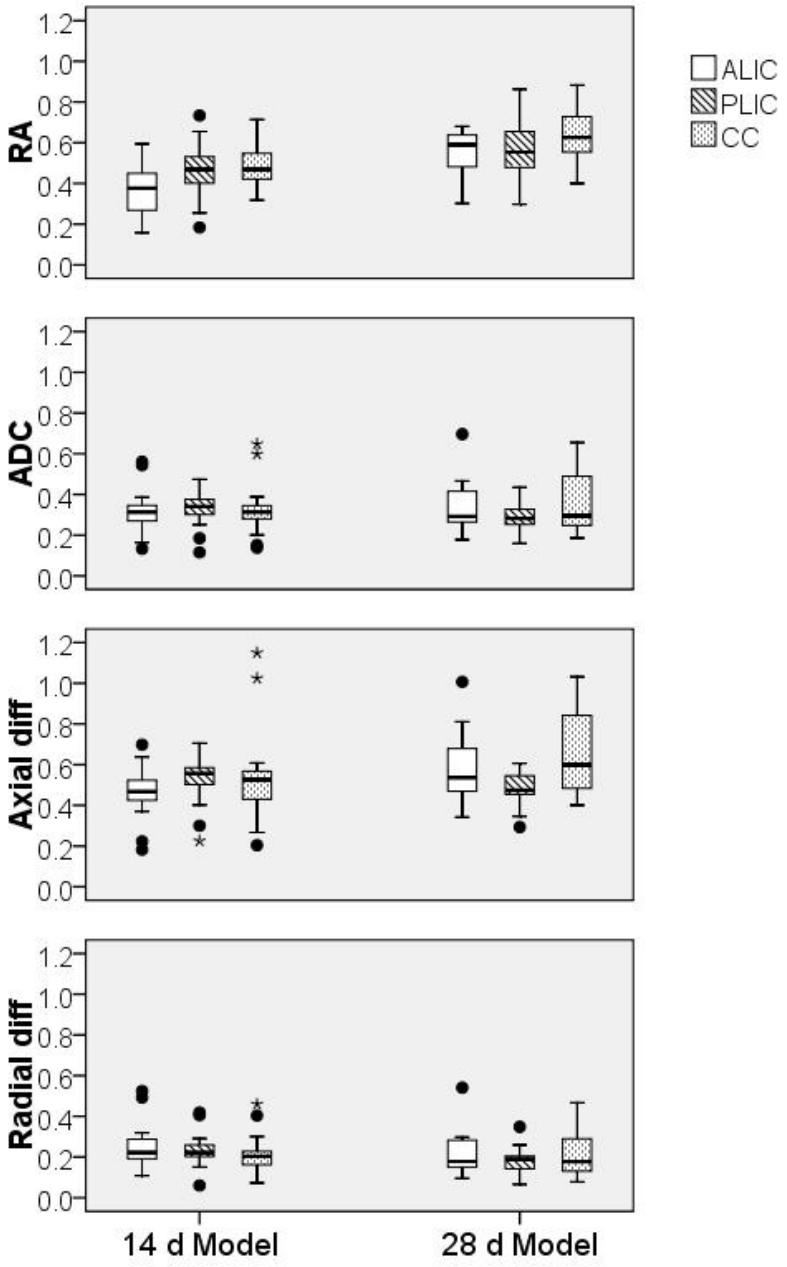

Figure 3.3. Values of RA, ADC (μm^2/ms), axial (μm^2/ms) and radial diffusivity (μm^2/ms) in hemispheric white matter in the 14 and 28 d models. Box plots represent the median value (horizontal line), interquartile range (IQR) (box) and range (error bars); shaded circles (●) represent values greater than 1.5 IQRs from the end of a box.

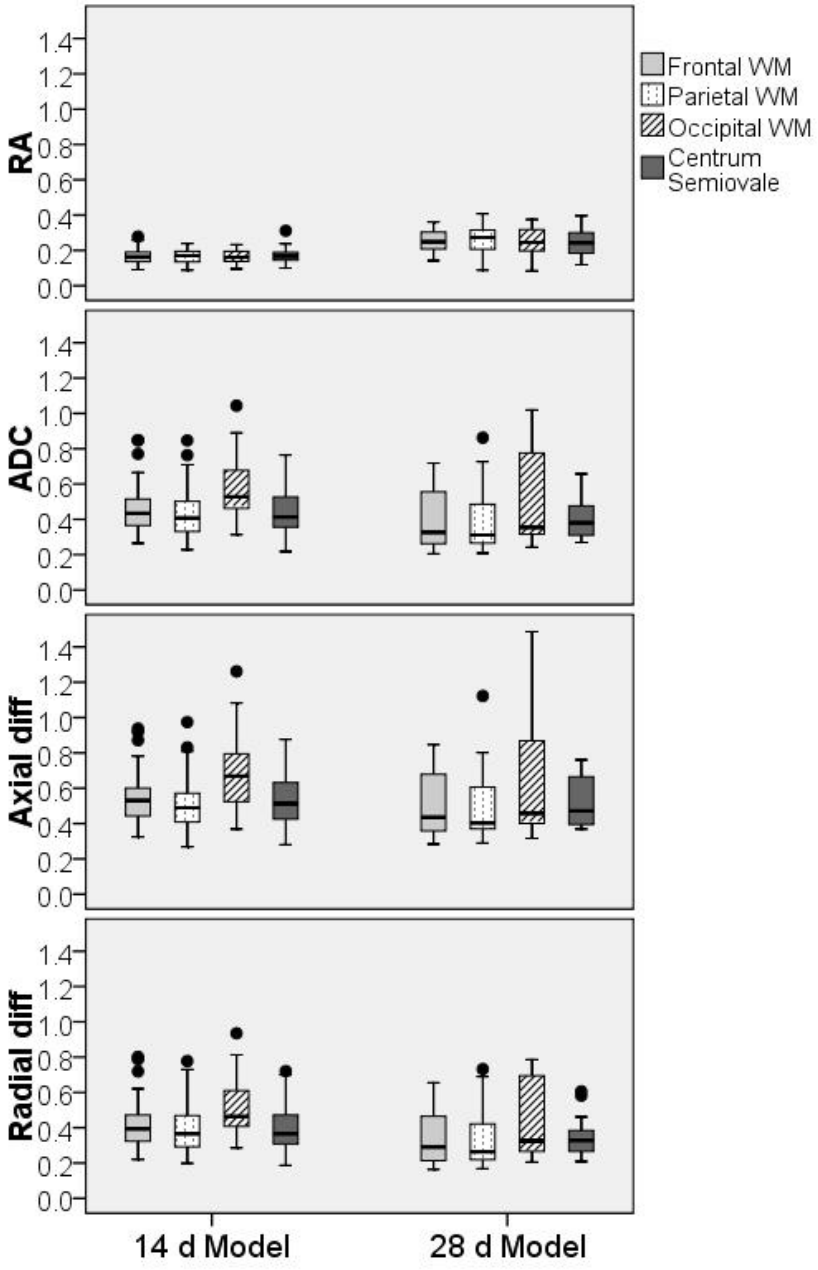

Table 3.2. Pearson's correlations between qualitative MRI scores (rows) and histopathology measures (columns). *$p < 0.05$, **$p < 0.01$

	WM Volume	Ventricular Volume	Deep WM Astrocytes	Subcortical WM Astrocytes	Deep WM Oligos	Subcortical WM Oligos
WM Signal	-.439*	.581**	.320	.435**		
WM Volume Loss	-.430*	.658**				-.344*
Ventriculomegaly	-.408*	.668**	.312			-.388*
Total WM Abnormality	-.393*	.652**				-.363*

Table 3.3. Pearson's correlations between diffusion parameters (rows) and histopathology measures (columns) in WM regions. The diffusion parameters relative anisotropy (RA), apparent diffusion coefficient (ADC), axial diffusivity and radial diffusivity were measured in the anterior and posterior limbs of the internal capsule (ALIC, PLIC), corpus callosum (CC), centrum semiovale, and frontal, parietal and occipital WM. *$p < 0.05$, **$p < 0.01$

	WM Volume	Ventricular Volume	Deep WM Astrocytes	Subcortical WM Astrocytes	Deep WM Oligos	Subcortical WM Oligos
RA						
ALIC	.408*	-.549**			.680**	.647**
PLIC	.348	-.376*	-.315		.527**	.578**
CC		-.453*			.511**	.449*
Frontal WM		-.514**			.587**	.533**
Parietal WM		-.516**			.592**	.687**
Occipital WM		-.321		.490**	.431*	.447*
Centrum Semi.				.594**		.316
ADC						
ALIC	-.454*	.395*	.476**			

	WM Volume	Ventricular Volume	Deep WM Astrocytes	Subcortical WM Astrocytes	Deep WM Oligos	Subcortical WM Oligos
ADC (cont'd)						
PLIC	-.372*	.365	.349		-.360	-.385*
CC	-.461*	.448*	.504**	.320		
Frontal WM	-.521**	.644**	.478**		-.421*	-.334
Parietal WM	-.583**	.597**	.500**			
Occipital WM	-.594**	.683**	.568**	.375*	-.381*	-.324
Centrum Semi.	-.372*	.538**			-.320	
Axial diffusivity						
ALIC	-.328		.406*	.432*		
PLIC	-.375*					
CC	-.370*	.325	.447*	.360*		
Frontal WM	-.563**	.635**	.541**		-.356	
Parietal WM	-.603**	.541**	.560**	.375*		
Occipital WM	-.632**	.637**	.642**	.522**		
Centrum Semi.	-.462*	.541**	.365*			
Radial diffusivity						
ALIC	-.475**	.500**	.481**		-.356	-.307
PLIC	-.350	.385*	.367*		-.426*	-.444*
CC	-.454*	.516**	.493**			
Frontal WM	-.478**	.628**	.422*		-.433*	-.349
Parietal WM	-.553**	.606**	.451*		-.322	-.309
Occipital WM	-.553**	.684**	.505**		-.427*	-.369*
Centrum Semi.	-.313	.524**			-.337	

Chapter 4

Relationship of Birth Weight and Cerebral Development

Abstract

Preterm birth is associated with high risk for adverse neurodevelopmental outcome. The role of birth weight in the prediction of these outcomes is unclear. We evaluated the relationship of birth weight to cerebral injury and development in a preterm baboon model. Baboons were delivered at 125 d gestation (dg, term ~ 185 dg) and ventilated for 14 d (n = 29) prior to euthanization, or delivered and euthanized at 140 dg (n = 11). Cerebral injury and development were evaluated using magnetic resonance imaging (MRI), diffusion tensor imaging (DTI) and histopathology. There was no relationship between birth weight and gender or severity of illness. Higher birth weight was associated with heavier brain weight ($p < .05$) and larger fronto-occipital distance, biparietal distance, transcerebellar distance and width of the basal ganglia (all $p \leq .001$). Birth weight did not relate to qualitative MRI scoring of cerebral injury. Higher birth weight was also associated with higher diffusion anisotropy in parietal WM ($p < .05$) and lower anisotropy in occipital cortex ($p < .05$) and thalamus ($p < .01$). Low birth weight may indicate subtle intrauterine insufficiencies that predispose to abnormal cerebral growth and maturation. Therefore, birth weight may be a better standard than gestational age to assess cerebral development in the premature infant.

Introduction

Prematurity is associated with long-term neurodevelopmental disabilities (Taylor et al., 2000; Anderson and Doyle, 2003; Marlow et al., 2005; Moster et al., 2008), yet the

role of gestational age or weight at birth in the prediction of these outcomes is not entirely clear. Separating these two factors presents challenges due to their collinearity with the most immature infants being the smallest. In addition, small for gestational age (SGA) infants are more likely than those with birth weights appropriate for gestational age (AGA) to be born preterm (Lackman et al., 2001). SGA infants have a 5-fold risk of mortality and a 2-3-fold risk of neonatal morbidities, such as bronchopulmonary dysplasia or retinopathy of prematurity, compared to AGA infants (Lackman et al., 2001; Regev et al., 2003; Bartels et al., 2005). SGA infants also have abnormal cerebral volumes and altered cortical folding on magnetic resonance imaging (MRI), suggesting that they are at increased risk for poor outcomes (Tolsa et al., 2004; Dubois et al., 2008b; Lodygensky et al., 2008). Yet evidence for the association between birth weight and long-term neurodevelopmental outcomes is mixed. Some studies have found that cerebral palsy, blindness, deafness and particularly cognitive and behavioral disabilities are more common in children born SGA (Sung et al., 1993; Hutton et al., 1997; Bardin et al., 2004; Feldman and Eidelman, 2006), while other studies have found no difference in outcomes (Gortner et al., 2003; Roelants-Van Rijn et al., 2004; Kan et al., 2008; Procianoy et al., 2009).

As usually defined, "SGA" refers to low birth weight, without any consideration of underlying cause. Infants with chromosomal and anatomic abnormalities or infective causes for low birth weight are generally excluded from analyses of outcome. Of the remaining SGA infants, some may be constitutionally small – so-called "normal SGA" – while others may have placental insufficiency leading to intrauterine growth restriction (IUGR). Estimations of gestational age have inherent errors due to method biases (Lynch

and Zhang, 2007; Callaghan and Dietz, 2010), so some AGA infants may even be incorrectly categorized as SGA, confounding analysis of outcomes. Thus, the question remains whether birth weight is independently associated with cerebral development.

An animal model of premature birth provides a unique opportunity to understand the connection between birth weight and cerebral injury and development. The premature baboon (*Papio papio)* model was developed to study respiratory outcomes of ventilatory strategies, but is also available to assess the impact of these therapies on the brain. This model is highly relevant because the premature baboon infant receives standard neonatal care; has no direct ischemic or inflammatory insult; and displays patterns of cerebral injury that resemble those in the human preterm infant (Dieni et al., 2004; Inder et al., 2005a). Human studies may be complicated by genetic variability in study populations, uncertainty of fetal gestational ages, and spontaneous preterm delivery. In contrast, the baboon model has less genetic variability, gestations timed by characteristic maternal sex skin changes, and elective deliveries. In the present study, baboon infants were delivered prematurely at 125 days of gestation (dg) (equivalent to 26 weeks human gestation; term ~ 185 dg), and received 14 days of neonatal care prior to sacrifice. Cerebral outcomes were evaluated using qualitative and quantitative assessments of *ex vivo* magnetic resonance imaging (MRI), including conventional T1- and T2-weighted imaging and diffusion tensor magnetic resonance imaging (DTI). Within this model, we sought to explore the relationship between birth weight and cerebral injury and development.

Methods

Studies were performed at the Southwest Foundation for Biomedical Research, San Antonio, TX. All animal husbandry, handling, and procedures were approved to conform to American Association for Accreditation of Laboratory Animal Care guidelines.

Delivery and Instrumentation. Pregnant baboon dams (*Papio papio*) with timed gestations were treated with 6 mg of intramuscular betamethasone 48 and 24 hours prior to elective hysterotomy under general anesthesia. Study animals were delivered at 125 ± 2 dg. At birth, animals were weighed, sedated, intubated and treated with 4 mL/kg of surfactant (Survanta, courtesy Ross Laboratories, Columbus, OH) prior to initiation of ventilatory support.

Respiratory Management and Treatment. Animals from three independent trials of therapeutic interventions were included. In each trial, animals were randomized to receive standard neonatal care, or standard care plus one additional pharmacotherapy. In all animals, initiation of positive pressure ventilation (InfantStar ventilator; Infrasonics, San Diego, CA) began immediately after delivery and continued for 14 days. In the estrogen study, animals were randomized to receive estradiol by a 0.5 mg, 21-day extended release subcutaneous pellet placed at 1 hour of life, to examine the effect of postnatal estrogen on the premature lung (McCurnin et al., 2009). In a second study, to examine the pulmonary effects of non-surgical closure of patent ductus arteriosus,

animals were randomized to receive ibuprofen (McCurnin et al., 2008). Animals in the third study were randomized to receive high-dose erythropoietin, which is thought to be neuroprotective. Blood pressure, heart rate, arterial pH and blood gases were monitored continuously. To assess the severity of illness of each animal, we calculated a modified CRIB score, which included only the three variables assessing acute physiologic stability (maximum base excess, and maximum and minimum appropriate FiO2 in the first 12 h) of the original six (Network, 1993).

Any baboon infant in these trials for whom high-resolution MR imaging was available was included in this analysis: standard care (n = 10), estrogen (n = 9), ibuprofen (n = 2) and erythropoietin (n = 8). At 139 dg, animals were euthanized with sodium pentabarbitone (130 mg/kg intravenously). For gestational control brains, additional pregnant baboon dams were treated with 6 mg of intramuscular betamethasone at 123 and 124 dg and animals delivered by elective hysterotomy at 140 dg (n = 11).

Conventional MRI. After sacrifice, brains were extracted, weighed and immersed in 4% paraformaldehyde in 0.1M phosphate buffer. MR Imaging was performed using a 33-cm clear bore, 4.7-tesla magnet controlled by a Varian INOVA console. The fixed brains were placed in sealed plastic containers filled with 4% paraformaldehyde, which fit inside a single-turn RF coil for imaging. T2-weighted images were acquired using spin echo pulse sequence, with 500-μm isotropic voxels, TE = 110 ms, and TR > 3 × T1 (> 7 s) so that T1 contrast was minimized. T1-weighted images were acquired using a modified driven equilibrium Fourier Transform (MDEFT)

sequence, with 500-μm isotropic voxels, TI = 600 ms, and TE minimized (= 17 ms); TR was set automatically to 2×TI, due to the timing requirements of the MDEFT sequence.

Quantitative measurements of the brain were made from T1- and T2-weighted images using Analyze v7.0 software (Rochester, MN): frontal-occipital distance, length of the corpus callosum, bifrontal and biparietal distances, craniocaudal distance, width of the basal ganglia, lateral ventricular distance, and transverse cerebellar distance. The images were also used to assess brain injury and development qualitatively by two readers blinded to treatment group. Scores from 0 (normal) to 3 (severe delay) were assigned for gyration, myelination, white matter abnormality, ventriculomegaly and hemorrhage. The subventricular zone and frontal tracts – populations of proliferating and migrating cells transiently present during development – were assessed to be absent (0), present (1), or prominent (2).

Diffusion Tensor MRI. Diffusion data were acquired using a spin-echo pulse sequence modified by the addition of a diffusion-sensitization gradient pulse pair. The brains were imaged using a 25-direction sampling scheme in which gradient strength was varied across each of the 25 gradient orientations to produce a range of *b*-values. An early set of acquisitions used *b*-values from 0 – 12,500 s/mm^2 (TE = 67 ms, TR = 3-7 s, nt ≥ 6, diffusion gradient duration = 15 ms, delay between diffusion gradients = 50 ms, and diffusion gradient amplitude = 0-38 Gauss/cm). Later acquisitions used *b*-values from 187 – 11,300 s/mm^2 (TE = 70 ms, TR = 4.7-6.7 s, nt = 4, diffusion gradient duration = 11.5 ms, delay between diffusion gradients = 50 ms, and diffusion gradient amplitude = 3-25 Gauss/cm). All diffusion images used 500-μm isotropic voxels.

Raw data from diffusion studies were phase-corrected using Bayesian probability analysis so that noise was Gaussian and centered about zero. A diffusion tensor was estimated for each voxel using a model selection algorithm. The mean and standard deviation of the eigenvalues of this diffusion tensor were used to calculate the apparent diffusion coefficient (ADC) and relative anisotropy (RA), respectively. Using Analyze software, regions of interest (ROIs) were manually drawn on horizontal slices of the four diffusion parameter maps. Regions included frontal, parietal and occipital white matter (WM); centrum semiovale; WM tracts, including the corpus callosum (CC) and the anterior and posterior limbs of the internal capsule (ALIC, PLIC); frontal, sensorimotor and occipital cortex; and caudate, putamen and thalamus (Figure 4.1).

Statistical analysis. Statistical analysis was performed using the Statistical Package for the Social Sciences, v17 (SPSS, Chicago, IL). Linear regression analysis was performed to determine whether each of the quantitative metrics, qualitative scores and regional diffusion values at sacrifice was significantly correlated with birth weight. Because premature birth and development *ex utero* is a known risk factor for cerebral injury or delayed maturation, animals were coded as premature (birth at 125 dg and treatment for 14 d) or control (birth at 140 dg). Both birth weight and premature/control status were included in a multiple regression model. Birth weight was considered to be significantly related to an outcome variable if its inclusion in the model resulted in a significant ($p < .05$) change in R^2. For those outcome variables that were significantly related to birth weight, the coefficient of birth weight in the model, β, is reported. The

relationships between 1) birth weight and gender, and 2) birth weight and severity of illness (modified CRIB score) were evaluated using Pierson's correlation coefficients.

Results

Birth weight, gender and illness. The mean birth weight of animals delivered at 125 dg (n = 29) was 387 g (range 325 – 440 g). Gestational controls delivered at 140 dg (n = 11) had a mean birth weight of 516 g (range 435 – 622 g). There was no relationship between birth weight and gender or between birth weight and severity of illness.

Conventional MRI – Brain metrics and qualitative brain injury. Brain weight at sacrifice was highly correlated with birth weight (Table 4.1). The coefficient of birth weight in the model was positive, indicating that infants with higher birth weights had heavier brains at sacrifice. The fronto-occipital, biparietal and transcerebellar distances and the width of the basal ganglia were also associated with birth weight (Table 4.1; Figure 4.2). Infants with higher birth weights had larger brain structures on imaging after sacrifice. There was no relationship between birth weight and cerebral injury (Table 4.1).

Diffusion tensor imaging. Higher birth weight was associated with higher anisotropy (RA) in parietal WM following sacrifice (Table 4.2). In occipital cortex and the thalamus, in contrast, higher birth weight was associated with lower RA (Figure 4.3). ADC was not associated with birth weight in any of the cerebral regions (Table 4.2).

Discussion

Weight at birth has a strong relationship to brain weight measures of cerebral size and microstructural maturity. These occurred in both study populations of prematurely born animals cared for in the neonatal intensive care unit and gestational controls. This suggests that birth weight is associated with cerebral growth, independent of premature birth and development *ex utero*. In contrast, qualitative cerebral injury was not related to birth weight. Both cerebral injury and delayed growth are common after premature birth, but our preterm baboon model suggests that they may be influenced, at least in part, by separate factors.

The relationship between birth weight and cerebral development was also demonstrated within the results from the diffusion imaging. In *ex vivo* brain imaging, diffusion parameters are influenced by cellular and microstructural properties of tissue, but not acute physiologic changes that impact diffusion in live subjects (Sun et al., 2003; Sun et al., 2005). Cortical anisotropy is high mid-gestation, due to the transient radial organization of the cortex, and decreases to near zero before term as cortical complexity increases (McKinstry et al., 2002). In contrast, anisotropy in the white matter increases during gestation as axons organize into tight bundles and begin to myelinate (Neil et al., 1998; Mukherjee et al., 2002). The magnitude of water diffusion, or ADC, decreases in both white matter and gray matter during gestation, as cellular density and tissue organization increase (Neil et al., 1998). If infants with higher birth weight have advanced cerebral maturation, cortical RA should be lower and WM RA higher in these

infants. As Table 2 shows, this is indeed the case. Thus, birth weight exerts a potent influence on cerebral growth and development, independent of gestational age.

Infants born prematurely, many of whom have low birth weight, are particularly vulnerable to white matter injury (Volpe, 2009). Abnormalities have also been noted within the cortex and deep nuclear gray matter (Pierson et al., 2007). In the prematurely delivered baboon, anisotropy was associated with birth weight in two GM regions – occipital cortex and thalamus – that are undergoing rapid changes in development from 125 to 140 dg (Dieni et al., 2004) but which are not classically associated with early injury in premature infants. Anisotropy in parietal WM was significantly associated with birth weight. Yet anisotropy in the posterior limb of the internal capsule was not, even though RA in the PLIC was lower in premature infants than in controls, consistent with studies of human preterm infants (Huppi et al., 2001; Cheong et al., 2009). This result supports the theory that low birth weight does not lead to postnatal cerebral injury directly, but instead may represent a marker for delayed cerebral development *in utero*. A key pathway to impaired fetal growth is placental insufficiency. In this baboon study, the placentas were examined for gross pathology at the time of delivery, and there were no abnormalities that would indicate insufficiency in any of the infants. Diagnosis of placental insufficiency is now often made by fetal Doppler ultrasound to measure umbilical artery (UA) blood flow velocity, but it remains unclear if an abnormal UA blood flow velocity predicts neurodevelopmental delays (Kirsten et al., 2000; McCowan et al., 2002). Furthermore, at least some SGA infants with normal UA blood flow have poor neurodevelopmental outcome (Figueras et al., 2008). It has been suggested that some SGA infants may have mild or early placental insufficiency that precedes

abnormalities in UA blood flow (McCowan et al., 2000; Rigano et al., 2001). A fetal sheep model demonstrated that a 12-h period of placental insufficiency during mid-gestation was sufficient to cause periventricular white matter damage and neuronal death in the cerebellum, hippocampus and cerebral cortex (Rees et al., 1999), abnormalities that are very similar to our own findings. Thus, abnormal cerebral maturation *in utero* may be a consequence of even relatively minor placental insufficiency, predisposing to the poor neurodevelopmental outcomes associated with prematurity.

There are clear limitations in our study including the small number of baboons studied and the diversity of clinical trials that the prematurely born baboons underwent. In addition, our findings are based on imaging characteristics with no underlying histology or behavioral outcomes. However, despite these limitations, our findings add new insights into the relationship between birth weight and brain development in a primate.

Conclusion

We have shown that low birth weight is associated with small brain metrics and immature diffusion characteristics, independent of prematurity. Low birth weight may indicate subtle intrauterine insufficiencies that predispose to abnormal cerebral growth and maturation. Thus, birth weight may be a better standard than gestational age to assess cerebral development. These findings assist our understanding of the pathway to adverse neurodevelopmental outcomes in small for gestational age infants.

Figures & Tables

Figure 4.1. RA maps of horizontal brain slices showing placement of ROIs. (*A)*, 125 + 14 dg premature brain (brain weight = 325 g); (*B)*, 140 dg control brain (brain weight = 501 g). Scale bar = 1 cm.

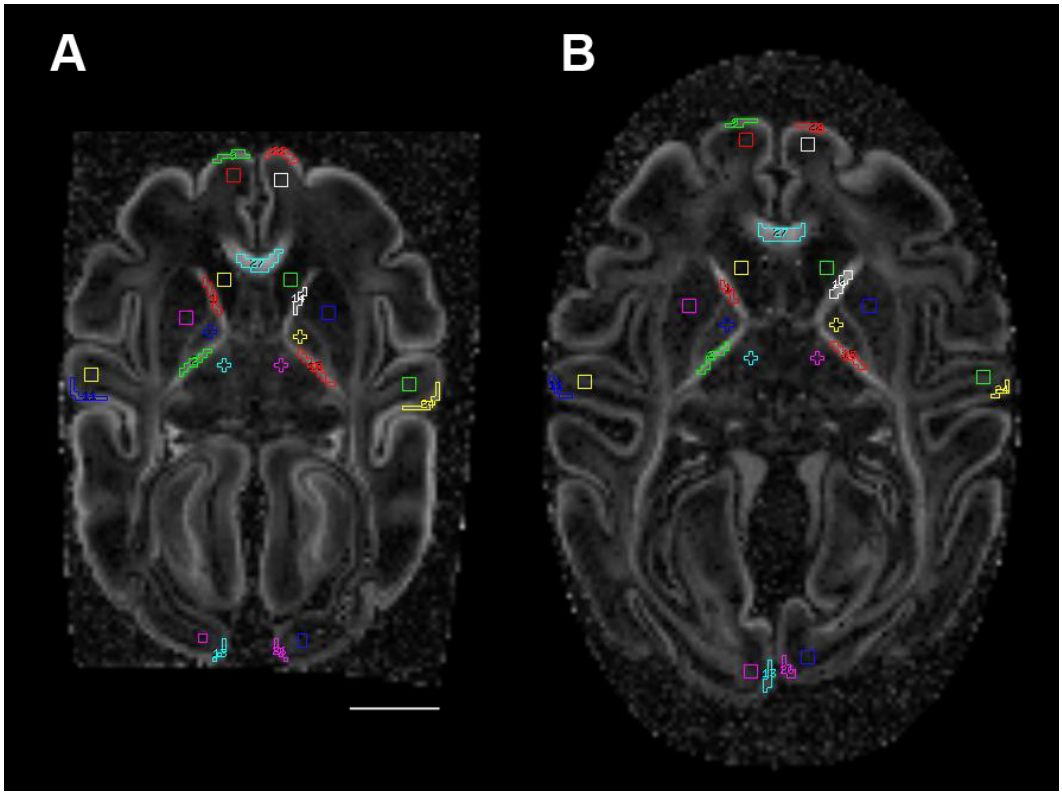

Table 4.1. The results of regression models of the effect of prematurity and birth weight on quantitative brain metrics and qualitative injury scores. R^2 values for the total model (including both predictive variables) are listed. If inclusion of birth weight in the regression model resulted in a significant ($p < .05$) change in R^2, the standardized coefficient of birth weight, β, is listed. * $p < .05$; † $p \leq .001$

	R^2	β
Brain weight (g)	.77*	.47
Brain Growth Metric (mm)		
Fronto-occipital distance	.70†	.85
Length corpus callosum	.05	
Bifrontal distance	.26	
Biparietal distance	.68†	.77
Craniocaudal distance	.05	
Width basal ganglia	.67†	.63
Lateral ventricular width	.15	
Transcerebellar distance	.60†	.74
Injury Score		
Gyration	.05	
Myelination	.07	
WM Abnormality	.28	
Ventriculomegaly	.08	
Hemorrhage	.03	
Subventricular Zone	.07	
Frontal Tracts	.02	

Figure 4.2. Scatter plot showing the relationship between birth weight and fronto-occipital distance. Linear fit lines were calculated in SPSS v17 (SPSS, Chicago, IL); R^2 for the linear model is shown.

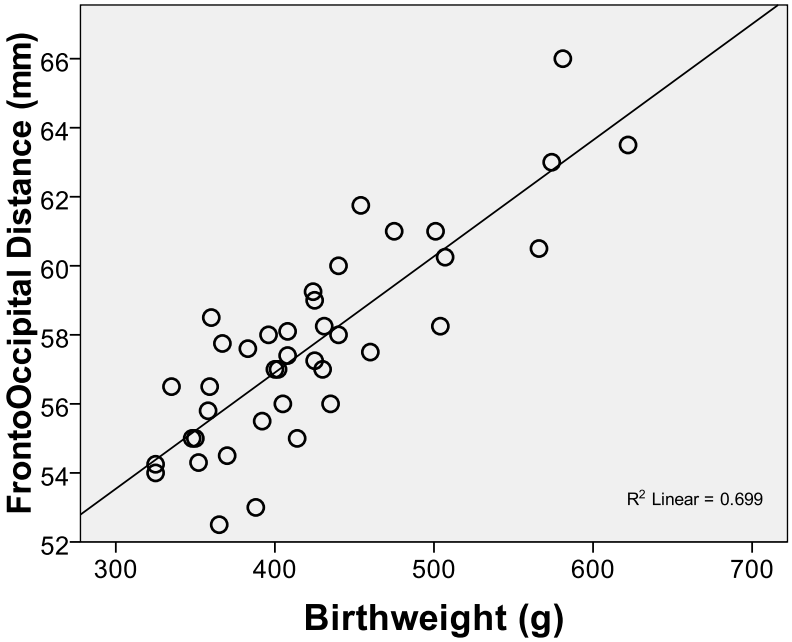

Table 4.2. The results of regression models of the effect of 1) prematurity and 2) birth weight on the diffusion imaging parameters relative anisotropy (RA) and apparent diffusion coefficient (ADC) in cerebral white matter (WM) and gray matter (GM). R^2 values for the total model (including both predictive variables) are listed. If inclusion of birth weight in the regression model resulted in a significant ($p < .05$) change in R^2, the standardized coefficient of birth weight, β, is listed. * $p < .05$; ** $p < .01$.

	RA		**ADC**	
	R²	**β**	***R²***	**β**
WM Tracts				
ALIC	.37		.01	
PLIC	.50		.01	
Corpus Callosum	.07		.27	
Hemispheric WM				
Frontal WM	.06		.21	
Parietal WM	.27*	.62	.10	
Occipital WM	.06		.34	
Centrum Semiovale	.17		.37	
Cortex				
Frontal Cortex	.06		.03	
Parietal Cortex	.07		.01	
Occipital Cortex	.22*	-.51	.15	
Deep nuclear GM				
Caudate	.09		.15	
Globus Pallidus	.12		.04	
Putamen	.19		.02	
Thalamus	.35**	-.63	.02	

Figure 4.3. Scatter plot showing the relationship between birth weight and RA in the occipital cortex. Linear fit lines were calculated in SPSS v17 (SPSS, Chicago, IL); R^2 for the linear model is shown.

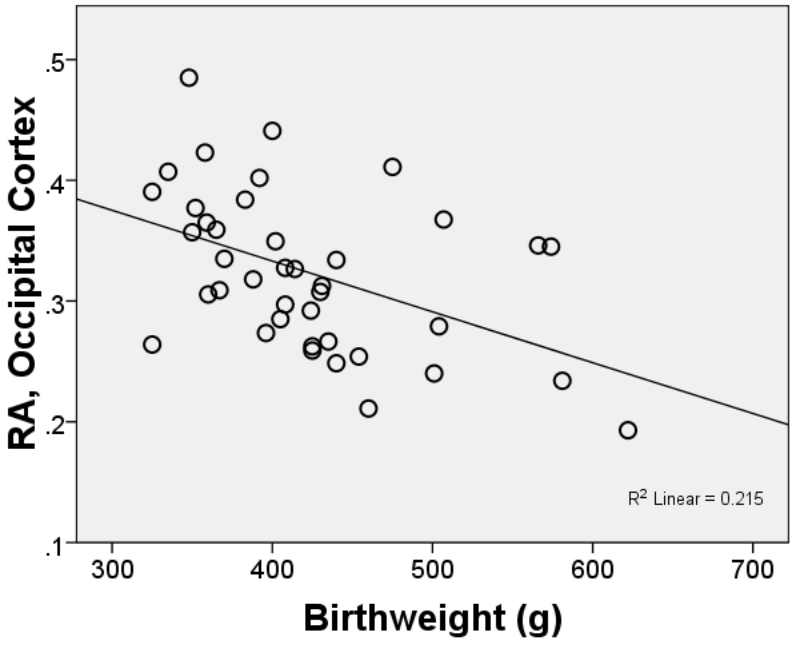

Chapter 5

Effects of Ventilation Strategies on Cerebral White Matter Development

Abstract

Many ventilatory strategies have been proposed to reduce the risk of bronchopulmonary dysplasia (BPD) in premature infants; their impact on the developing brain is unclear. We evaluated cerebral WM outcomes among ventilation strategies in the preterm baboon brain. Baboons were delivered at 125 d gestation (dg, term ~ 185 dg) and maintained in an animal intensive care unit. In a 14 d model, animals (n = 22) were randomized to positive pressure ventilation (PPV) alone, PPV + ibuprofen, or PPV + estrogen. In a 28 d model, animals (n = 14) were randomized to PPV, high frequency oscillatory ventilation (HFOV), early extubation to nasal continuous positive airway pressure (EnCPAP) or delayed extubation to nCPAP (DnCPAP). Gestational control animals were delivered at 140 dg (n = 7) or 153 dg (n = 3). Cerebral white matter (WM) in fixed brains was evaluated using magnetic resonance imaging (MRI) and diffusion tensor imaging (DTI). Few differences in cerebral injury and development were detected among 140 dg models. The 153 dg HFOV group had higher qualitative WM signal abnormality, ventriculomegaly and WM volume loss scores on MRI (all $p < .05$); higher WM apparent diffusion coefficient, axial and radial diffusivity ($p \leq .001$); and lower anisotropy in the ALIC ($p < .05$) than gestational controls and nCPAP groups. While there was a trend toward some WM abnormality in the DnCPAP group, EnCPAP animals did not differ significantly from controls. Protracted ventilation appears to predict cerebral injury in the preterm baboon model at 153 dg.

Introduction

Improvements in respiratory management of preterm infants in the last two decades have contributed to survival rates that now exceed 85% (Fanaroff et al., 2007). Among infants who survive, however, there is a high rate of long-term physical, behavioral, and cognitive impairments (Wilson-Costello et al., 2005; Moster et al., 2008). In order to reduce the risk of these adverse outcomes, we must understand the impact of clinical interventions on brain development in premature infants.

Ventilation strategies currently used in neonates have variable effects on lung and brain outcomes. High frequency oscillatory ventilation (HFOV) was proposed to reduce the risk of bronchopulmonary dysplasia (BPD) compared to conventional mechanical ventilation, although meta-analyses of human studies have demonstrated that ventilation strategy, rather than modality, is the crucial factor (Thome et al., 2005; Cools et al., 2010). The impact of HFOV on the brain is unclear. Some studies have found that HFOV is associated with a greater risk of intracranial hemorrhage and white matter injury than conventional ventilation (Wiswell et al., 1996; Moriette et al., 2001), while other studies have shown no difference in postnatal (Keszler et al., 1997) or two-year outcomes (Marlow et al., 2006) between the two types of ventilation. As the potential risks of ventilation were recognized, early extubation to nasal continuous positive airway pressure (nCPAP) was proposed as a safer alternative. The use of nCPAP has been associated with fewer days of ventilation (Morley et al., 2008) and decreased rates of BPD (Meyer et al., 2004; Kirchner et al., 2005). However, two-year neurodevelopmental

outcomes in infants treated with nCPAP do not appear different than those of ventilated infants (Stack and Jalaludin, 2007).

The impact of mechanical ventilation on respiratory and cerebral outcomes might be improved by the use of adjuvant therapies to correct anatomic and biochemical disturbances that are common in premature infants. For instance, a persistent patent ductus arteriosus is associated with increased risk of BPD (Marshall et al., 1999). In a primate model of lung injury, closure of a patent ductus arteriosus by the administration of ibuprofen improved pulmonary mechanics (McCurnin et al., 2008). Further, nitric oxide synthase, which promotes maturation in the developing lung by generating endogenous nitric oxide, is expressed at lower levels in prematurely-born infants than *in utero* (Afshar et al., 2003). In the primate model, postnatal administration of estradiol increased lung nitric oxide synthase, and treated infants showed improved lung function and decreased need for ventilatory support (McCurnin et al., 2009).

To examine the neuropathological effects of randomized ventilatory strategies on cerebral injury and development, an animal model is necessary. The immature baboon (*Papio papio)* model was developed to study respiratory outcomes, but is also available to assess the impact of therapies on the brain. This model is highly relevant to the preterm human infant because the baboons receive no "intentional" ischemic or inflammatory insult as in other animal models, but instead receive standard neonatal care (Dieni et al., 2004; Inder et al., 2005a). Baboons are delivered prematurely at 125 days of gestation (dg, term ~185 dg), equivalent to 26 weeks human gestation, and are maintained in an animal intensive care unit for either 14 or 28 d prior to euthanization. Cerebral outcomes of specific ventilatory strategies in this model have been previously

evaluated by histopathology (Loeliger et al., 2006; Loeliger et al., 2009b; Loeliger et al., 2009a; Loeliger et al., 2010). In the present study, we use conventional MRI and DTI of fixed brain to show the variability of cerebral WM outcomes among these same ventilation strategies – positive pressure ventilation (PPV), HFOV, early extubation to nCPAP, delayed extubation to nCPAP, treatment with ibuprofen, and treatment with estrogen.

Methods

Animal tissue was prepared at the Southwest Foundation for Biomedical Research, San Antonio, TX. All animal husbandry, handling, and procedures were approved to conform to American Association for Accreditation of Laboratory Animal Care guidelines. MR imaging was done at the Washington University School of Medicine in St. Louis.

Delivery and Instrumentation. Pregnant baboon dams (*Papio papio*) were treated with 6 mg of intramuscular betamethasone 48 and 24 hours prior to elective hysterotomy under general anesthesia. Timed gestations were determined by characteristic sex skin changes and confirmed by serial fetal ultrasounds. Study animals were delivered at 126 ± 2 dg. At birth, animals were weighed, sedated, intubated and treated with 4 mL/kg bolus of exogenous surfactant (Survanta, courtesy Ross Laboratories, Columbus, OH) through the endotracheal tube.

Respiratory Management and Treatment. The management, monitoring and treatment strategies of all baboon infants in this analysis have been described in detail in previous publications (Yoder et al., 2000; Thomson et al., 2006; McCurnin et al., 2008; McCurnin et al., 2009).

In a 140 dg model, initiation of PPV (InfantStar ventilator; Infrasonics, San Diego, CA) began immediately after delivery and continued for 14 days. In a study of the effect of postnatal estradiol on the premature lung, animals were randomized to the PPV group, which received routine care, or to the estrogen group, which received routine care plus subcutaneous placement of a 0.5 mg, 21-day extended release estradiol pellet at 1 hour of life (McCurnin et al., 2009). In a second study, to examine the pulmonary effects of non-surgical closure of patent ductus arteriosus, animals were randomized to the PPV group or to an ibuprofen group; 10 mg/kg ibuprofen was administrated intravenously at 24 hours of life, and four additional 5 mg/kg doses delivered at subsequent 24-h intervals (McCurnin et al., 2008). At 139 dg, animals were euthanized with sodium pentabarbitone (130 mg/kg intravenously).

In a 153 dg model, animals were ventilated for 28 days according to prior antenatal assignment. One group was maintained on PPV, while another was converted to high-frequency oscillatory ventilation (HFOV) at 5 min of age (Yoder et al., 2000). In a separate study, animals were initially ventilated on PPV, then extubated to nasal continuous positive airway pressure at either 24 hours (EnCPAP) or 5 days (DnCPAP) of life (Thomson et al., 2006). At 153 dg, animals were euthanized.

Tissue collection. After euthanization, brains were extracted, weighed and immersed in 4% paraformaldehyde in 0.1M phosphate buffer. Twenty-two brains from the 140 dg models (PPV, n = 5; Ibuprofen, n = 8; Estrogen, n = 9) and fourteen brains from the 153 dg models (HFOV, n = 5; EnCPAP, n = 4; DnCPAP, n = 5) were available for *ex vivo* MRI and/or DTI. For gestational control brains, additional pregnant baboon dams were treated with 6 mg of intramuscular betamethasone at 123 and 124 dg, animals delivered by elective hysterotomy at 140 dg (n = 7) or 153 dg (n = 3), and euthanized immediately.

Qualitative MRI. Imaging was performed using a 33-cm clear bore, 4.7-tesla magnet controlled by a Varian INOVA console. The fixed brains were placed in sealed plastic containers filled with 4% paraformaldehyde, which fit inside a single-turn RF coil for imaging. T2-weighted images were acquired using a spin-echo pulse sequence, with TE = 100 ms (≈ T2) and TR set to 8–11 s, depending on the number of slices being acquired. Slice thickness was 500 μm; in-plane resolution was 500 μm x 500 μm.

MR images were scored qualitatively by two experienced readers blinded to treatment group. WM abnormality was graded using three 3-point scales previously described (Inder et al., 2003b) to assess the nature and extent of WM signal abnormality, WM volume loss and ventriculomegaly.

Diffusion MRI. Diffusion data were acquired using a spin-echo pulse sequence modified by the addition of a diffusion-sensitization gradient pulse pair. All of the 153 dg and 10 of the 140 dg brains were imaged using a 6-direction sampling scheme, with b

= 2038 s/mm^2 (TE = 80 ms, TR = 3-7 s, 600-μm isotropic voxel size, diffusion gradient duration = 15 ms, delay between diffusion gradients = 50 ms, and diffusion gradient amplitude = 3.75 Gauss/cm). A reference image was obtained with b = 0 s/mm^2. The remainder of the 140 dg brains were imaged using a 25-direction sampling scheme in which gradient strength was varied across each of the 25 gradient orientations to produce b-values ranging from 0 - 12,500 s/mm^2 (TE = 67 ms, TR = 3-7 s, 500-μm isotropic voxel size, diffusion gradient duration = 15 ms, delay between diffusion gradients = 50 ms, and diffusion gradient amplitude = 0-38 Gauss/cm).

Raw data from diffusion studies were phase-corrected using Bayesian probability analysis so that noise was Gaussian and centered about zero. A diffusion tensor was estimated for each voxel. For the single b-value data, the signal was assumed to decay to zero; for the 25 b-value data, the data were modeled as a monoexponential function plus a constant (Kroenke et al., 2006). The mean and standard deviation of the eigenvalues of this diffusion tensor were used to calculate the apparent diffusion coefficient (ADC) and relative anisotropy (RA), respectively; axial diffusivity, equal to the principal eigenvalue, and radial diffusivity, the mean of the two minor eigenvalues, were also determined. Using Analyze software, regions of interest were defined manually on horizontal slices in frontal, parietal and occipital white matter, in the centrum semiovale, and in white matter tracts, including the corpus callosum (CC) and the anterior and posterior limbs of the internal capsule (ALIC, PLIC).

Statistical analysis. Statistical analysis was performed using the Statistical Package for the Social Sciences, v17 (SPSS, Chicago, IL). Independent samples t tests

were used to determine the statistical significance of differences in diffusion parameters between 140 dg and 153 dg controls. The likelihood ratio was calculated to compare frequencies of qualitative MRI scores among ventilation groups; 140 dg models were evaluated separately from 153 dg models. Differences in diffusion parameters among models were evaluated using one-way ANOVA with *post hoc* analysis (Bonferroni correction). Diffusion values are expressed as group mean ± SEM.

Results

Normal changes in diffusion values with gestational age. Compared to 140 dg controls, 153 dg controls had lower ADC, axial diffusivity and radial diffusivity in the PLIC, and lower radial diffusivity with higher RA in the ALIC (Table 5.1). Differences between gestational ages in other WM regions did not reach significance, but ADC, axial and radial diffusivity tended to be lower, and RA to be higher, at 153 dg.

Qualitative MRI scores across models. *140 dg models*. There were no statistically significant differences among treatments in frequency of WM signal abnormality, WM volume or ventriculomegaly score (Table 5.2). *153 dg models*. There was a significant effect of treatment on WM signal scores at 153 dg, and a trend toward an effect of treatment on WM volume loss and ventriculomegaly scores (Table 5.2). To understand which of the treatments were associated with abnormality, pair-wise analyses of groups were performed. The HFOV group had higher WM signal abnormality scores and WM volume loss scores than gestational controls and both nCPAP groups (all $p <$

.05). Ventriculomegaly scores in the HFOV group were significantly different from 153 dg controls ($p < .05$) but not from nCPAP groups. The DnCPAP group tended to have higher ventriculomegaly scores compared to 153 dg controls ($p = .05$); otherwise, the EnCPAP and DnCPAP groups did not have higher qualitative scores.

Diffusion values across models. *140 dg models.* Compared to 140 dg controls, ADC, axial and radial diffusivity tended to be higher in hemispheric white matter (frontal, parietal, occipital, centrum semiovale) in all preterm groups; these differences reached significance in the ibuprofen group (Figure 5.1). There were no differences in diffusivity among the 140 d models. Estrogen-treated animals had significantly lower RA in the ALIC than gestational controls, while ibuprofen-treated animals had significantly lower RA in the ALIC compared to both controls and the estrogen-treated group (Figure 5.2). In general, WM tracts tended to have lower anisotropy in all preterm groups compared to controls.

153 dg models. The HFOV group had higher ADC, axial and radial diffusivity in WM compared to gestational controls and both nCPAP groups (Figure 5.1). The HFOV group also had lower RA in the ALIC compared to controls and the EnCPAP animals, and tended to be lower than the DnCPAP group (Figure 5.2). The DnCPAP group tended to have higher ADC and lower anisotropy compared to 153 dg controls, while the EnCPAP group was not significantly different.

Discussion

Technical considerations. Fixation affects diffusion parameters in tissue, so that one must exercise caution in interpreting data obtained from fixed tissue. RA values are unchanged by fixation, whereas ADC, axial diffusivity and radial diffusivity are ~30% lower (Sun et al., 2003). Alterations in ADC that survive fixation, such as those reported in this study, do not reflect acute physiologic change or injury. Rather they are a consequence of differences in tissue density/microstructure. Such differences might be in increase in tissue density related to brain maturation (leading to a lower ADC) or a decrease in tissue density related to injury or slowed maturation (leading to a higher ADC). We saw more diffusion abnormalities at 153 dg than at 140 dg, suggesting that WM injury may not have evolved to changes in tissue microstructure by 140 dg.

Another potential concern is that our analysis includes data obtained with two different sets of b values: a 6-direction, single amplitude acquisition, and a 25-direction, 25 amplitude acquisition. In particular, a 25 amplitude acquisition allowed modeling signal decay with a positive constant, whereas the single amplitude acquisition did not; the difference in model selection algorithms between the two data sets could introduce a potential source of bias in our analysis. Recalculating the correlations between DTI parameters and histopathology using only the 6-direction data, which included all of the 153 dg brains and around half of the 140 dg brains, gave the same pattern of correlations. Thus, we included all the data in the final analysis.

Diffusion changes in normal development. In control, fixed baboon brain, WM ADC values decrease and RA values rise during development. These changes parallel those of the live human infant and demonstrate that the fixed baboon brain is a reasonable model of cerebral development in humans. As brain WM matures, water diffusivity decreases as brain water content drops and tissue density increases. RA increases in association with the organization of axons into bundles and subsequent myelination (Huppi et al., 1998a; Neil et al., 1998; Neil et al., 2002). During the period from 140 dg to 153 dg (equivalent to 26 weeks gestation through term in human infants), the anterior and posterior limbs of the internal capsule showed the most significant diffusion changes, probably because these tracts undergo more rapid and earlier myelination than hemispheric WM or the CC (Gilles et al., 1983; Brody et al., 1987).

WM Injury associated with premature birth. Diffusion abnormalities in preterm baboons generally paralleled those reported in human studies. Premature infants have lower anisotropy in the internal capsule and corpus callosum at term equivalent age compared to term infants (Anjari et al., 2007; Rose et al., 2008). The abnormalities in anisotropy are primarily due to higher radial diffusivity in these regions (Counsell et al., 2006). Similarly, premature baboons had lower RA and higher radial diffusivity, particularly in the internal capsule, by 153 dg. Many studies of human infants have compared diffusion parameters in infants with overt WM signal abnormality on conventional MRI to those with normal-appearing WM (Huppi et al., 2001; Miller et al., 2002; Counsell et al., 2003; Cheong et al., 2009). These studies have shown that premature infants have lower anisotropy and higher ADC in WM with signal

abnormalities. In our baboon data, animals with the most WM signal abnormality also had the most abnormal diffusion values.

Comparison of ventilation models. Although none of the 140 dg preterm groups had significant qualitative WM abnormality compared to gestational controls, the brains from animals treated with ibuprofen did have lower anisotropy and higher diffusivity in some WM regions. Because diffusion data were only available for two animals in the PPV group, our statistical analysis was limited, and we cannot say whether ibuprofen treatment has adverse consequences on cerebral development when administered to ventilated infants. Previous histopathological analysis in the preterm baboon showed that ibuprofen therapy is not associated with significant differences in histopathology compared to ventilation alone (Loeliger et al., 2010). The collective evidence suggests that neither ibuprofen nor estrogen treatment is associated with significant positive or negative impact to the 140 dg brain.

The severity and extent of cerebral abnormalities on MRI and DTI were greater at 153 dg, equivalent to 40 weeks postmenstrual age in human infants, than at 140 dg. This may indicate that injury acquired during early postnatal life continues to evolve after two weeks. Alternatively, it may demonstrate the cumulative nature of cerebral insults caused by ventilation and/or other environmental factors. In addition, we must consider that microstructural changes are necessary before diffusion parameter differences are detectable in fixed tissue. Microstructural changes are likely more prevalent at 153 dg than 140 dg.

In our comparison of 153 dg ventilation models, no PPV animals were available for *ex vivo* MRI. However, HFOV was associated with far more alterations in qualitative MRI scores and diffusion abnormalities than either nCPAP group. This is consistent with previous histopathological studies, which showed that HFOV was not associated with greater histopathological cerebral WM injury than PPV (Loeliger et al., 2009a), and that EnCPAP was associated with less injury than either PPV or DnCPAP (Loeliger et al., 2006). In the preterm baboon, it appears that duration of ventilation correlates with cerebral injury: one day of ventilation (EnCPAP) produced less WM abnormality than five days of ventilation (DnCPAP), which produced much less WM abnormality than 28 days of ventilation (HFOV, PPV). In human infants, the risk of cerebral injury and subsequent neurodevelopmental disability has been shown to increase substantially with protracted ventilation (Walsh et al., 2005). Indeed, many investigators have shown that cerebral WM abnormalities on MRI (Aida et al., 1998; Miller et al., 2005; Woodward et al., 2006) or DTI (Arzoumanian et al., 2003; Drobyshevsky et al., 2007; Krishnan et al., 2007; Rose et al., 2007) at term-equivalent age predict long-term neurodevelopmental outcomes.

Conclusion

We have shown that the extent of cerebral white matter injury evident on qualitative MRI and DTI varied among ventilatory strategies. In the 140 dg model, treatment with ibuprofen and estrogen did not have a detectable impact on cerebral development. Among 153 dg models, cerebral injury was significantly related to length

of ventilation. Consequently, early extubation to nCPAP was associated with the least WM abnormalities. These results support the use of a prospective randomized clinical trial to evaluate the impact of EnCPAP on long-term neurodevelopmental outcomes in premature human infants.

Figures & Tables

Table 5.1. Diffusion parameters in gestational control animals. Diffusion values were measured in manually defined regions of interest in the anterior and posterior limbs of the internal capsule (ALIC, PLIC); corpus callosum (CC); centrum semiovale and frontal, parietal and occipital WM. Values are presented as group mean ± SEM. Differences between groups were evaluated using t-tests; *$p < 0.05$ *versus* 140 dg.

WM Region		ADC ($\mu m^2/ms$)	Axial diff.	Radial diff.	RA
ALIC	140 dg	0.29 ± 0.02	0.49 ± 0.03	0.20 ± 0.01	0.48 ± 0.03
	153 dg	0.24 ± 0.04	0.45 ± 0.06	0.13 ± 0.02*	0.65 ± 0.02*
PLIC	140 dg	0.32 ± 0.02	0.56 ± 0.03	0.20 ± 0.01	0.55 ± 0.02
	153 dg	0.22 ± 0.03*	0.38 ± 0.03*	0.13 ± 0.04*	0.70 ± 0.11
CC	140 dg	0.25 ± 0.02	0.43 ± 0.03	0.16 ± 0.01	0.52 ± 0.04
	153 dg	0.27 ± 0.04	0.55 ± 0.05	0.16 ± 0.04	0.69 ± 0.09
Frontal WM	140 dg	0.36 ± 0.04	0.44 ± 0.04	0.32 ± 0.03	0.19 ± 0.02
	153 dg	0.30 ± 0.05	0.38 ± 0.05	0.27 ± 0.06	0.24 ± 0.06
Parietal WM	140 dg	0.33 ± 0.03	0.41 ± 0.03	0.29 ± 0.03	0.19 ± 0.01
	153 dg	0.27 ± 0.03	0.35 ± 0.03	0.23 ± 0.04	0.28 ± 0.05
Occipital WM	140 dg	0.42 ± 0.03	0.51 ± 0.04	0.37 ± 0.03	0.18 ± 0.01
	153 dg	0.32 ± 0.04	0.38 ± 0.03	0.28 ± 0.04	0.20 ± 0.04
Centrum Sem.	140 dg	0.32 ± 0.03	0.40 ± 0.03	0.28 ± 0.02	0.21 ± 0.02
	153 dg	0.35 ± 0.02	0.43 ± 0.02	0.31 ± 0.02	0.17 ± 0.02

Table 5.2. Frequency of qualitative white matter scores (WM signal, WM volume loss, Ventriculomegaly) in 140 dg and 153 dg treatment models. To determine whether there was a significant effect of treatment on WM score, likelihood ratios (df = 6) were calculated for 140 dg treatments and 153 dg treatments; significant likelihood ratios are indicated; *$p < 0.05$, † $p < 0.10$.

WM Abnormality		**Likelihood ratio**	**Model**	**Frequency of Score, *N***		
				1	***2***	***3***
WM Signal	140 dg	7.18	Control	1	4	0
			PPV	2	2	1
			Ibuprofen	6	1	1
			Estrogen	4	3	1
	153 dg	14.55*	Control	3	0	0
			EnCPAP	3	1	0
			DnCPAP	3	2	0
			HFOV	0	3	2
Volume Loss	140 dg	8.73	Control	5	0	0
			PPV	3	1	1
			Ibuprofen	7	0	1
			Estrogen	4	3	1
	153 dg	11.77†	Control	3	0	0
			EnCPAP	4	0	0
			DnCPAP	4	1	0
			HFOV	1	2	2
Ventriculomegaly	140 dg	3.70	Control	4	1	0
			PPV	3	1	1
			Ibuprofen	3	4	1
			Estrogen	4	3	1
	153 dg	10.73†	Control	3	0	0
			EnCPAP	3	1	0
			DnCPAP	2	3	0
			HFOV	1	2	2

Figure 5.1. Apparent diffusion coefficient (ADC), axial and radial diffusivity values ($\mu m^2/ms$) in occipital white matter among 140 dg treatment groups *(left column)* and 153 groups *(right column)*. Box plots represent the median value (horizontal line), interquartile range (IQR) (box) and range (error bars) of scores in each group. A * or ** above a treatment group indicates a significant difference from GCs; a horizontal line indicates a significant difference between groups. $*p < 0.05$, $**p \leq 0.001$.

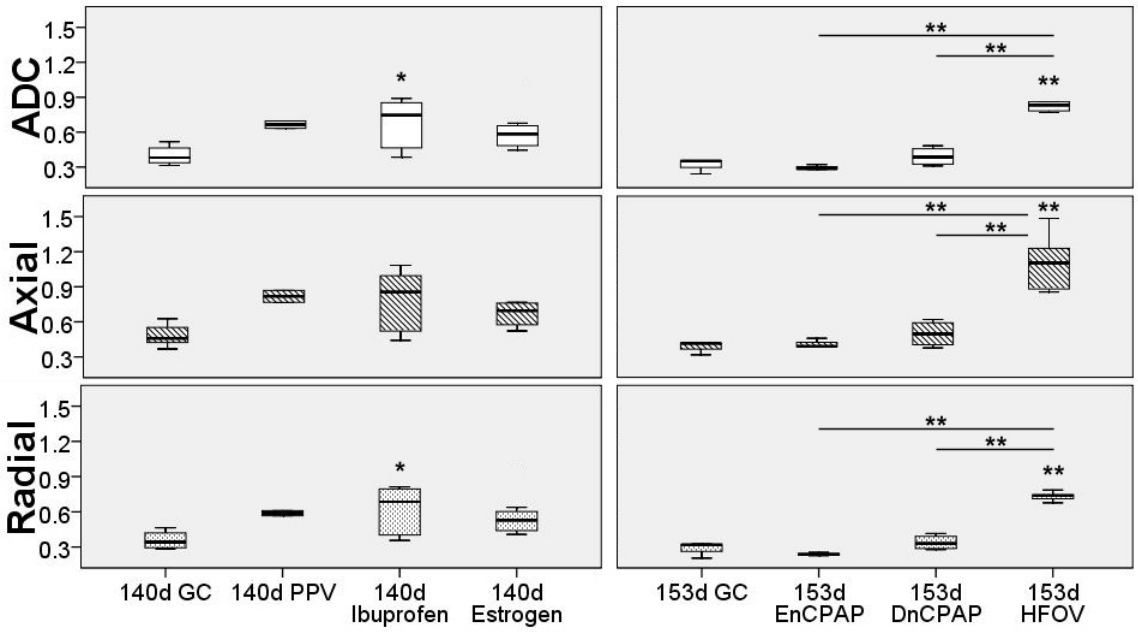

Figure 5.2. Relative anisotropy (RA) in anterior limb of the internal capsule among 140 dg treatment groups *(left column)* and 153 groups *(right column)*. Box plots represent the median value (horizontal line), interquartile range (IQR) (box) and range (error bars) of scores in each group. A * or ** below a treatment group indicates a significant difference from GCs; a horizontal line indicates a significant difference between groups. *$p < 0.05$, **$p \leq 0.001$.

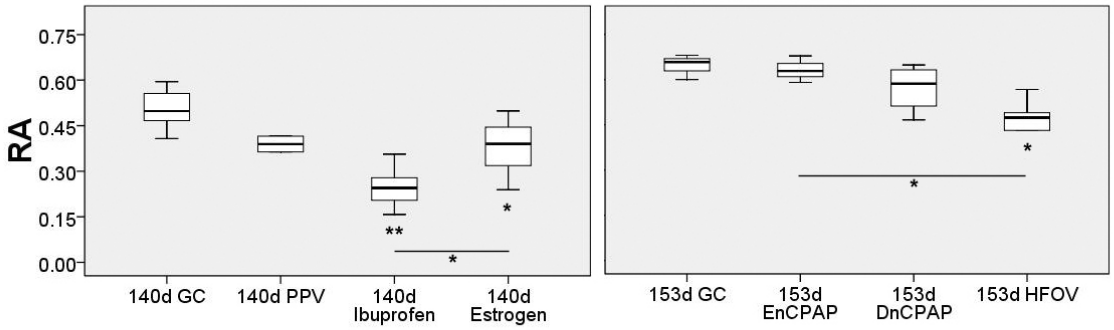

Chapter 6

Effects of Erythropoietin on the Preterm Baboon Brain

Abstract

High dose erythropoietin (EPO) has emerged as a potential neuroprotective strategy in preterm infants. The safety of EPO and the mechanisms by which it might improve cerebral outcomes in this population are unclear. We evaluated the cerebral effects of high dose EPO in baboons delivered at 125 days of gestation (dg, term ~ 185 dg) and ventilated for 14 d prior to euthanization. Premature baboons were randomized to receive high dose EPO for 14 d (n = 8) or no EPO (n = 8). Cerebral outcomes, evaluated on magnetic resonance imaging (MRI), diffusion tensor imaging (DTI) and histopathology, were compared to 140 dg gestational controls (n = 6). Cerebral growth metrics were decreased in both preterm groups ($p < .05$), while ventricular size was increased in the No EPO group compared to controls ($p < .001$) and EPO-treated animals ($p < .05$). Preterm animals had lower diffusion anisotropy in the posterior limb of the internal capsule compared to controls ($p < .001$), while only the No EPO group had lower anisotropy in the anterior limb of the internal capsule ($p < .05$) and higher axial and radial diffusivity in the corpus callosum ($p < .05$), frontal WM ($p < .01$) and occipital WM ($p < .001$). EPO-treated animals also had greater density of proliferative cells in the subventricular zone ($p < .05$) compared to the No EPO group. Administration of high dose EPO does not adversely affect cerebral development in the preterm infant and appears to protect against disturbances in cerebral tissue microstructure.

Introduction

Approximately two percent of infants in the United States are born extremely prematurely (Heron et al., 2010), with the majority surviving, but with a high risk for long-term physical, behavioral, and cognitive impairments (Wilson-Costello et al., 2005; Moster et al., 2008). Adverse neurodevelopmental outcomes in preterm infants have been associated with brain injury, including intraventricular hemorrhage (IVH) and cerebral white matter (WM) injury (Miller et al., 2005; Woodward et al., 2006; Drobyshevsky et al., 2007). Cerebral injury appears to be mediated by ischemia and reperfusion, in addition to inflammation (Back, 2006; Khwaja and Volpe, 2008). However, outcomes are not fully explained by the presence of injury, and it appears that preterm birth, along with exposures in the neonatal intensive care unit, may impact the sequence of typical cerebral development. Factors that have been suggested as being detrimental to cerebral development include endotracheal ventilation; drugs such as analgesics, anesthetic agents and postnatal steroids; inadequate nutrition; and pain and stress (Gressens et al., 2002; Degos et al., 2008). Therefore, strategies to both reduce the risk of injury and enhance the sequence of normal development in the preterm infant may include reducing infants' exposure to potentially deleterious agents and/or administering additional neuroprotective therapies.

Erythropoietin (EPO) has a primary role in promoting red blood cell maturation but has recently emerged as a candidate for neuroprotection in the developing brain. EPO receptors are present in the brain as early as 5 weeks of gestation, and EPO is produced by astrocytes and neurons throughout development (Juul et al., 1999; Dame et

al., 2000). Expression of EPO and its receptors are upregulated in response to cerebral insults, such as hypoxia (Widness et al., 1986). This upregulation may represent a compensatory response to severe or chronic hypoxia (Teramo et al., 2002; Teramo and Widness, 2009), though it remains unclear as to whether endogenous EPO levels can be upregulated sufficiently to provide neuroprotection. Thus, exogenous EPO administration may be required to achieve the levels that appear necessary for neuroprotection. Recombinant human EPO (rhEPO) has been used safely for the last two decades to treat anemia in the preterm infant. No adverse effects have been noted with low dose rhEPO. Of particular relevance, experimental data has shown that rhEPO protects neurons from hypoxia and glutamate toxicity *in vitro* (Konishi et al., 1993; Morishita et al., 1997) and improves outcomes in a neonatal rat model of hypoxic-ischemic cerebral injury (McPherson et al., 2007). In human preterm infants treated for anemia with rhEPO, improved neurodevelopmental outcomes have been noted by some investigators (Bierer et al., 2006).

The use of rhEPO as a neuroprotective agent in the preterm infant has recently been investigated. Two small Phase I/II clinical trials delivering three doses ≤3000 U/kg rhEPO within the first three days of life showed no adverse effects of high-dose EPO treatment (Fauchere et al., 2008; Juul et al., 2008). A recent retrospective cohort study of preterm infants found that higher cumulative rhEPO doses in the first six weeks of life were associated with improved MDI, but not PDI, scores in evaluations after 12 months (Brown et al., 2009).

Although high doses of rhEPO may be neuroprotective, there remains limited data on its safety or on the major mechanisms for improved outcomes in the setting of the

preterm infant. Thus, we aimed to utilize the premature baboon (*Papio papio)* model to evaluate the impact of neuroprotective doses of rhEPO on histological and magnetic resonance imaging (MRI) measures of cerebral injury and development. This model is highly relevant because the baboon infants receive standard neonatal care; have no direct ischemic or inflammatory insult to produce injury; and display patterns of cerebral injury that closely resemble the human preterm infant (Dieni et al., 2004; Inder et al., 2005a). In the present study, baboon infants were delivered prematurely at 125 days of gestation (dg), equivalent to 26 weeks human gestation; term: ~185 dg), and received 14 days of neonatal care prior to sacrifice. Infants were randomized at birth to receive rhEPO (initial 2000 U/kg loading dose, followed by 500 U/kg maintenance doses over a two-week period). This dosing regimen has low individual doses, similar to treatment protocols for anemia, and a high cumulative dose over the two-week period. Cerebral outcomes were evaluated by qualitative scoring of magnetic resonance imaging (MRI), diffusion tensor magnetic resonance imaging (DTI) and histopathology.

Methods

Studies were performed at the Southwest Foundation for Biomedical Research, San Antonio, TX. All animal husbandry, handling, and procedures were approved to conform to American Association for Accreditation of Laboratory Animal Care guidelines.

Delivery and Instrumentation. Pregnant baboon dams (*Papio papio*) with timed gestations were treated with 6 mg of intramuscular betamethasone 48 and 24 hours prior to elective hysterotomy under general anesthesia. Study animals were delivered at 125±2 dg. At birth, animals were weighed, sedated, intubated and treated with 4 mL/kg of surfactant (Survanta, courtesy Ross Laboratories, Columbus, OH) prior to initiation of ventilatory support.

Respiratory Management and Treatment. Initiation of positive pressure ventilation (InfantStar ventilator; Infrasonics, San Diego, CA) began immediately after delivery and continued for 14 days. All other aspects of cardiovascular, nutritional and neonatal care were similar to that of the standard neonatal intensive care unit and have been previously published (McCurnin et al., 2008; McCurnin et al., 2009). Infants were randomized before birth to an EPO group (n=8) or a no EPO group (n=8). Recombinant human EPO (Procrit – Amgen, Thousand Oaks, CA) was administered intravenously: a 2000 U/kg loading dose was given at two hours of age or as soon as the central venous line was in place, followed by 500 U/kg maintenance doses every 12 hours for the first 72 hours and every 24 hours on subsequent days. Animals randomized to EPO treatment also received supplemental iron (1 mg/kg/d; Ferrlicit – Watson Pharma, Corona, CA) beginning on day 7, and Vitamin B12 (3 μg/kg/d) and folic acid (100 μg/kg/d) beginning on day 3. Serum EPO levels were measured in premature animals at 0, 0.5, 3, 6, 12 and 72 hours of life, and at 3-day intervals thereafter until the time of sacrifice (~14 days/336 hours of life) (Figure 6.1).

Tissue collection. After sacrifice, brains were weighed and immersed in 4% paraformaldehyde in 0.1M phosphate buffer. For gestational control brains, additional pregnant baboon dams were treated with 6 mg of intramuscular betamethasone at 123 and 124 dg and animals delivered by elective hysterotomy at 140 dg (n=6).

Physiologic data. PaO_2, $PaCO_2$, pH, FiO_2, mean arterial BP, and heart rate were monitored continuously throughout the experimental period. As described previously (Loeliger et al., 2009b), the "interval flux" of these physiologic variables was calculated by subtracting the minimum value of each variable from its maximum value during each time period (6-h time periods for the first 48 h and daily periods thereafter). The maximum flux and mean flux over the entire experimental course were evaluated.

Conventional MRI. MR imaging was performed using a 33-cm clear bore, 4.7-tesla magnet controlled by a Varian INOVA console. The fixed brains were placed in sealed plastic containers filled with 4% paraformaldehyde, which fit inside a single-turn RF coil for imaging. T2-weighted images were acquired using spin echo pulse sequence, with isotropic voxels 0.5 x 0.5 x 0.5 mm, TE = 110 ms, and TR > 3×T1 (> 7 s) so that T1 contrast was minimized. T1-weighted images were acquired using a modified driven equilibrium Fourier Transform (MDEFT) sequence, with isotropic voxels 0.5 x 0.5 x 0.5 mm, TI = 600 ms, and TE minimized (= 17 ms); TR was set automatically to 2 × TI, due to the timing requirements of the MDEFT sequence.

All imaging analysis was undertaken blinded to the group assignment. Quantitative measurements of the brain were made from T1- and T2-weighted images

using Analyze v7.0 software (Rochester, MN): frontal-occipital, craniocaudal, bifrontal and biparietal distances, length of the corpus callosum, interhemispheric distance, width of the basal ganglia, lateral ventricular width and transverse cerebellar distance. Conventional MR images were also used to assess brain injury and development qualitatively. Scores from 0 (normal) to 3 (severe delay) were assigned for gyration, myelination, white matter abnormality, hemorrhage, and ventricular dilatation. The subventricular zone and frontal tracts – populations of proliferating and migrating cells transiently present during development – were assessed to be absent (0), present (1), or prominent (2).

Diffusion Tensor MRI. Diffusion data were acquired using a spin-echo pulse sequence, with diffusion-sensitization gradient pulse pair. The brains were imaged using a 25-direction sampling scheme in which gradient strength was varied across each of the 25 gradient orientations to produce *b*-values ranging from 187 – 11,300 s/mm^2 (TE = 70 ms, TR = 4.7-6.7 s, 500 μm isotropic voxel size, diffusion gradient duration = 11.5 ms, delay between diffusion gradients = 50 ms, and diffusion gradient amplitude = 3-25 Gauss/cm).

Raw data from diffusion studies were phase-corrected using Bayesian probability analysis so that noise was Gaussian and centered about zero. A diffusion tensor was estimated for each voxel using a model selection algorithm. The mean and standard deviation of the eigenvalues of this diffusion tensor were used to calculate the apparent diffusion coefficient (ADC) and relative anisotropy (RA), respectively; axial diffusivity, equal to the principal eigenvalue, and radial diffusivity, the mean of the two minor

eigenvalues, were also determined. Using Analyze software, regions of interest were manually drawn on axial slices in frontal, parietal and occipital white matter (WM); centrum semiovale; WM tracts, including the corpus callosum (CC) and the anterior and posterior limbs of the internal capsule (ALIC, PLIC); frontal, sensorimotor and occipital cortex; and caudate, putamen and thalamus.

Histology. One-centimeter horizontal blocks from the left forebrain were processed to paraffin, and 8-μm sections at the mid-thalamic level were collected. A stereology system (StereoInvestigator v9.0, MBF Bioscience, Williston, VT) was used to count cells. Analyses were performed on coded slides blinded to treatment group.

Areal density of astrocytes. Rabbit anti-cow glial fibrillary acidic protein (GFAP; 1:500, Sigma, St Louis, MO) was used to identify astrocytes. GFAP-IR cells were counted in areas (0.2 mm^2) in frontal, parietal, and occipital WM corresponding to diffusion ROIs.

Areal density of oligodendrocytes. Rat anti-bovine myelin basic protein (MBP, 1:100; Chemicon, USA) was used to identify oligodendrocytes. MBP-IR oligodendrocytes were counted in areas (0.2 mm^2) in frontal, parietal, and occipital WM corresponding to diffusion ROIs.

Ki67-IR cell density in subventricular zone. The density of proliferating cells was determined by assessing Ki67-IR cells in the entirety of the SVZ found along the posterolateral border of the lateral ventricle.

Semiquantitative radial glia scores. The number and extent of GFAP-IR fibers from the SVZ to the cortex were assessed in the parietal region. Scores of 0 – 3 were assigned: 0 –

no radial glial fibers observed; 1 – occasional fibers; 2 – moderate number of fibers; 3 – considerable number of fibers, extending all the way to cortex.

Semiquantitative myelination scores. At 140 dg, myelination assessed by MBP-IR is prominent in the internal capsule, with fibers extending through parietal WM to the cortex, and in the optic radiations. The extent of myelination was scored against this standard on a scale of 0 – 3: 0 = no myelination; 1 – myelinated fibers limited to internal capsule; 2 – some myelinated fibers in parietal WM and optic radiations; 3 – dense bundles of fibers in parietal WM extending to cortex, and through the entire extent of the optic radiations.

Statistical analysis. Statistical analysis was performed using the Statistical Package for the Social Sciences, v17 (SPSS, Chicago, IL). To compare birth weight, gestational age, and mean and maximum flux of physiology measures in the EPO and No EPO groups, independent-samples t-tests were used. For those variables that were not normally distributed, the Mann-Whitney test was used. To compare gender ratio between the two groups, the Fisher's exact test was used. To evaluate whether treatment group was significantly associated with qualitative MRI scores, which were not normally distributed, a Kruskal-Wallis analysis was used. For any variables found to be significant, the differences between each pair of groups (control–EPO, control–No EPO, EPO–No EPO) were evaluated using Mann-Whitney analyses, and the Type I error rate controlled by using a Bonferroni correction (dividing the $p = 0.05$ cut-off by the number of tests used – three). Differences in brain and body weights, quantitative brain metrics,

DTI parameters, and histopathological measures among groups were evaluated with one-way ANOVA with *post-hoc* Bonferroni correction.

Results

Premature group characteristics and physiology. There were no differences between the premature infant groups (EPO and No EPO) in any of the measured physiologic variables (PaO_2, $PaCO_2$, pH, FiO_2, mean arterial BP, and HR), nor in birth weight (EPO, 381 ± 11 g; No EPO, 393 ± 14 g), gestational age at birth (EPO, 124.8 ± 0.5 d; No EPO, 125.1 ± 0.7 d), or sex (M/F: EPO, 5/3; No EPO, 7/1).

Brain and body weights. Brain and body weights at sacrifice were reduced in EPO and No EPO groups compared to gestational controls ($p \leq 0.001$). There was a trend toward higher brain-to-body weight ratio in the EPO group compared to both gestational controls and the No EPO group (Table 6.1).

Quantitative brain metrics. The biparietal cerebral distance ($p \leq 0.001$), width of the basal ganglia ($p < 0.01$), and the transcerebellar distance ($p < 0.05$) were smaller in both premature groups compared to controls (Table 6.1). The lateral ventricular width was larger in the No EPO group compared to controls ($p \leq 0.001$) and to the EPO group ($p < 0.05$); lateral ventricular width in the EPO group was not different from controls. The length of the corpus callosum, bifrontal distance and craniocaudal distance did not differ among groups.

Qualitative assessment of brain injury on MRI. T2-weighted axial slices of representative brains from each group are shown in Figure 6.2. Only two brains, both from the No EPO group, showed evidence of hemorrhage. There were no differences in gyration, subventricular zone or frontal tracts scores among the groups. The WM index was increased in both EPO and No EPO groups compared to gestational controls (Figure 6.3). Among the components of the WM Index, WM abnormality was increased ($p < 0.01$) in both premature groups, while there was a trend for ventriculomegaly score to be increased only in the No EPO group ($p = 0.03$). Myelination scores in the premature group did not differ from controls. The EPO group did not differ significantly from the No EPO group on any of the qualitative scores.

DTI parameters. Mean values for the diffusion parameters are shown in Table 6.2. The No EPO group had lower RA in the ALIC ($p < 0.05$) and PLIC ($p < 0.001$) and higher axial and radial diffusivity in the PLIC (both $p < 0.01$) and CC (both $p < 0.05$) compared to controls, while the EPO-treated group had lower RA ($p < 0.001$) and higher axial and radial diffusivity (both $p < 0.05$) only in the PLIC. ADC, axial and radial diffusivity were higher in frontal (all $p < 0.01$) and occipital WM (all $p < 0.001$) in the No EPO group compared to controls; there was a trend toward higher values in parietal WM in this group as well. The EPO group did not differ from controls in any of these hemispheric WM regions, but it did differ from the No EPO group in the occipital WM ($p < 0.001$). In the centrum semiovale, RA was lower and ADC, axial and radial diffusivity were higher in both premature groups (all $p < 0.05$). ADC and axial diffusivity were

higher in the occipital cortex (both $p < 0.01$) in the No EPO group, but not the EPO group, compared to controls. There were no differences among groups in other cortical regions.

Histopathology. The density of Ki67-IR cells in the SVZ was lower in the No EPO group compared to controls ($p < 0.01$) and to the EPO group ($p < 0.05$) (Table 6.3; Figure 6.4*A*-*C*). The EPO group did not differ from controls. Myelination was less extensive in both premature groups compared to controls (both $p < 0.001$) (Figure 6.4*D*-*L*). The density of MBP-IR oligodendrocytes did not differ among groups in any of the WM regions (Table 6.3). The density of reactive astrocytes in occipital WM was lower in the EPO group compared to the No EPO group ($p < 0.05$) and controls ($p = 0.106$); the density of astrocytes did not significantly differ among treatments in frontal or parietal WM (Table 6.3: Figure 6.4*M*-*O*). The extent of GFAP-IR radial glial fibers (Figure 6.4*O*) was not different among groups (Table 6.3).

Discussion

This study demonstrates that a high dose of recombinant erythropoietin can be administered to extremely preterm primates over the first 2 weeks of life with no evidence of adverse effect on cerebral injury and development. Indeed, there was evidence of a trend toward neuroprotection with reduction in ventricular size and less widespread disturbance in white matter microstructure on diffusion imaging.

With specific relationship to cerebral growth and development, all of the premature animals were smaller than age-matched gestational controls at necropsy. Brain weight and size were correspondingly small, although the trend toward increased brain/body weight ratio in the EPO group may indicate brain sparing. Otherwise, there was no indication that high-dose EPO improves brain growth after two weeks.

The premature animals displayed a variety of cerebral abnormalities on MRI and histopathology compared to controls, particularly in the white matter. Although only two of the animals showed evidence of hemorrhage, they were both in the No EPO group, indicating that EPO may protect against intracranial bleeding, as has been suggested in a recent trial of human infants (Juul et al., 2008). Ventriculomegaly was a common finding in the premature brains, noted both by quantitative metrics and on qualitative examination. EPO treatment reduced the incidence of moderate-to-severe ventriculomegaly (EPO, 1/8 *vs*. No EPO, 4/8). Although this difference was not statistically significant, it may be of clinical importance, as moderate/severe ventriculomegaly has been associated with an increased risk of abnormal neurodevelopmental outcome (Miller et al., 2005; Woodward et al., 2006). Alterations in DTI parameters demonstrated a similar trend toward a neuroprotective effect of EPO. The ADC in fixed tissue is ~30% lower than in live tissue, while RA, axial and radial diffusivity are unchanged by fixation (Sun et al., 2003). As all the tissue in this analysis was fixed, comparisons among the baboon infant groups are valid. Cerebral WM in the premature baboon infants was characterized by lower anisotropy and higher ADC, axial and radial diffusivity compared to gestational controls, as has been found in human infants (Huppi et al., 2001; Miller et al., 2002; Counsell et al., 2003; Counsell et al.,

2006; Anjari et al., 2007; Rose et al., 2008; Cheong et al., 2009). The pattern of differences between EPO and No EPO groups suggested a regional variability in EPO neuroprotection. While the PLIC and the centrum semiovale – regions associated with motor function – were altered in both premature groups, other regions of hemispheric WM (frontal, parietal, and especially occipital) and the CC were only significantly altered in the No EPO group. This pattern of regional protection fits with evidence from two studies that found EPO treatment to be associated with improved cognitive but not motor outcomes at 12 – 27 months of corrected age (Bierer et al., 2006; Brown et al., 2009).

One of the ways in which EPO is proposed to exert its neuroprotective effects is by promoting oligodendrocyte maturation (Sugawa et al., 2002), as mature oligodendrocytes are less vulnerable to injury than pre-oligodendrocytes. It was surprising, therefore, that there was no difference in the number of mature MBP-IR oligodendrocytes among any of the groups. Still, there were fewer reactive astrocytes found in the occipital WM in EPO-treated animals than those in the No EPO group, and cell proliferation in the SVZ surrounding the posterior portion of the lateral ventricles was preserved in EPO brains compared to controls, while it was decreased in the No EPO group. These changes suggest that EPO's neuroprotective effects may be mediated by many mechanisms, including reduction of injury by glutamate toxicity, nitric oxide and inflammation, anti-apoptotic effects on neurons, or by improving blood flow to the damaged white matter.

Conclusion

We conclude that high-dose EPO treatment is not associated with deleterious effects on cerebral growth and development and appears to provide protection against ventriculomegaly and alterations in WM development. Long-term follow-up of EPO-treated baboon infants is not feasible, and therefore we cannot know whether the trends toward EPO protection of histopathological and imaging parameters would correspond with improved neurodevelopmental outcomes. Still, these findings support the further investigation of high-dose EPO treatment in the premature human infant. Magnetic resonance imaging of preterm infants in such randomized trials may assist in defining the neuroprotective mechanisms.

Figures & Tables

Figure 6.1. Serum erythropoietin concentrations at time (h) after birth in premature animals treated (EPO) or not treated (No EPO) with high dose erythropoietin (2000 U/kg loading dose given at two h of life or as soon as the central venous line was in place, followed by 500 U/kg maintenance doses every 12 hours for the first 72 hours and every 24 hours on subsequent days).

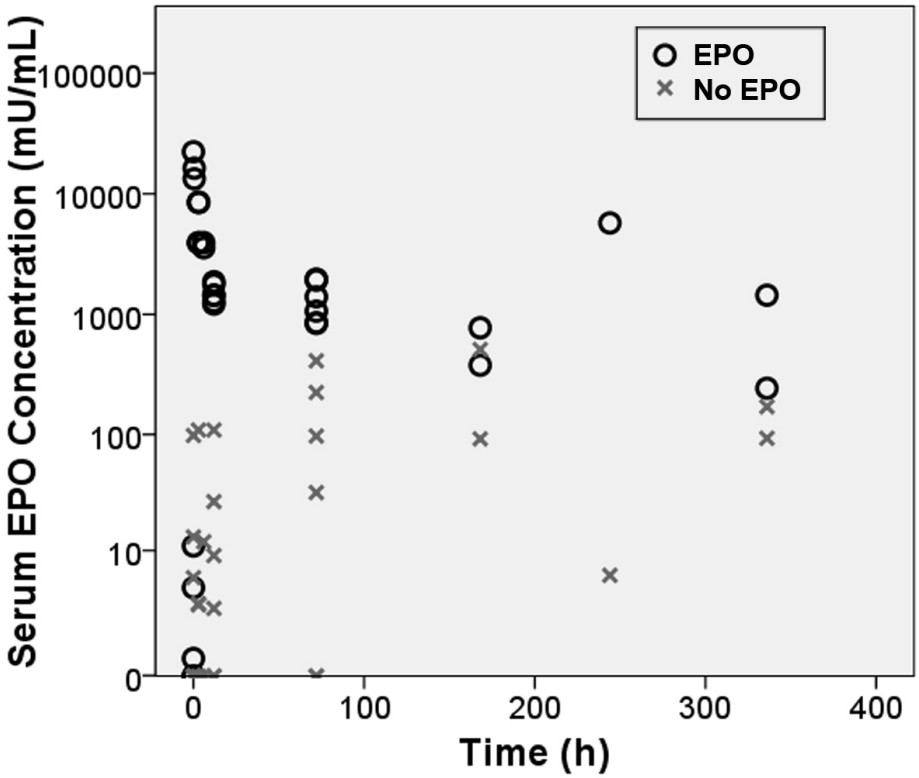

Table 6.1. Cerebral growth metrics. Brain weight of fixed brain was measured at the time of imaging. Fronto-occipital, bifrontal, biparietal, craniocaudal and transcerebellar distances, length of corpus callosum, width of basal ganglia, and lateral ventricular width were measured on MR images. Values are mean ± SEM. † $p < 0.05$; * $p < 0.01$; ** $p \leq 0.001$ *vs.* controls.

	Control	**EPO**	**No EPO**
Brain weight (g)	57 ± 2	44 ± 2**	40 ± 2**
Body weight at necropsy (g)	477 ± 13	347 ± 12**	359 ± 19**
Brain/body weight ratio	0.12 ± 0.01	0.13 ± 0.01	0.11 ± 0.01
Fronto-occipital distance (mm)	59.1 ± 0.9	56.0 ± 0.7†	56.7 ± 0.6
Bifrontal distance (mm)	40.0 ± 0.9	38.1 ± 0.5	38.0 ± 0.6
Biparietal distance (mm)	43.6 ± 1.0	39.0 ± 0.6**	39.4 ± 0.6**
Craniocaudal distance (mm)	35.0 ± 0.8	34.9 ± 0.5	33.8 ± 1.0
Length corpus callosum (mm)	32.6 ± 0.5	31.5 ± 1.5	30.3 ± 1.1
Lateral ventricular width (mm)	0.9 ± 0.1	1.2 ± 0.2	2.1 ± 0.3**
Width basal ganglia (mm)	24.2 ± 0.7	21.6 ± 0.3*	21.1 ± 0.5**
Transcerebellar distance (mm)	25.2 ± 0.7	22.9 ± 0.6†	21.6 ± 0.4**

Figure 6.2. T2-weighted, axial slices of representative brains from each treatment group. The brain from a 140 dg control (*A*) demonstrates normal cerebral size, cortical gyration, and signal characteristics in WM and deep nuclear GM. Brains from premature animals delivered prematurely at 125 dg and ventilated for 14 d (*B,C*) show delayed cerebral growth. Premature animals not treated with EPO (*C*) had significantly larger ventricles than EPO-treated animals (*B*).

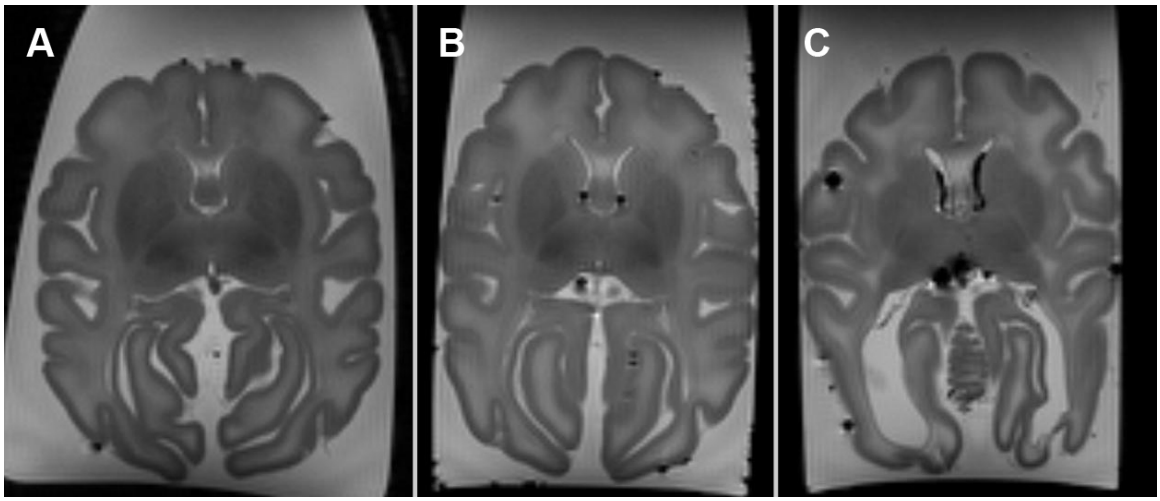

Figure 6.3. Qualitative WM injury scores, evaluated on MRI by two readers blinded to treatment group, in 140 dg controls and premature animals treated (EPO) and not treated (No EPO) with high dose erythropoietin. Box plots represent the median value (horizontal line), interquartile range (IQR) (box) and range (error bars) of scores in each group. WM Index represents the sum of myelination, WM abnormality and ventriculomegaly scores. * $p < 0.01$ *vs.* 140 dg controls.

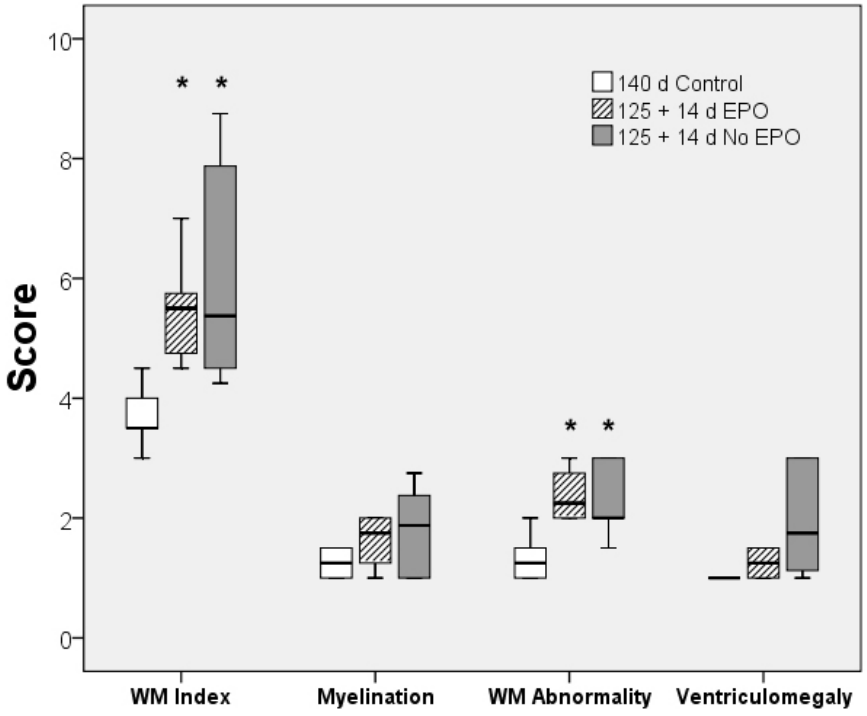

Table 6.2. Diffusion parameters. Relative anisotropy (RA), apparent diffusion coefficient (ADC), axial and radial diffusivity were measured in cerebral regions of interest. Values are group mean ± SEM. † $p < 0.05$; * $p < 0.01$; ** $p \leq 0.001$ *vs.* controls. ALIC, PLIC: anterior, posterior limbs of the internal capsule; CC: corpus callosum.

	Control	EPO	No EPO
RA			
ALIC	0.46 ± 0.01	0.38 ± 0.02	0.35 ± 0.03†
PLIC	0.55 ± 0.02	0.44 ± 0.01**	0.42 ± 0.02**
CC	0.52 ± 0.02	0.48 ± 0.02	0.48 ± 0.02
Frontal WM	0.13 ± 0.01	0.14 ± 0.01	0.12 ± 0.01
Parietal WM	0.16 ± 0.01	0.15 ± 0.01	0.12 ± 0.01
Occipital WM	0.15 ± 0.01	0.13 ± 0.01	0.10 ± 0.01**
Centrum Semiovale	0.15 ± 0.01	0.09 ± 0.01**	0.11 ± 0.01*
Frontal Cortex	0.34 ± 0.02	0.40 ± 0.02	0.36 ± 0.03
Parietal Cortex	0.30 ± 0.01	0.34 ± 0.01	0.33 ± 0.02
Occipital Cortex	0.27 ± 0.02	0.32 ± 0.02	0.33 ± 0.02
ADC (μm^2/ms)			
ALIC	0.27 ± 0.01	0.27 ± 0.01	0.29 ± 0.02
PLIC	0.30 ± 0.01	0.30 ± 0.01	0.30 ± 0.01
CC	0.24 ± 0.01	0.28 ± 0.01	0.34 ± 0.03†
Frontal WM	0.31 ± 0.01	0.38 ± 0.01	0.50 ± 0.06*
Parietal WM	0.33 ± 0.02	0.34 ± 0.01	0.48 ± 0.08
Occipital WM	0.41 ± 0.02	0.51 ± 0.02	0.76 ± 0.05**
Centrum Semiovale	0.34 ± 0.02	0.51 ± 0.04†	0.54 ± 0.04*
Frontal Cortex	0.35 ± 0.01	0.34 ± 0.01	0.36 ± 0.01
Parietal Cortex	0.37 ± 0.01	0.35 ± 0.01	0.37 ± 0.01
Occipital Cortex	0.33 ± 0.01	0.34 ± 0.01	0.38 ± 0.01*

	Control	EPO	No EPO
Axial diffusivity (μm^2/ms)			
ALIC	0.45 ± 0.02	0.41 ± 0.01	0.43 ± 0.01
PLIC	0.54 ± 0.02	0.48 ± 0.01†	0.46 ± 0.01*
CC	0.42 ± 0.02	0.47 ± 0.01	0.57 ± 0.05†
Frontal WM	0.35 ± 0.01	0.44 ± 0.01	0.57 ± 0.06*
Parietal WM	0.38 ± 0.02	0.39 ± 0.01	0.53 ± 0.08
Occipital WM	0.48 ± 0.03	0.58 ± 0.02	0.85 ± 0.05**
Centrum Semiovale	0.40 ± 0.02	0.57 ± 0.04†	0.60 ± 0.05*
Frontal Cortex	0.51 ± 0.02	0.53 ± 0.02	0.53 ± 0.02
Parietal Cortex	0.52 ± 0.01	0.52 ± 0.01	0.53 ± 0.01
Occipital Cortex	0.45 ± 0.01	0.49 ± 0.01	0.54 ± 0.02*
Radial diffusivity (μm^2/ms)			
ALIC	0.18 ± 0.01	0.20 ± 0.01	0.22 ± 0.02
PLIC	0.19 ± 0.01	0.21 ± 0.01*	0.21 ± 0.01*
CC	0.15 ± 0.00	0.19 ± 0.01	0.23 ± 0.03†
Frontal WM	0.29 ± 0.01	0.35 ± 0.01	0.46 ± 0.06*
Parietal WM	0.30 ± 0.02	0.31 ± 0.01	0.45 ± 0.08
Occipital WM	0.38 ± 0.02	0.47 ± 0.02	0.72 ± 0.05**
Centrum Semiovale	0.31 ± 0.02	0.48 ± 0.04*	0.51 ± 0.04*
Frontal Cortex	0.26 ± 0.01	0.24 ± 0.01	0.27 ± 0.01
Parietal Cortex	0.29 ± 0.01	0.27 ± 0.01	0.28 ± 0.02
Occipital Cortex	0.27 ± 0.01	0.26 ± 0.01	0.29 ± 0.01

Table 6.3. Histopathology measurements. The density of Ki67-IR proliferative cells was measured in the subventricular zone (SVZ) along the lateral edge of the occipital ventricular horn. Extent of MBP-IR myelination and GFAP-IR radial glia fibers were evaluated semiquantitatively. The densities of MBP-IR oligodendrocytes (cells/mm^2) and GFAP-IR astrocytes (cells/mm^2) were determined in areas (0.2 mm^2) in frontal, parietal and occipital WM corresponding to diffusion regions of interest. Values are mean ± SEM. * $p < 0.01$; ** $p \leq 0.001$ *vs.* controls.

	Control	**EPO**	**No EPO**
Ki67-IR cells in SVZ	495 ± 48	433 ± 28	281 ± 36*
Extent of myelination	2.7 ± 0.2	1.4 ± 0.2**	1.4 ± 0.2**
MBP-IR oligodendrocytes			
Frontal WM	3.2 ± 1.0	2.3 ± 1.0	2.0 ± 0.6
Parietal WM	13.1 ± 1.4	8.0 ± 1.8	8.1 ± 1.9
Occipital WM	6.0 ± 1.1	4.2 ± 0.9	4.1 ± 0.7
Extent of radial glia fibers	1.8 ± 0.3	1.8 ± 0.2	2.1 ± 0.2
GFAP-IR astrocytes			
Frontal WM	201 ± 16	162 ± 19	214 ± 16
Parietal WM	186 ± 13	185 ± 11	218 ± 17
Occipital WM	202 ± 18	133 ± 18	211 ± 23

Figure 6.4 (*next page*). *A – C*. Ki67-IR in the subventricular zone (SVZ); a lower density of Ki67-IR cells was found in the No EPO group (*C*, $p < 0.01$) compared to controls (*A*) and EPO-treated animals (*B*). *D – L*. MBP-IR in the internal capsule (IC; *D – F*), optic radiations (OR; *G – I*) and parietal WM (*J – L*). The extent of myelination was decreased ($p \leq 0.001$) in both EPO (*E, H, K*) and No EPO (*F, I, L*) groups compared to controls (*D, G, J*). There was no difference in density of MBP-IR oligodendrocytes (black arrows) in parietal WM (*J – L*) among the groups. *M – O*. GFAP-IR in the parietal WM. There was no difference in the density of GFAP-IR astrocytes (black arrows) in the EPO (*N*) and No EPO group (*O*) compared to controls (*M*). Note the GFAP-IR radial glia fibers (gray arrowhead) extending through subcortical WM in the No EPO animal (*O*); there was no difference in the extent of radial glia fibers among the groups.

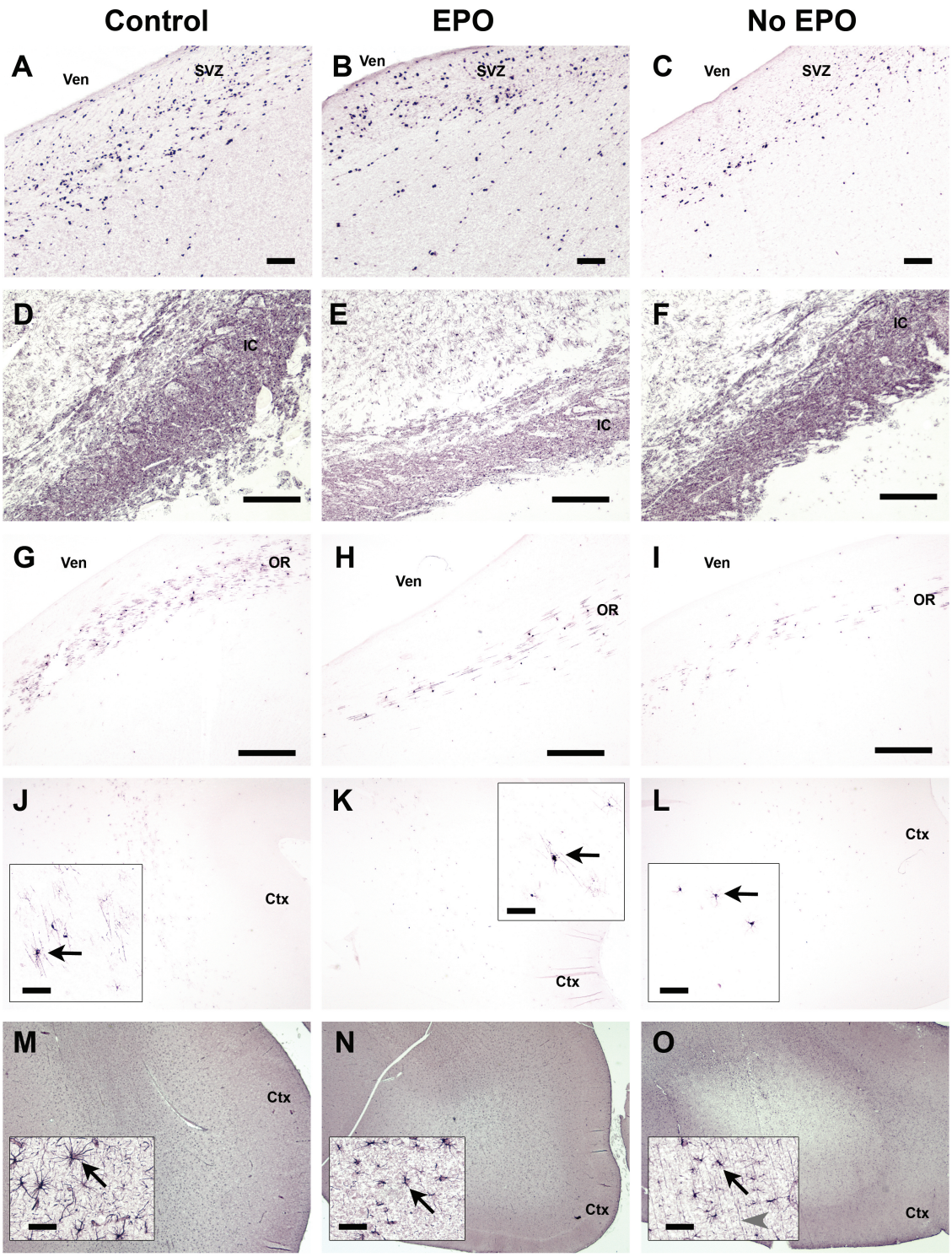
Control
EPO
No EPO
A
Ven
SVZ
B
Ven
SVZ
C
Ven
SVZ
D
IC
E
IC
F
IC
G
Ven
OR
H
Ven
OR
I
Ven
OR
J
Ctx
K
Ctx
L
Ctx
M
Ctx
N
Ctx
O
Ctx

Chapter 7
Conclusions and Future Directions

Improving outcomes of preterm birth

Over the past two decades, the management of the youngest and smallest preterm infants has improved dramatically. Survival rates are now nearly 90% (Fanaroff et al., 2007). Yet the many clinical interventions that are required to ensure the survival of infants may have deleterious effects on the developing brain. High rates of survival therefore provide both the motivation and the primary challenge for those wishing to improve long-term outcomes in prematurely-born children.

To identify therapies that would reduce the risk of neurodevelopmental disability, we need to understand how cerebral development is altered in the preterm infant. Investigation of cerebral pathology in survivors of preterm birth is limited to indirect assessment by imaging modalities. MRI in particular has proven to be a safe and accurate tool for evaluating cerebral development in preterm infants (Neil and Inder, 2004). MRI abnormalities may have value as prognostic markers (Myers and Ment, 2009), but have only limited utility for clarifying pathogenetic mechanisms of cerebral injury and identifying potential therapeutic interventions. Without a clear understanding of the imaging correlates of perinatal brain pathology, MRI will only be a tool for predicting bad outcomes, and not for identifying ways to improve them.

Value of the preterm baboon model

An animal model is the only surrogate for neuropathological analyses in surviving preterm infants. To be relevant, any preterm animal model must demonstrate a pattern of

injury consistent with that found in modern preterm human populations. As the cause of preterm birth cannot be identified in around half of all cases (Committee on Understanding Premature Birth and Assuring Healthy Outcomes, 2006), the results from a direct injury animal model (e.g. induction of hypoxia-ischemia or inflammation) may not be applicable to a large percentage of human infants. In this respect, the preterm baboon model differs from all other animal models and provides its greatest advantage. The cerebral pattern of injury in premature baboons is strikingly similar to that seen in human preterm infants (Dieni et al., 2004), and is produced simply as a result of keeping the baboons alive in an *ex utero* intensive care environment.

Contributions of the present studies

The investigation of the preterm baboon model presented in the first six chapters overcomes limitations inherent in human research studies, and therefore provides a unique understanding of cerebral injury and development in the primate brain.

(i) *Characterize variation in normal WM development.* Previous descriptions of normal development in the human brain have been limited by their study populations. In autopsy studies, investigators are careful to include only infants with accidental or other "non-neural" causes of death. Similarly, imaging studies in live human infants generally include prematurely-born infants without evidence of severe morbidity. To what extent each of these types of study populations are representative of true normal development – or even relevant to each other – may only be speculated.

Electively delivered baboons are likely to have cerebral characteristics that are more representative of normal development *in utero* (Chapter 2). WM diffusion anisotropy increased during gestation, particularly between 140 and 185 dg. The internal capsule, corpus callosum and optic radiations were the first WM regions to show anisotropy changes, followed by the centrum semiovale and other hemispheric WM. Anisotropy changes preceded T2 MRI signal changes and histological evidence of myelination. The changes in MRI and DTI in the preterm baboon paralleled those in human infants, indicating that the preterm baboon model is highly relevant to the preterm infant.

Because the baboon gestations were timed and deliveries elective, it was possible to investigate other factors that may be related to cerebral development. Birth weight was found to correlate with imaging markers of cerebral maturation, independent of gestational age at birth (Chapter 4). Unlike previous studies comparing birth weight and brain development or neurodevelopmental outcomes in human infants, baboons with low birth weight were not growth restricted *in utero*. This suggests that subtle nutritional or placental insufficiencies may affect fetal growth and cerebral development, and even small differences in birth weight may indicate intrauterine compromise. Therefore, birth weight may be a better standard than gestational age to evaluate cerebral development.

(ii) *Imaging correlates of cerebral pathology.* Until now, there has been a gap between neuropathological and imaging descriptions of cerebral injury associated with premature birth. Conclusions about the pathologic nature of abnormalities on MRI and DTI have far outpaced the few attempts to compare histopathological and imaging findings in premature infants (Schouman-Claeys et al., 1993; Felderhoff-Mueser et al.,

1999; Roelants-van Rijn et al., 2001; Guimiot et al., 2008). This is not particularly surprising, however, given that the majority of premature infants survive. Comparison of *in vivo* imaging and neuropathological analysis at autopsy, therefore, is generally limited to those infants with suspected encephalopathy who eventually succumbed to respiratory disease or other morbidities in the neonatal period. Often, these are the infants with the most severe or overt forms of WM pathology, limiting our understanding of imaging correlates of subtle cerebral abnormalities.

The preterm baboon model bridges the gap between characterization of imaging abnormalities and description of pathological injury (Chapter 3). In particular, diffuse astrocytosis was associated with increased T2-weighted signal abnormality and increased ADC in WM, while loss of oligodendrocytes was associated with increased radial diffusivity and decreased anisotropy. Qualitative assessment of MRI abnormalities accurately identified infants with cerebral pathologies, but individual WM scores were not specific. Higher T2 signal and ADC values were shown to correlate with astrocytosis, while increased radial diffusivity and a corresponding decrease in RA reflected the loss of oligodendrocytes. Understanding the microstructural correlates of alterations in diffusion anisotropy, which were shown for the first time in the primate brain in this analysis, will improve interpretation of diffusion imaging studies in premature infants.

(iii) *Impact of individual therapies.* Many aspects of the neonatal intensive care environment are known or suspected to impact the developing brain (Gressens et al., 2002; Degos et al., 2008). The particular therapeutic strategies used in each infant depend on his or her perinatal course and postnatal morbidities and the standards of

practice, both formal and informal, of the institution and clinicians. A wide variation in clinical care and other confounding factors, such as maternal or demographic characteristics, complicate even prospective randomized controlled trials of individual therapeutic interventions.

In the preterm baboon, elective deliveries and randomization of treatment strategies prior to birth allow investigation of the specific effects of individual therapies. Ventilation strategies differentially impact the developing brain (Chapter 5). Prolonged mechanical ventilation was associated with increased cerebral injury and delayed development, while extubation to nasal CPAP within the first day of life significantly reduced the risk of injury. The impact of high-dose erythropoietin, which has been shown to be neuroprotective in other animal models and in adults after stroke, was also evaluated (Chapter 6). Erythropoietin was not associated with any injury to the preterm brain, and it appears to induce proliferation of cells in the subventricular zone, which may increase the capacity for WM repair. These results may help guide clinicians to appropriate ventilation and neuroprotective strategies.

Future directions

Many questions remain about the developing brain and how it is impacted by preterm birth. Three key areas of investigation that could be the targets of future investigations in the preterm baboon model are outlined here.

(i) *Early WM pathology*. In this analysis, DTI parameters in fixed brains correlated strongly with pathology by 153 dg (equivalent to term postmenstrual age in

human infants). At 140 dg, however, there were few changes in pathology, and these did not correlate strongly with imaging findings. One explanation is that our pathology was limited to investigation of certain chronic tissue changes – loss of mature oligodendrocytes, astrocytosis, WM volume loss – for technical reasons. It is possible that diffusion parameters at 140 dg reflect early, transient activation of microglia or necrosis of pre-OLs or other cell populations, subacute histopathological changes that have been described in previous neuropathological studies (Marin-Padilla, 1997; Folkerth, 2007). However, immunohistochemistry for activated microglia or necrosis of pre-oligodendrocytes are technically challenging or impossible in paraformaldehyde-fixed tissue. In addition, WM abnormalities at 140 dg may reflect physiological abnormalities, in addition to microstructural changes. These physiological abnormalities can be detected in live human infants by transient decreases in ADC (Cowan et al., 1994). Although ADC pseudonormalizes by the seventh day post-injury (McKinstry et al., 2002), diffusion imaging (axial and radial diffusivity) may still reflect physiological changes. Yet *ex vivo* brain imaging detects only structural, not physiological abnormalities (Sun et al., 2005). Therefore, *in vivo* diffusion imaging of live premature baboons and histopathological analysis of fresh, not fixed, brain tissue, may further our understanding of imaging correlates of early WM changes.

(ii) *Regional development and injury in the preterm brain.* In this analysis, diffusion parameters were evaluated in small, manually-selected regions of interest in the brain. ROI-based analysis has limitations, including that *a priori* definitions of brain regions are required, and that it can be difficult to systematically apply regions reliably across large study populations. Advanced computational techniques may improve upon

ROI analysis to detect regional differences in the brain. One of these techniques is WM tractography, which uses diffusion anisotropy maps to delineate WM tracts. In human infants, tractography has been used to identify the pattern of normal WM development (Berman et al., 2005; Yoo et al., 2005; Dubois et al., 2008a; Huang et al., 2009) and regional abnormalities in preterm infants (Hoon et al., 2002; Partridge et al., 2006; Anjari et al., 2007; Counsell et al., 2007). Tractography has many technical challenges, not the least of which is that anisotropy is very low in all but a few regions of WM for most of the third trimester, so that only a few tracts may be identified in preterm infants. This problem may be overcome by using more advanced probabilistic methods of tracking (Counsell et al., 2007). In addition, some tract-based methods require alignment of all subjects' data into a common space; infants with severely abnormal brain anatomy due to, for example, ventricular dilation – which is quite frequent in the preterm population – may be difficult to register to other subjects, diluting differences in anisotropy. Despite these hurdles, WM tractography may be valuable to identify non-subjectively the most vulnerable regions across populations of preterm baboons.

Another technique for defining regional cerebral abnormalities is volumetric analysis using high-resolution T1- and T2-weighted imaging. Volumetric studies have proven particularly useful at identifying cortical and deep nuclear gray matter abnormalities in the term-equivalent human infant (Ajayi-Obe et al., 2000). These abnormalities are associated with neurodevelopmental outcome (Adamson et al., 2005; Inder et al., 2005b). Despite our high-resolution diffusion data, we found few differences in GM regions, even though we know from human studies that prematurity is associated with these abnormalities. Volumetric, rather than diffusion-based methods, may be a

better method for identifying GM abnormalities. Identifying alterations in cortex, basal ganglia, thalamus and hippocampus associated with preterm birth or particular interventions in the preterm baboon would help elucidate how these therapies injure the preterm brain and cause long-term neurodevelopmental disability. Both WM tractography and volumetric analysis could be implemented readily in the preterm baboon, as high-resolution, high-quality MRI and DTI data are currently available.

(iii) *Evaluation of potential neuroprotective agents.* Because the preterm baboon model produces a wide variety of cerebral abnormality, including subtle WM disturbances that are so common in human infants, it is ideal for evaluating novel neuroprotective strategies. High-dose erythropoietin (Chapter 6) is just one of many therapies proposed to be neuroprotective. Other therapeutic agents proposed to protect the premature lung have already been tested in the preterm baboon; cerebral outcomes remain to be evaluated. For example, a superoxide dismutase (SOD) mimetic, the metalloporphyrin AEOL 10113, was administered by intravenous infusion (0.5 mg/kg/d) in the preterm baboon model. AEOL 10113 may be indirectly neuroprotective, by reducing the risk of lung disease and its associated neuropathology. Alternatively, this SOD mimetic may protect the brain directly, as it is administered systemically. Because AEOL 10113 is an antioxidant, it may protect pre-oligodendrocytes, the key cellular targets in WM injury, from reactive oxygen species if it can cross the blood-brain barrier. Subjective evaluation of MRI evidence does not show much improvement in cerebral outcomes with administration of AEOL 10113 (Figure 7.1); however, a careful and systematic approach may yet reveal qualitative or diffusion differences. If an antioxidant or other therapy is shown to be neuroprotective in the preterm baboon, translating it to

clinical use would be relatively straightforward in a technical sense, as the timing and dosage would be nearly identical for baboon and human infants. Therefore, the baboon model is ideal for evaluating the novel therapeutic interventions that will be proposed for use in premature human infants. It will continue to be a powerful tool as our understanding of the nature and pathogenesis of cerebral injury in the developing brain is further refined.

Figures

Figure 7.1. T2-weighted, axial slices from MR images of brains imaged at the equivalent of 140 dg. The brain from a 140 dg control (*A*) demonstrates normal cerebral size, cortical gyration, and signal characteristics in WM and deep nuclear GM. Brains from four premature animals delivered prematurely at 125 dg and ventilated for 14 d (*B,C*) show delayed cerebral growth. Brains from two premature animals treated with the superoxide dismutase mimetic 10113C (*C*) show smaller ventricles and less hyperintense WM signal compared to brains from two premature animals receiving no treatment (*B*).

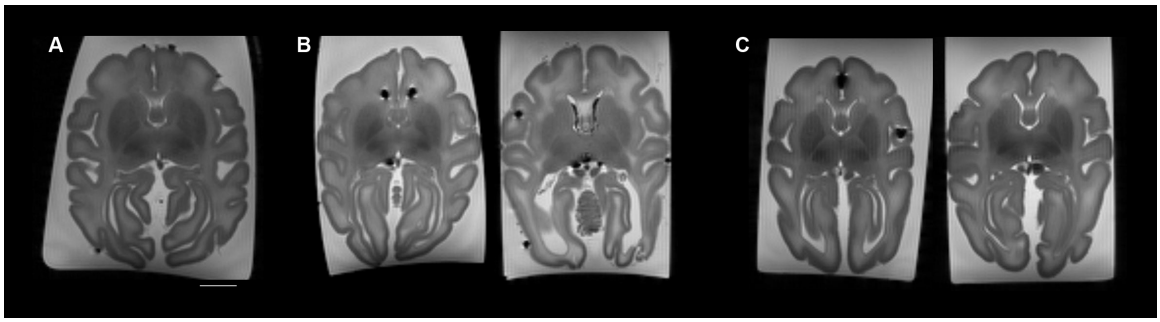

References

Aarnoudse-Moens CS, Weisglas-Kuperus N, van Goudoever JB, Oosterlaan J (2009) Meta-analysis of neurobehavioral outcomes in very preterm and/or very low birth weight children. Pediatrics 124:717-728.

Adamson C, Johnston L, Inder T, Rees S, Mareels I, Egan G (2005) A tracking approach to parcellation of the cerebral cortex. Med Image Comput Comput Assist Interv 8:294-301.

Afshar S, Gibson LL, Yuhanna IS, Sherman TS, Kerecman JD, Grubb PH, Yoder BA, McCurnin DC, Shaul PW (2003) Pulmonary NO synthase expression is attenuated in a fetal baboon model of chronic lung disease. Am J Physiol Lung Cell Mol Physiol 284:L749-758.

Aida N, Nishimura G, Hachiya Y, Matsui K, Takeuchi M, Itani Y (1998) MR imaging of perinatal brain damage: comparison of clinical outcome with initial and follow-up MR findings. AJNR Am J Neuroradiol 19:1909-1921.

Ajayi-Obe M, Saeed N, Cowan FM, Rutherford MA, Edwards AD (2000) Reduced development of cerebral cortex in extremely preterm infants. Lancet 356:1162-1163.

Anderson P, Doyle LW (2003) Neurobehavioral outcomes of school-age children born extremely low birth weight or very preterm in the 1990s. JAMA 289:3264-3272.

Anjari M, Srinivasan L, Allsop JM, Hajnal JV, Rutherford MA, Edwards AD, Counsell SJ (2007) Diffusion tensor imaging with tract-based spatial statistics reveals local white matter abnormalities in preterm infants. Neuroimage 35:1021-1027.

Arzoumanian Y, Mirmiran M, Barnes PD, Woolley K, Ariagno RL, Moseley ME, Fleisher BE, Atlas SW (2003) Diffusion tensor brain imaging findings at term-equivalent age may predict neurologic abnormalities in low birth weight preterm infants. AJNR Am J Neuroradiol 24:1646-1653.

Back SA (2006) Perinatal white matter injury: the changing spectrum of pathology and emerging insights into pathogenetic mechanisms. Ment Retard Dev Disabil Res Rev 12:129-140.

Back SA, Luo NL, Borenstein NS, Levine JM, Volpe JJ, Kinney HC (2001) Late oligodendrocyte progenitors coincide with the developmental window of vulnerability for human perinatal white matter injury. J Neurosci 21:1302-1312.

Back SA, Han BH, Luo NL, Chricton CA, Xanthoudakis S, Tam J, Arvin KL, Holtzman DM (2002) Selective vulnerability of late oligodendrocyte progenitors to hypoxia-ischemia. J Neurosci 22:455-463.

Banker BQ, Larroche JC (1962) Periventricular leukomalacia of infancy. A form of neonatal anoxic encephalopathy. Arch Neurol 7:386-410.

Bardin C, Piuze G, Papageorgiou A (2004) Outcome at 5 years of age of SGA and AGA infants born less than 28 weeks of gestation. Semin Perinatol 28:288-294.

Barkovich AJ, Kjos BO, Jackson DE, Jr., Norman D (1988) Normal maturation of the neonatal and infant brain: MR imaging at 1.5 T. Radiology 166:173-180.

Barnette AR, Neil JJ, Kroenke CD, Griffith JL, Epstein AA, Bayly PV, Knutsen AK, Inder TE (2009) Characterization of brain development in the ferret via MRI. Pediatr Res 66:80-84.

Bartels DB, Kreienbrock L, Dammann O, Wenzlaff P, Poets CF (2005) Population based study on the outcome of small for gestational age newborns. Arch Dis Child Fetal Neonatal Ed 90:F53-59.

Bassan H, Feldman HA, Limperopoulos C, Benson CB, Ringer SA, Veracruz E, Soul JS, Volpe JJ, du Plessis AJ (2006) Periventricular hemorrhagic infarction: risk factors and neonatal outcome. Pediatr Neurol 35:85-92.

Beaulieu C (2002) The basis of anisotropic water diffusion in the nervous system - a technical review. NMR Biomed 15:435-455.

Berman JI, Mukherjee P, Partridge SC, Miller SP, Ferriero DM, Barkovich AJ, Vigneron DB, Henry RG (2005) Quantitative diffusion tensor MRI fiber tractography of sensorimotor white matter development in premature infants. Neuroimage 27:862-871.

Bierer R, Peceny MC, Hartenberger CH, Ohls RK (2006) Erythropoietin concentrations and neurodevelopmental outcome in preterm infants. Pediatrics 118:e635-640.

Billiards SS, Haynes RL, Folkerth RD, Borenstein NS, Trachtenberg FL, Rowitch DH, Ligon KL, Volpe JJ, Kinney HC (2008) Myelin abnormalities without oligodendrocyte loss in periventricular leukomalacia. Brain Pathol 18:153-163.

Bretthorst GL (2008a) Automatic phasing of MR images. Part I: Linearly varying phase. Journal of Magnetic Resonance 191:184-192.

Bretthorst GL (2008b) Automatic phasing of MR images. Part II: Voxel-wise phase estimation. Journal of Magnetic Resonance 191:193-201.

Brody BA, Kinney HC, Kloman AS, Gilles FH (1987) Sequence of central nervous system myelination in human infancy. I. An autopsy study of myelination. J Neuropathol Exp Neurol 46:283-301.

Brown MS, Eichorst D, Lala-Black B, Gonzalez R (2009) Higher cumulative doses of erythropoietin and developmental outcomes in preterm infants. Pediatrics 124:e681-687.

Budde MD, Xie M, Cross AH, Song SK (2009) Axial diffusivity is the primary correlate of axonal injury in the experimental autoimmune encephalomyelitis spinal cord: a quantitative pixelwise analysis. J Neurosci 29:2805-2813.

Budde MD, Kim JH, Liang HF, Schmidt RE, Russell JH, Cross AH, Song SK (2007) Toward accurate diagnosis of white matter pathology using diffusion tensor imaging. Magn Reson Med 57:688-695.

Bui T, Daire JL, Chalard F, Zaccaria I, Alberti C, Elmaleh M, Garel C, Luton D, Blanc N, Sebag G (2006) Microstructural development of human brain assessed in utero by diffusion tensor imaging. Pediatr Radiol 36:1133-1140.

Bystron I, Blakemore C, Rakic P (2008) Development of the human cerebral cortex: Boulder Committee revisited. Nat Rev Neurosci 9:110-122.

Bystron I, Rakic P, Molnar Z, Blakemore C (2006) The first neurons of the human cerebral cortex. Nat Neurosci 9:880-886.

Callaghan WM, Dietz PM (2010) Differences in Birth Weight for Gestational Age Distributions According to the Measures Used to Assign Gestational Age. American Journal of Epidemiology 171:826-836.

Cheong JL, Thompson DK, Wang HX, Hunt RW, Anderson PJ, Inder TE, Doyle LW (2009) Abnormal white matter signal on MR imaging is related to abnormal tissue microstructure. AJNR Am J Neuroradiol 30:623-628.

Chi JG, Dooling EC, Gilles FH (1977) Gyral development of the human brain. Ann Neurol 1:86-93.
Childs AM, Ramenghi LA, Cornette L, Tanner SF, Arthur RJ, Martinez D, Levene MI (2001) Cerebral maturation in premature infants: quantitative assessment using MR imaging. AJNR Am J Neuroradiol 22:1577-1582.
Childs AM, Ramenghi LA, Evans DJ, Ridgeway J, Saysell M, Martinez D, Arthur R, Tanner S, Levene MI (1998) MR features of developing periventricular white matter in preterm infants: evidence of glial cell migration. AJNR Am J Neuroradiol 19:971-976.
Committee on Understanding Premature Birth and Assuring Healthy Outcomes BoHSP (2006) Preterm birth: causes, consequences, and prevention. In: National Academies Press.
Cools F, Askie LM, Offringa M, Asselin JM, Calvert SA, Courtney SE, Dani C, Durand DJ, Gerstmann DR, Henderson-Smart DJ, Marlow N, Peacock JL, Pillow JJ, Soll RF, Thome UH, Truffert P, Schreiber MD, Van Reempts P, Vendettuoli V, Vento G (2010) Elective high-frequency oscillatory versus conventional ventilation in preterm infants: a systematic review and meta-analysis of individual patients' data. Lancet.
Counsell SJ, Allsop JM, Harrison MC, Larkman DJ, Kennea NL, Kapellou O, Cowan FM, Hajnal JV, Edwards AD, Rutherford MA (2003) Diffusion-weighted imaging of the brain in preterm infants with focal and diffuse white matter abnormality. Pediatrics 112:1-7.
Counsell SJ, Shen Y, Boardman JP, Larkman DJ, Kapellou O, Ward P, Allsop JM, Cowan FM, Hajnal JV, Edwards AD, Rutherford MA (2006) Axial and radial diffusivity in preterm infants who have diffuse white matter changes on magnetic resonance imaging at term-equivalent age. Pediatrics 117:376-386.
Counsell SJ, Dyet LE, Larkman DJ, Nunes RG, Boardman JP, Allsop JM, Fitzpatrick J, Srinivasan L, Cowan FM, Hajnal JV, Rutherford MA, Edwards AD (2007) Thalamo-cortical connectivity in children born preterm mapped using probabilistic magnetic resonance tractography. Neuroimage 34:896-904.
Cowan FM, Pennock JM, Hanrahan JD, Manji KP, Edwards AD (1994) Early detection of cerebral infarction and hypoxic ischemic encephalopathy in neonates using diffusion-weighted magnetic resonance imaging. Neuropediatrics 25:172-175.
Dame C, Bartmann P, Wolber E, Fahnenstich H, Hofmann D, Fandrey J (2000) Erythropoietin gene expression in different areas of the developing human central nervous system. Brain Res Dev Brain Res 125:69-74.
Degos V, Loron G, Mantz J, Gressens P (2008) Neuroprotective strategies for the neonatal brain. Anesth Analg 106:1670-1680.
Dehay C, Kennedy H (2007) Cell-cycle control and cortical development. Nat Rev Neurosci 8:438-450.
Dieni S, Inder T, Yoder B, Briscoe T, Camm E, Egan G, Denton D, Rees S (2004) The pattern of cerebral injury in a primate model of preterm birth and neonatal intensive care. J Neuropathol Exp Neurol 63:1297-1309.
Dietrich RB, Bradley WG, Zaragoza EJt, Otto RJ, Taira RK, Wilson GH, Kangarloo H (1988) MR evaluation of early myelination patterns in normal and developmentally delayed infants. AJR Am J Roentgenol 150:889-896.

Dommergues MA, Gallego J, Evrard P, Gressens P (1998) Iron supplementation aggravates periventricular cystic white matter lesions in newborn mice. Eur J Paediatr Neurol 2:313-318.

Drobyshevsky A, Bregman J, Storey P, Meyer J, Prasad PV, Derrick M, MacKendrick W, Tan S (2007) Serial diffusion tensor imaging detects white matter changes that correlate with motor outcome in premature infants. Dev Neurosci 29:289-301.

Drobyshevsky A, Song SK, Gamkrelidze G, Wyrwicz AM, Derrick M, Meng F, Li L, Ji X, Trommer B, Beardsley DJ, Luo NL, Back SA, Tan S (2005) Developmental changes in diffusion anisotropy coincide with immature oligodendrocyte progression and maturation of compound action potential. J Neurosci 25:5988-5997.

Dubois J, Dehaene-Lambertz G, Perrin M, Mangin JF, Cointepas Y, Duchesnay E, Le Bihan D, Hertz-Pannier L (2008a) Asynchrony of the early maturation of white matter bundles in healthy infants: quantitative landmarks revealed noninvasively by diffusion tensor imaging. Hum Brain Mapp 29:14-27.

Dubois J, Benders M, Borradori-Tolsa C, Cachia A, Lazeyras F, Ha-Vinh Leuchter R, Sizonenko SV, Warfield SK, Mangin JF, Huppi PS (2008b) Primary cortical folding in the human newborn: an early marker of later functional development. Brain 131:2028-2041.

Fanaroff AA, Stoll BJ, Wright LL, Carlo WA, Ehrenkranz RA, Stark AR, Bauer CR, Donovan EF, Korones SB, Laptook AR, Lemons JA, Oh W, Papile LA, Shankaran S, Stevenson DK, Tyson JE, Poole WK (2007) Trends in neonatal morbidity and mortality for very low birthweight infants. Am J Obstet Gynecol 196:147 e141-148.

Fauchere JC, Dame C, Vonthein R, Koller B, Arri S, Wolf M, Bucher HU (2008) An approach to using recombinant erythropoietin for neuroprotection in very preterm infants. Pediatrics 122:375-382.

Felderhoff-Mueser U, Rutherford MA, Squier WV, Cox P, Maalouf EF, Counsell SJ, Bydder GM, Edwards AD (1999) Relationship between MR imaging and histopathologic findings of the brain in extremely sick preterm infants. AJNR Am J Neuroradiol 20:1349-1357.

Feldman R, Eidelman AI (2006) Neonatal state organization, neuromaturation, mother-infant interaction, and cognitive development in small-for-gestational-age premature infants. Pediatrics 118:e869-878.

Figueras F, Eixarch E, Meler E, Iraola A, Figueras J, Puerto B, Gratacos E (2008) Small-for-gestational-age fetuses with normal umbilical artery Doppler have suboptimal perinatal and neurodevelopmental outcome. Eur J Obstet Gynecol Reprod Biol 136:34-38.

Fishell G, Kriegstein AR (2003) Neurons from radial glia: the consequences of asymmetric inheritance. Curr Opin Neurobiol 13:34-41.

Folkerth RD (2007) The neuropathology of acquired pre- and perinatal brain injuries. Semin Diagn Pathol 24:48-57.

Garel C (2004) MR imaging of the fetal brain : normal development and cerebral pathologies. Berlin ; New York: Springer.

Gilles FH, Murphy SF (1969) Perinatal telencephalic leucoencephalopathy. J Neurol Neurosurg Psychiatry 32:404-413.

Gilles FH, Leviton A, Dooling EC (1983) The Developing human brain : growth and epidemiologic neuropathology. Boston: J. Wright-PSG.
Gortner L, van Husen M, Thyen U, Gembruch U, Friedrich HJ, Landmann E (2003) Outcome in preterm small for gestational age infants compared to appropriate for gestational age preterms at the age of 2 years: a prospective study. Eur J Obstet Gynecol Reprod Biol 110 Suppl 1:S93-97.
Gressens P (2000) Mechanisms and disturbances of neuronal migration. Pediatr Res 48:725-730.
Gressens P, Rogido M, Paindaveine B, Sola A (2002) The impact of neonatal intensive care practices on the developing brain. J Pediatr 140:646-653.
Guimiot F, Garel C, Fallet-Bianco C, Menez F, Khung-Savatovsky S, Oury JF, Sebag G, Delezoide AL (2008) Contribution of diffusion-weighted imaging in the evaluation of diffuse white matter ischemic lesions in fetuses: correlations with fetopathologic findings. AJNR Am J Neuroradiol 29:110-115.
Haynes RL, Folkerth RD, Keefe RJ, Sung I, Swzeda LI, Rosenberg PA, Volpe JJ, Kinney HC (2003) Nitrosative and oxidative injury to premyelinating oligodendrocytes in periventricular leukomalacia. J Neuropathol Exp Neurol 62:441-450.
Heron M, Sutton PD, Xu J, Ventura SJ, Strobino DM, Guyer B (2010) Annual summary of vital statistics: 2007. Pediatrics 125:4-15.
Hoon AH, Jr., Lawrie WT, Jr., Melhem ER, Reinhardt EM, Van Zijl PC, Solaiyappan M, Jiang H, Johnston MV, Mori S (2002) Diffusion tensor imaging of periventricular leukomalacia shows affected sensory cortex white matter pathways. Neurology 59:752-756.
Huang H, Xue R, Zhang J, Ren T, Richards LJ, Yarowsky P, Miller MI, Mori S (2009) Anatomical characterization of human fetal brain development with diffusion tensor magnetic resonance imaging. J Neurosci 29:4263-4273.
Huppi PS, Maier SE, Peled S, Zientara GP, Barnes PD, Jolesz FA, Volpe JJ (1998a) Microstructural development of human newborn cerebral white matter assessed in vivo by diffusion tensor magnetic resonance imaging. Pediatr Res 44:584-590.
Huppi PS, Warfield S, Kikinis R, Barnes PD, Zientara GP, Jolesz FA, Tsuji MK, Volpe JJ (1998b) Quantitative magnetic resonance imaging of brain development in premature and mature newborns. Ann Neurol 43:224-235.
Huppi PS, Murphy B, Maier SE, Zientara GP, Inder TE, Barnes PD, Kikinis R, Jolesz FA, Volpe JJ (2001) Microstructural brain development after perinatal cerebral white matter injury assessed by diffusion tensor magnetic resonance imaging. Pediatrics 107:455-460.
Hutton JL, Pharoah PO, Cooke RW, Stevenson RC (1997) Differential effects of preterm birth and small gestational age on cognitive and motor development. Arch Dis Child Fetal Neonatal Ed 76:F75-81.
Inder T, Neil J, Kroenke C, Dieni S, Yoder B, Rees S (2005a) Investigation of cerebral development and injury in the prematurely born primate by magnetic resonance imaging and histopathology. Dev Neurosci 27:100-111.
Inder T, Huppi PS, Zientara GP, Maier SE, Jolesz FA, di Salvo D, Robertson R, Barnes PD, Volpe JJ (1999a) Early detection of periventricular leukomalacia by diffusion-weighted magnetic resonance imaging techniques. J Pediatr 134:631-634.

Inder TE, Anderson NJ, Spencer C, Wells S, Volpe JJ (2003a) White matter injury in the premature infant: a comparison between serial cranial sonographic and MR findings at term. AJNR Am J Neuroradiol 24:805-809.
Inder TE, Wells SJ, Mogridge NB, Spencer C, Volpe JJ (2003b) Defining the nature of the cerebral abnormalities in the premature infant: a qualitative magnetic resonance imaging study. J Pediatr 143:171-179.
Inder TE, Warfield SK, Wang H, Huppi PS, Volpe JJ (2005b) Abnormal cerebral structure is present at term in premature infants. Pediatrics 115:286-294.
Inder TE, Huppi PS, Warfield S, Kikinis R, Zientara GP, Barnes PD, Jolesz F, Volpe JJ (1999b) Periventricular white matter injury in the premature infant is followed by reduced cerebral cortical gray matter volume at term. Ann Neurol 46:755-760.
Jevtovic-Todorovic V, Hartman RE, Izumi Y, Benshoff ND, Dikranian K, Zorumski CF, Olney JW, Wozniak DF (2003) Early exposure to common anesthetic agents causes widespread neurodegeneration in the developing rat brain and persistent learning deficits. J Neurosci 23:876-882.
Johnson SA, Young C, Olney JW (2008) Isoflurane-induced neuroapoptosis in the developing brain of nonhypoglycemic mice. J Neurosurg Anesthesiol 20:21-28.
Juul SE, Yachnis AT, Rojiani AM, Christensen RD (1999) Immunohistochemical localization of erythropoietin and its receptor in the developing human brain. Pediatr Dev Pathol 2:148-158.
Juul SE, McPherson RJ, Bauer LA, Ledbetter KJ, Gleason CA, Mayock DE (2008) A phase I/II trial of high-dose erythropoietin in extremely low birth weight infants: pharmacokinetics and safety. Pediatrics 122:383-391.
Kan E, Roberts G, Anderson PJ, Doyle LW (2008) The association of growth impairment with neurodevelopmental outcome at eight years of age in very preterm children. Early Hum Dev 84:409-416.
Kanold PO (2004) Transient microcircuits formed by subplate neurons and their role in functional development of thalamocortical connections. Neuroreport 15:2149-2153.
Keszler M, Modanlou HD, Brudno DS, Clark FI, Cohen RS, Ryan RM, Kaneta MK, Davis JM (1997) Multicenter controlled clinical trial of high-frequency jet ventilation in preterm infants with uncomplicated respiratory distress syndrome. Pediatrics 100:593-599.
Khwaja O, Volpe JJ (2008) Pathogenesis of cerebral white matter injury of prematurity. Arch Dis Child Fetal Neonatal Ed 93:F153-161.
Kinney HC, Back SA (1998) Human oligodendroglial development: relationship to periventricular leukomalacia. Semin Pediatr Neurol 5:180-189.
Kinney HC, Brody BA, Kloman AS, Gilles FH (1988) Sequence of central nervous system myelination in human infancy. II. Patterns of myelination in autopsied infants. J Neuropathol Exp Neurol 47:217-234.
Kirchner L, Weninger M, Unterasinger L, Birnbacher R, Hayde M, Krepler R, Pollak A (2005) Is the use of early nasal CPAP associated with lower rates of chronic lung disease and retinopathy of prematurity? Nine years of experience with the Vermont Oxford Neonatal Network. J Perinat Med 33:60-66.
Kirsten GF, Van Zyl JI, Van Zijl F, Maritz JS, Odendaal HJ (2000) Infants of women with severe early pre-eclampsia: the effect of absent end-diastolic umbilical artery

doppler flow velocities on neurodevelopmental outcome. Acta Paediatr 89:566-570.
Konishi Y, Chui DH, Hirose H, Kunishita T, Tabira T (1993) Trophic effect of erythropoietin and other hematopoietic factors on central cholinergic neurons in vitro and in vivo. Brain Res 609:29-35.
Kostovic I, Jovanov-Milosevic N (2006) The development of cerebral connections during the first 20-45 weeks' gestation. Semin Fetal Neonatal Med 11:415-422.
Kostovic I, Judas M, Rados M, Hrabac P (2002) Laminar organization of the human fetal cerebrum revealed by histochemical markers and magnetic resonance imaging. Cereb Cortex 12:536-544.
Kriegstein AR, Noctor SC (2004) Patterns of neuronal migration in the embryonic cortex. Trends Neurosci 27:392-399.
Krishnan ML, Dyet LE, Boardman JP, Kapellou O, Allsop JM, Cowan F, Edwards AD, Rutherford MA, Counsell SJ (2007) Relationship between white matter apparent diffusion coefficients in preterm infants at term-equivalent age and developmental outcome at 2 years. Pediatrics 120:e604-609.
Kroenke CD, Bretthorst GL, Inder TE, Neil JJ (2005) Diffusion MR imaging characteristics of the developing primate brain. Neuroimage 25:1205-1213.
Kroenke CD, Bretthorst GL, Inder TE, Neil JJ (2006) Modeling water diffusion anisotropy within fixed newborn primate brain using Bayesian probability theory. Magn Reson Med 55:187-197.
Kroenke CD, Van Essen DC, Inder TE, Rees S, Bretthorst GL, Neil JJ (2007) Microstructural changes of the baboon cerebral cortex during gestational development reflected in magnetic resonance imaging diffusion anisotropy. J Neurosci 27:12506-12515.
Lackman F, Capewell V, Richardson B, daSilva O, Gagnon R (2001) The risks of spontaneous preterm delivery and perinatal mortality in relation to size at birth according to fetal versus neonatal growth standards. Am J Obstet Gynecol 184:946-953.
Larroque B, Marret S, Ancel PY, Arnaud C, Marpeau L, Supernant K, Pierrat V, Roze JC, Matis J, Cambonie G, Burguet A, Andre M, Kaminski M, Breart G (2003) White matter damage and intraventricular hemorrhage in very preterm infants: the EPIPAGE study. J Pediatr 143:477-483.
Leviton A, Gilles FH (1984) Acquired perinatal leukoencephalopathy. Ann Neurol 16:1-8.
Ligam P, Haynes RL, Folkerth RD, Liu L, Yang M, Volpe JJ, Kinney HC (2009) Thalamic damage in periventricular leukomalacia: novel pathologic observations relevant to cognitive deficits in survivors of prematurity. Pediatr Res 65:524-529.
Limperopoulos C, Benson CB, Bassan H, Disalvo DN, Kinnamon DD, Moore M, Ringer SA, Volpe JJ, du Plessis AJ (2005) Cerebellar hemorrhage in the preterm infant: ultrasonographic findings and risk factors. Pediatrics 116:717-724.
Liu F, Garland M, Duan Y, Stark RI, Xu D, Dong Z, Bansal R, Peterson BS, Kangarlu A (2008) Study of the development of fetal baboon brain using magnetic resonance imaging at 3 Tesla. Neuroimage 40:148-159.

Lodygensky GA, Seghier ML, Warfield SK, Tolsa CB, Sizonenko S, Lazeyras F, Huppi PS (2008) Intrauterine growth restriction affects the preterm infant's hippocampus. Pediatr Res 63:438-443.

Loeliger M, Inder TE, Shields A, Dalitz P, Cain S, Yoder B, Rees SM (2009a) High-frequency oscillatory ventilation is not associated with increased risk of neuropathology compared with positive pressure ventilation: a preterm primate model. Pediatr Res 66:545-550.

Loeliger M, Shields A, McCurnin D, Clyman RI, Yoder B, Inder TE, Rees SM (2010) Ibuprofen Treatment for Closure Of Patent Ductus Arteriosus Is Not Associated With Increased Risk Of Neuropathology. Pediatr Res.

Loeliger M, Inder T, Cain S, Ramesh RC, Camm E, Thomson MA, Coalson J, Rees SM (2006) Cerebral outcomes in a preterm baboon model of early versus delayed nasal continuous positive airway pressure. Pediatrics 118:1640-1653.

Loeliger M, Inder TE, Dalitz PA, Cain S, Camm EJ, Yoder B, McCurnin D, Shaul PW, Clyman R, Rees SM (2009b) Developmental and neuropathological consequences of ductal ligation in the preterm baboon. Pediatr Res 65:209-214.

Lynch CD, Zhang J (2007) The research implications of the selection of a gestational age estimation method. Paediatr Perinat Ep 21:86-96.

Maalouf EF, Duggan PJ, Counsell SJ, Rutherford MA, Cowan F, Azzopardi D, Edwards AD (2001) Comparison of findings on cranial ultrasound and magnetic resonance imaging in preterm infants. Pediatrics 107:719-727.

Maalouf EF, Duggan PJ, Rutherford MA, Counsell SJ, Fletcher AM, Battin M, Cowan F, Edwards AD (1999) Magnetic resonance imaging of the brain in a cohort of extremely preterm infants. J Pediatr 135:351-357.

Marin-Padilla M (1970) Prenatal and early postnatal ontogenesis of the human motor cortex: a golgi study. I. The sequential development of the cortical layers. Brain Res 23:167-183.

Marin-Padilla M (1996) Developmental neuropathology and impact of perinatal brain damage. I: Hemorrhagic lesions of neocortex. J Neuropathol Exp Neurol 55:758-773.

Marin-Padilla M (1997) Developmental neuropathology and impact of perinatal brain damage. II: white matter lesions of the neocortex. J Neuropathol Exp Neurol 56:219-235.

Marin O, Rubenstein JL (2003) Cell migration in the forebrain. Annu Rev Neurosci 26:441-483.

Marlow N, Wolke D, Bracewell MA, Samara M (2005) Neurologic and developmental disability at six years of age after extremely preterm birth. N Engl J Med 352:9-19.

Marlow N, Greenough A, Peacock JL, Marston L, Limb ES, Johnson AH, Calvert SA (2006) Randomised trial of high frequency oscillatory ventilation or conventional ventilation in babies of gestational age 28 weeks or less: respiratory and neurological outcomes at 2 years. Arch Dis Child Fetal Neonatal Ed 91:F320-326.

Marshall DD, Kotelchuck M, Young TE, Bose CL, Kruyer L, O'Shea TM (1999) Risk factors for chronic lung disease in the surfactant era: a North Carolina population-based study of very low birth weight infants. North Carolina Neonatologists Association. Pediatrics 104:1345-1350.

McArdle CB, Richardson CJ, Hayden CK, Nicholas DA, Amparo EG (1987a) Abnormalities of the neonatal brain: MR imaging. Part II. Hypoxic-ischemic brain injury. Radiology 163:395-403.
McArdle CB, Richardson CJ, Nicholas DA, Mirfakhraee M, Hayden CK, Amparo EG (1987b) Developmental features of the neonatal brain: MR imaging. Part I. Gray-white matter differentiation and myelination. Radiology 162:223-229.
McArdle CB, Richardson CJ, Hayden CK, Nicholas DA, Crofford MJ, Amparo EG (1987c) Abnormalities of the neonatal brain: MR imaging. Part I. Intracranial hemorrhage. Radiology 163:387-394.
McCowan LM, Harding JE, Stewart AW (2000) Umbilical artery Doppler studies in small for gestational age babies reflect disease severity. BJOG 107:916-925.
McCowan LM, Pryor J, Harding JE (2002) Perinatal predictors of neurodevelopmental outcome in small-for-gestational-age children at 18 months of age. Am J Obstet Gynecol 186:1069-1075.
McCurnin D, Seidner S, Chang LY, Waleh N, Ikegami M, Petershack J, Yoder B, Giavedoni L, Albertine KH, Dahl MJ, Wang ZM, Clyman RI (2008) Ibuprofen-induced patent ductus arteriosus closure: physiologic, histologic, and biochemical effects on the premature lung. Pediatrics 121:945-956.
McCurnin DC, Pierce RA, Willis BC, Chang LY, Yoder BA, Yuhanna IS, Ballard PL, Clyman RI, Waleh N, Maniscalco W, Crapo JD, Grubb PH, Shaul PW (2009) Postnatal estradiol up-regulates lung nitric oxide synthases and improves lung function in bronchopulmonary dysplasia. Am J Respir Crit Care Med 179:492-500.
McKinstry RC, Mathur A, Miller JH, Ozcan A, Snyder AZ, Schefft GL, Almli CR, Shiran SI, Conturo TE, Neil JJ (2002) Radial organization of developing preterm human cerebral cortex revealed by non-invasive water diffusion anisotropy MRI. Cereb Cortex 12:1237-1243.
McPherson RJ, Demers EJ, Juul SE (2007) Safety of high-dose recombinant erythropoietin in a neonatal rat model. Neonatology 91:36-43.
Meyer M, Mildenhall L, Wong M (2004) Outcomes for infants weighing less than 1000 grams cared for with a nasal continuous positive airway pressure-based strategy. J Paediatr Child Health 40:38-41.
Miller SP, Cozzio CC, Goldstein RB, Ferriero DM, Partridge JC, Vigneron DB, Barkovich AJ (2003) Comparing the diagnosis of white matter injury in premature newborns with serial MR imaging and transfontanel ultrasonography findings. AJNR Am J Neuroradiol 24:1661-1669.
Miller SP, Vigneron DB, Henry RG, Bohland MA, Ceppi-Cozzio C, Hoffman C, Newton N, Partridge JC, Ferriero DM, Barkovich AJ (2002) Serial quantitative diffusion tensor MRI of the premature brain: development in newborns with and without injury. J Magn Reson Imaging 16:621-632.
Miller SP, Ferriero DM, Leonard C, Piecuch R, Glidden DV, Partridge JC, Perez M, Mukherjee P, Vigneron DB, Barkovich AJ (2005) Early brain injury in premature newborns detected with magnetic resonance imaging is associated with adverse early neurodevelopmental outcome. J Pediatr 147:609-616.

Miot-Noirault E, Barantin L, Akoka S, Le Pape A (1997) T2 relaxation time as a marker of brain myelination: experimental MR study in two neonatal animal models. J Neurosci Methods 72:5-14.
Moriette G, Paris-Llado J, Walti H, Escande B, Magny JF, Cambonie G, Thiriez G, Cantagrel S, Lacaze-Masmonteil T, Storme L, Blanc T, Liet JM, Andre C, Salanave B, Breart G (2001) Prospective randomized multicenter comparison of high-frequency oscillatory ventilation and conventional ventilation in preterm infants of less than 30 weeks with respiratory distress syndrome. Pediatrics 107:363-372.
Morishita E, Masuda S, Nagao M, Yasuda Y, Sasaki R (1997) Erythropoietin receptor is expressed in rat hippocampal and cerebral cortical neurons, and erythropoietin prevents in vitro glutamate-induced neuronal death. Neuroscience 76:105-116.
Morley CJ, Davis PG, Doyle LW, Brion LP, Hascoet JM, Carlin JB (2008) Nasal CPAP or intubation at birth for very preterm infants. N Engl J Med 358:700-708.
Moseley ME, Cohen Y, Mintorovitch J, Chileuitt L, Shimizu H, Kucharczyk J, Wendland MF, Weinstein PR (1990) Early detection of regional cerebral ischemia in cats: comparison of diffusion- and T2-weighted MRI and spectroscopy. Magn Reson Med 14:330-346.
Moster D, Lie RT, Markestad T (2008) Long-term medical and social consequences of preterm birth. N Engl J Med 359:262-273.
Muglia LJ, Katz M (2010) The enigma of spontaneous preterm birth. N Engl J Med 362:529-535.
Mukherjee P, Miller JH, Shimony JS, Philip JV, Nehra D, Snyder AZ, Conturo TE, Neil JJ, McKinstry RC (2002) Diffusion-tensor MR imaging of gray and white matter development during normal human brain maturation. AJNR Am J Neuroradiol 23:1445-1456.
Murphy BP, Inder TE, Huppi PS, Warfield S, Zientara GP, Kikinis R, Jolesz FA, Volpe JJ (2001) Impaired cerebral cortical gray matter growth after treatment with dexamethasone for neonatal chronic lung disease. Pediatrics 107:217-221.
Murphy BP, Inder TE, Rooks V, Taylor GA, Anderson NJ, Mogridge N, Horwood LJ, Volpe JJ (2002) Posthaemorrhagic ventricular dilatation in the premature infant: natural history and predictors of outcome. Arch Dis Child Fetal Neonatal Ed 87:F37-41.
Myers E, Ment LR (2009) Long-term outcome of preterm infants and the role of neuroimaging. Clin Perinatol 36:773-789, vi.
Neil J, Miller J, Mukherjee P, Huppi PS (2002) Diffusion tensor imaging of normal and injured developing human brain - a technical review. NMR Biomed 15:543-552.
Neil JJ, Inder TE (2004) Imaging perinatal brain injury in premature infants. Semin Perinatol 28:433-443.
Neil JJ, Shiran SI, McKinstry RC, Schefft GL, Snyder AZ, Almli CR, Akbudak E, Aronovitz JA, Miller JP, Lee BC, Conturo TE (1998) Normal brain in human newborns: apparent diffusion coefficient and diffusion anisotropy measured by using diffusion tensor MR imaging. Radiology 209:57-66.
Network TIN (1993) The CRIB (clinical risk index for babies) score: a tool for assessing initial neonatal risk and comparing performance of neonatal intensive care units. . Lancet 342:193-198.

Nguyen The Tich S, Anderson PJ, Shimony JS, Hunt RW, Doyle LW, Inder TE (2009) A novel quantitative simple brain metric using MR imaging for preterm infants. AJNR Am J Neuroradiol 30:125-131.
Nitsos I, Rees S (1990) The effects of intrauterine growth retardation on the development of neuroglia in fetal guinea pigs. An immunohistochemical and an ultrastructural study. Int J Dev Neurosci 8:233-244.
Noctor SC, Martinez-Cerdeno V, Ivic L, Kriegstein AR (2004) Cortical neurons arise in symmetric and asymmetric division zones and migrate through specific phases. Nat Neurosci 7:136-144.
Olney JW, Farber NB, Wozniak DF, Jevtovic-Todorovic V, Ikonomidou C (2000) Environmental agents that have the potential to trigger massive apoptotic neurodegeneration in the developing brain. Environ Health Perspect 108 Suppl 3:383-388.
Partridge SC, Vigneron DB, Charlton NN, Berman JI, Henry RG, Mukherjee P, McQuillen PS, Karl TR, Barkovich AJ, Miller SP (2006) Pyramidal tract maturation after brain injury in newborns with heart disease. Ann Neurol 59:640-651.
Partridge SC, Mukherjee P, Henry RG, Miller SP, Berman JI, Jin H, Lu Y, Glenn OA, Ferriero DM, Barkovich AJ, Vigneron DB (2004) Diffusion tensor imaging: serial quantitation of white matter tract maturity in premature newborns. Neuroimage 22:1302-1314.
Paus T, Collins DL, Evans AC, Leonard G, Pike B, Zijdenbos A (2001) Maturation of white matter in the human brain: a review of magnetic resonance studies. Brain Res Bull 54:255-266.
Pierson CR, Folkerth RD, Billiards SS, Trachtenberg FL, Drinkwater ME, Volpe JJ, Kinney HC (2007) Gray matter injury associated with periventricular leukomalacia in the premature infant. Acta Neuropathol 114:619-631.
Prayer D, Kasprian G, Krampl E, Ulm B, Witzani L, Prayer L, Brugger PC (2006) MRI of normal fetal brain development. Eur J Radiol 57:199-216.
Procianoy RS, Koch MS, Silveira RC (2009) Neurodevelopmental outcome of appropriate and small for gestational age very low birth weight infants. J Child Neurol 24:788-794.
Provenzale JM, Liang L, DeLong D, White LE (2007) Diffusion tensor imaging assessment of brain white matter maturation during the first postnatal year. AJR Am J Roentgenol 189:476-486.
Rados M, Judas M, Kostovic I (2006) In vitro MRI of brain development. Eur J Radiol 57:187-198.
Rees S, Harding R, Walker D (2008) An adverse intrauterine environment: implications for injury and altered development of the brain. Int J Dev Neurosci 26:3-11.
Rees S, Stringer M, Just Y, Hooper SB, Harding R (1997) The vulnerability of the fetal sheep brain to hypoxemia at mid-gestation. Brain Res Dev Brain Res 103:103-118.
Rees S, Breen S, Loeliger M, McCrabb G, Harding R (1999) Hypoxemia near mid-gestation has long-term effects on fetal brain development. J Neuropathol Exp Neurol 58:932-945.

Rees SM, Camm EJ, Loeliger M, Cain S, Dieni S, McCurnin D, Shaul PW, Yoder B, McLean C, Inder TE (2007) Inhaled nitric oxide: effects on cerebral growth and injury in a baboon model of premature delivery. Pediatr Res 61:552-558.

Regev RH, Lusky A, Dolfin T, Litmanovitz I, Arnon S, Reichman B (2003) Excess mortality and morbidity among small-for-gestational-age premature infants: a population-based study. J Pediatr 143:186-191.

Rice JE, 3rd, Vannucci RC, Brierley JB (1981) The influence of immaturity on hypoxic-ischemic brain damage in the rat. Ann Neurol 9:131-141.

Riddle A, Luo NL, Manese M, Beardsley DJ, Green L, Rorvik DA, Kelly KA, Barlow CH, Kelly JJ, Hohimer AR, Back SA (2006) Spatial heterogeneity in oligodendrocyte lineage maturation and not cerebral blood flow predicts fetal ovine periventricular white matter injury. J Neurosci 26:3045-3055.

Rigano S, Bozzo M, Ferrazzi E, Bellotti M, Battaglia FC, Galan HL (2001) Early and persistent reduction in umbilical vein blood flow in the growth-restricted fetus: a longitudinal study. Am J Obstet Gynecol 185:834-838.

Righini A, Bianchini E, Parazzini C, Gementi P, Ramenghi L, Baldoli C, Nicolini U, Mosca F, Triulzi F (2003) Apparent diffusion coefficient determination in normal fetal brain: a prenatal MR imaging study. AJNR Am J Neuroradiol 24:799-804.

Roelants-Van Rijn AM, Van der Grond J, Stigter RH, De Vries LS, Groenendaal F (2004) Cerebral structure and metabolism and long-term outcome in small-for-gestational-age preterm neonates. Pediatric Research 56:285-290.

Roelants-van Rijn AM, Nikkels PG, Groenendaal F, van Der Grond J, Barth PG, Snoeck I, Beek FJ, de Vries LS (2001) Neonatal diffusion-weighted MR imaging: relation with histopathology or follow-up MR examination. Neuropediatrics 32:286-294.

Rose J, Mirmiran M, Butler EE, Lin CY, Barnes PD, Kermoian R, Stevenson DK (2007) Neonatal microstructural development of the internal capsule on diffusion tensor imaging correlates with severity of gait and motor deficits. Dev Med Child Neurol 49:745-750.

Rose SE, Hatzigeorgiou X, Strudwick MW, Durbridge G, Davies PS, Colditz PB (2008) Altered white matter diffusion anisotropy in normal and preterm infants at term-equivalent age. Magn Reson Med 60:761-767.

Schouman-Claeys E, Henry-Feugeas MC, Roset F, Larroche JC, Hassine D, Sadik JC, Frija G, Gabilan JC (1993) Periventricular leukomalacia: correlation between MR imaging and autopsy findings during the first 2 months of life. Radiology 189:59-64.

Shepherd TM, Thelwall PE, Stanisz GJ, Blackband SJ (2009) Aldehyde fixative solutions alter the water relaxation and diffusion properties of nervous tissue. Magn Reson Med 62:26-34.

Song SK, Sun SW, Ramsbottom MJ, Chang C, Russell J, Cross AH (2002) Dysmyelination revealed through MRI as increased radial (but unchanged axial) diffusion of water. Neuroimage 17:1429-1436.

Song SK, Yoshino J, Le TQ, Lin SJ, Sun SW, Cross AH, Armstrong RC (2005) Demyelination increases radial diffusivity in corpus callosum of mouse brain. Neuroimage 26:132-140.

Stack JA, Jalaludin B (2007) Developmental outcomes at the age of two years for very premature babies managed with nasal prong continuous positive airway pressure. J Paediatr Child Health 43:480-485.
Sugawa M, Sakurai Y, Ishikawa-Ieda Y, Suzuki H, Asou H (2002) Effects of erythropoietin on glial cell development; oligodendrocyte maturation and astrocyte proliferation. Neurosci Res 44:391-403.
Sun SW, Neil JJ, Song SK (2003) Relative indices of water diffusion anisotropy are equivalent in live and formalin-fixed mouse brains. Magn Reson Med 50:743-748.
Sun SW, Neil JJ, Liang HF, He YY, Schmidt RE, Hsu CY, Song SK (2005) Formalin fixation alters water diffusion coefficient magnitude but not anisotropy in infarcted brain. Magn Reson Med 53:1447-1451.
Sung IK, Vohr B, Oh W (1993) Growth and neurodevelopmental outcome of very low birth weight infants with intrauterine growth retardation: comparison with control subjects matched by birth weight and gestational age. J Pediatr 123:618-624.
Taylor HG, Klein N, Minich NM, Hack M (2000) Middle-school-age outcomes in children with very low birthweight. Child Dev 71:1495-1511.
Teramo KA, Widness JA (2009) Increased fetal plasma and amniotic fluid erythropoietin concentrations: markers of intrauterine hypoxia. Neonatology 95:105-116.
Teramo KA, Schwartz R, Clemons GK, Widness JA (2002) Amniotic fluid erythropoietin concentrations differentiate between acute and chronic causes of fetal death. Acta Obstet Gynecol Scand 81:245-251.
Thome UH, Carlo WA, Pohlandt F (2005) Ventilation strategies and outcome in randomised trials of high frequency ventilation. Arch Dis Child Fetal Neonatal Ed 90:F466-473.
Thomson MA, Yoder BA, Winter VT, Giavedoni L, Chang LY, Coalson JJ (2006) Delayed extubation to nasal continuous positive airway pressure in the immature baboon model of bronchopulmonary dysplasia: lung clinical and pathological findings. Pediatrics 118:2038-2050.
Tolsa CB, Zimine S, Warfield SK, Freschi M, Sancho Rossignol A, Lazeyras F, Hanquinet S, Pfizenmaier M, Huppi PS (2004) Early alteration of structural and functional brain development in premature infants born with intrauterine growth restriction. Pediatr Res 56:132-138.
Trivedi R, Husain N, Rathore RK, Saksena S, Srivastava S, Malik GK, Das V, Pradhan M, Pandey CM, Gupta RK (2009) Correlation of diffusion tensor imaging with histology in the developing human frontal cerebrum. Dev Neurosci 31:487-496.
Valkama AM, Paakko EL, Vainionpaa LK, Lanning FP, Ilkko EA, Koivisto ME (2000) Magnetic resonance imaging at term and neuromotor outcome in preterm infants. Acta Paediatr 89:348-355.
van der Knaap MS, van Wezel-Meijler G, Barth PG, Barkhof F, Ader HJ, Valk J (1996) Normal gyration and sulcation in preterm and term neonates: appearance on MR images. Radiology 200:389-396.
Van Essen DC (1997) A tension-based theory of morphogenesis and compact wiring in the central nervous system. Nature 385:313-318.
Volpe JJ (2003) Cerebral white matter injury of the premature infant-more common than you think. Pediatrics 112:176-180.

Volpe JJ (2009) Brain injury in premature infants: a complex amalgam of destructive and developmental disturbances. Lancet Neurol 8:110-124.

Walsh MC, Morris BH, Wrage LA, Vohr BR, Poole WK, Tyson JE, Wright LL, Ehrenkranz RA, Stoll BJ, Fanaroff AA (2005) Extremely low birthweight neonates with protracted ventilation: mortality and 18-month neurodevelopmental outcomes. J Pediatr 146:798-804.

Wang S, Wu EX, Cai K, Lau HF, Cheung PT, Khong PL (2009) Mild hypoxic-ischemic injury in the neonatal rat brain: longitudinal evaluation of white matter using diffusion tensor MR imaging. AJNR Am J Neuroradiol 30:1907-1913.

Widness JA, Teramo KA, Clemons GK, Garcia JF, Cavalieri RL, Piasecki GJ, Jackson BT, Susa JB, Schwartz R (1986) Temporal response of immunoreactive erythropoietin to acute hypoxemia in fetal sheep. Pediatr Res 20:15-19.

Wilson-Costello D, Friedman H, Minich N, Fanaroff AA, Hack M (2005) Improved survival rates with increased neurodevelopmental disability for extremely low birth weight infants in the 1990s. Pediatrics 115:997-1003.

Wimberger DM, Roberts TP, Barkovich AJ, Prayer LM, Moseley ME, Kucharczyk J (1995) Identification of "premyelination" by diffusion-weighted MRI. J Comput Assist Tomogr 19:28-33.

Wiswell TE, Graziani LJ, Kornhauser MS, Cullen J, Merton DA, McKee L, Spitzer AR (1996) High-frequency jet ventilation in the early management of respiratory distress syndrome is associated with a greater risk for adverse outcomes. Pediatrics 98:1035-1043.

Woodward LJ, Anderson PJ, Austin NC, Howard K, Inder TE (2006) Neonatal MRI to predict neurodevelopmental outcomes in preterm infants. N Engl J Med 355:685-694.

Yoder BA, Siler-Khodr T, Winter VT, Coalson JJ (2000) High-frequency oscillatory ventilation: effects on lung function, mechanics, and airway cytokines in the immature baboon model for neonatal chronic lung disease. Am J Respir Crit Care Med 162:1867-1876.

Yoo SS, Park HJ, Soul JS, Mamata H, Park H, Westin CF, Bassan H, Du Plessis AJ, Robertson RL, Jr., Maier SE, Ringer SA, Volpe JJ, Zientara GP (2005) In vivo visualization of white matter fiber tracts of preterm- and term-infant brains with diffusion tensor magnetic resonance imaging. Invest Radiol 40:110-115.